AD-A111 140 AIR FORCE INST OF TECH WRIGHT-PATTERSON AFB OH SCHOO--ETC F/G 20/5
CHARACTERIZATION OF AN HF-PUMPED CO2 LASER.(U)
OCT 81 G P PERRAM
UNCLASSIFIED AFIT/GEP/PH/81D-7 NL

1 of 2
AD
A111 140

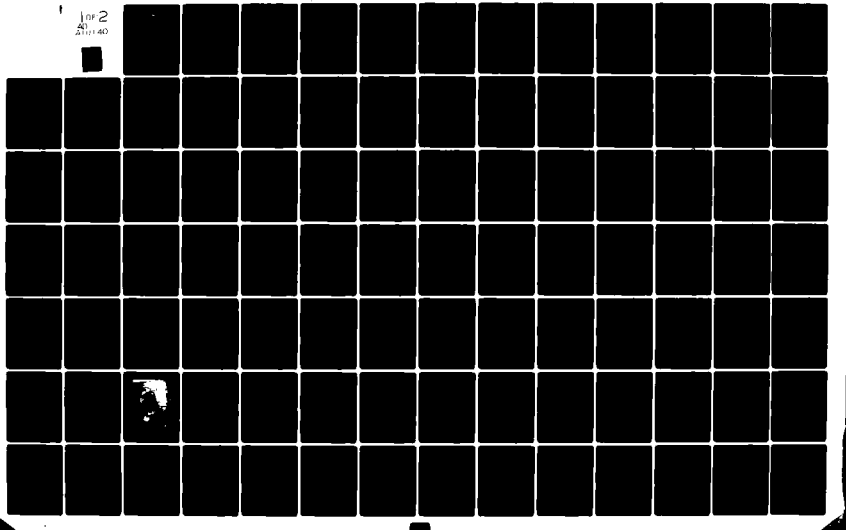

LEVEL II

1

AD A111140

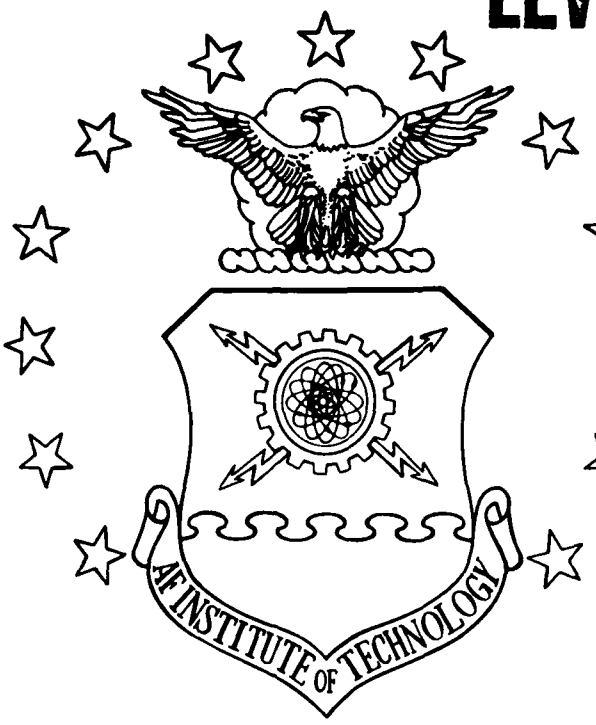


DTIC
ELECTE
FEB 19 1982
S
D
E

UNITED STATES AIR FORCE

AIR UNIVERSITY

# AIR FORCE INSTITUTE OF TECHNOLOGY

Wright-Patterson Air Force Base, Ohio

DTIC FILE COPY

This document has been approved for public release and sale; its distribution is unlimited.

82 02 18 067

II

(1)

# CHARACTERIZATION OF AN HF-PUMPED $CO_2$ LASER

THESIS

AFIT/GEP/PH/81D-7

Glen P. Perram
2nd Lt USAF

AFIT/GEP/PH/81D-7

# CHARACTERIZATION OF AN HF-PUMPED $CO_2$ LASER

THESIS

Presented to the Faculty of the School of Engineering
of the Air Force Institute of Technology
Air University
in Partial Fulfillment of the
Requirements for the Degree of
Master of Science

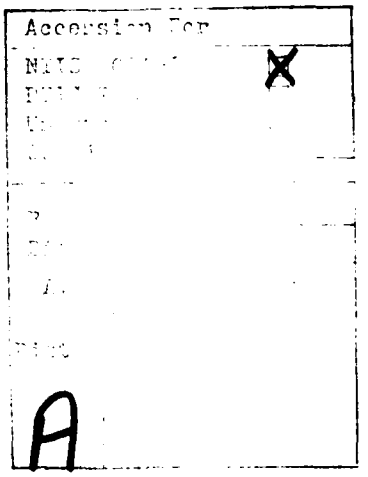


by

Glen P. Perram, B.S.
2nd Lt USAF
Graduate Engineering Physics

October 1981

## Preface

The purpose of this study was to characterize the performance of an optically pumped molecular laser and determine the effect of pump frequency on output power. Specifically, the $P_2(6)$ transition in a chemical HF laser is used to pump $^{12}C^{18}O_2$ molecules from the ground state to the 101 vibrational energy level. A population inversion is established between the 101 and 100 energy levels and lasing action is achieved at 4.3 microns. The results of a theoretical analysis and an experimental study are used to maximize the system's performance, clarify the principles of operation, and to resolve discrepancies between theory and prior experimental observations.

I would like to acknowledge the support of the Avionics Laboratory, AFWAL, WPAFB, OH in conducting this study, particularly Dr. W. Schuebel for sponsoring the project and J. Brandelik for his advice, instruction, and guidance. The support of my AFIT thesis advisor, Dr. E.A. Dorko, and thesis committee members, Major J.H. Erkkila and Dr. W.B. Roh was greatly appreciated, as were the discussions and information provided by Capt. R.J. Cook, AFIT/ENP, and Capt R. Walters, AFWL. The technical support provided by C. Shortt, AFIT Shop supervisor, A.M. Becraft, Avionics Lab, R. Wade, Glassblower-Avionics Lab, S. Derby, Avionics Lab, J.R. Gabriel, AFIT, and particularly, P. Dunigan and M. Lovingshimer, TSSI contractors-Avionics Lab, is gratefully acknowledged.

## Contents

## List of Figures

List of Figures
(Continued)

## List of Figures
(Continued)

## List of Tables

## Notation

| Symbol | Variable |
|---|---|
| $C$ | speed of light |
| $K$ | boltzman constant |
| $h$ | planck constant |
| $R_U$ | universal gas consatnt |
| $X$ | horizontal spatial coordinate |
| $Y$ | vertcal spatial coordinate |
| $Z$ | axial spatial coordinate |
| $V$ | volume |
| $A$ | area |
| $L$ | length |
| $q$ | axial mode number |
| $\upsilon$ | vibrational quantum number |
| $J$ | rotational quantum number |
| $\beta$ | rotational constant |
| $A_{21}$ | Einstein coefficient for spontaneous emission |
| $B_{12}, B_{21}$ | Einstein coefficient for stimulated emission |
| $\eta$ | ratio of specific heats, |
| $C_P$ | heat capacity at constant pressure |
| $C_V$ | heat capacity at constant volume |
| $\nu$ | frequency |
| $\nu_o$ | linecenter frequency |
| $\delta$ | offset frequency, HF frequency - $CO_2$ linecenter freq |
| $\bar{\nu}$ | wave number |
| $\lambda$ | wavelength |
| $\lambda_o$ | linecenter wavelength |

## Notation

(Continued)

| Symbol | Variable |
|---|---|
| $\gamma$ | gain coefficient |
| $\gamma_{TH}$ | threshold gain coefficient |
| $\alpha$ | absorption coefficient |
| $\alpha_o$ | distributed loss coefficient |
| $\sigma$ | absorption crossection |
| $\sigma_{AB}$ | collisional crossection |
| $G$ | lineshape factor |
| $\Delta \nu_N$ | natural linewidth |
| $\Delta \nu_C$ | collisional linewidth |
| $\Delta \nu_D$ | doppler linewidth |
| $\Delta \nu_T$ | total linewidth |
| $\omega$ | beam spot size |
| $\theta_{1/2}$ | beam divergence, half angle |
| $R$ | complex radius of curvature |
| $T$ | absolute temperature |
| $M$ | mass |
| $M_{\#}$ | Mach number |
| $\epsilon$ | energy/mole |
| $\epsilon_D$ | dissociation energy/mole |
| $E$ | energy |
| $V$ | potential |
| $N$ | total number |
| $N_\varphi$ | total photon number |
| $\eta$ | number density |

## Notation

(Continued)

| Symbol | Variable |
|---|---|
| $[\,]$ | concentration |
| $\Delta$ | population inversion |
| $P$ | power |
| $I$ | intensity |
| $I_o$ | incident intensity |
| $I_S$ | saturation intensity |
| $I_\nu$ | intensity as a function of frequency |
| $D$ | atomic diameter |
| $U$ | velocity |
| $a_S$ | speed of sound |
| $a$ | radius |
| $\Lambda$ | mean free path |
| $\rho$ | reflectivity |
| $R$ | radius of curvature |
| $r$ | repetition rate |
| $\tau$ | characteristic time |
| $\tau_R$ | radiative lifetime |
| $\tau_C$ | cavity photon lifetime |
| $K$ | rate constant |
| $H$ | Hamiltonian |
| $\psi$ | wavefunction |
| $\mu$ | dipole moment or viscosity |
| $P$ | pressure |
| $\underline{E}$ | electric field |

## Notation

(Continued)

| Symbol | Variable |
|---|---|
| $S$ | strain |
| $\xi$ | piezoelctric constant |
| $i$ | current |

## Abstract

Optical pumping of the 000 - $(10°1)_{II}$ transition in $^{12}C^{18}O_2$ by the $P_2(6)$ transition of an $SF_6$:$H_2$ electric discharge HF chemical laser was used to establish a population inversion between the $(10°1)_{II}$ and $(10°0)_{I}$ levels of $^{12}C^{18}O_2$ and lasing at 4.3 microns.

The HF pump laser was characterized and maximum power achieved at 79% $SF_6$/ 21% $H_2$, 88 torr total pressure, a 12kV discharge voltage, and 300 pulses/sec. Lasing on the $P_2(4)$, $P_2(5)$, and $P_2(6)$ transitions was observed with a beam divergence of 9 mrad. A pulse-to-pulse variation in output power of a factor of six and a frequency instability greater than 200 MHz/msec. was observed. A 156 micro-Joule, 106 nsec pulse was observed multiline.

The $P_2(6)$ TEM 00 HF beam at 37.5 micro-J was coupled into a .5 inch diameter pyrex cell with 7 torr $^{12}C^{18}O_2$ with a 25 cm focal length $CaF_2$ lens. A 26 nsec $CO_2$ pulse was observed in the forward propogating direction. $CO_2$ lasing was erratic, due to near threshold pumping conditions.

A theoretical model of the kinetics of the $SF_6$ + $H_2$ / electric discharge was established. Pulse widths predicted by this theory and those observed experimentally agree well. The predicted power amplitude is larger than observed, due to losses not included in the model.

The dependence of $CO_2$ output power on HF frequency was not observed experimentally. The contradiction between established theory and previous experimental results was explained, however.

# Introduction

## Background

Laser sources are needed across a wide portion of the electromagnetic spectrum. The infrared region is particularly important for several laser applications: (1) multi-photon IR beam photochemistry, (2) laser isotope seperation, (3) laser methods for obtaining pure materials, and (4) military applications [1:1317]. Several molecular lasers, including $CO_2$, CO, $N_2O$, HF and DF, operate in the mid-infrared region, but do not adequately cover this band. Resonant frequency conversion can be used to increase the number of sources in the mid-IR by using one of the molecular lasers to optically pump a second laser medium. One advantage of such systems is the high power obtainable [2:68].

A $CO_2$ laser optically pumped by an HF laser was developed for the Avionics Laboratory, Air Force Wright Aeronautical Laboratories, Wright-Patterson Air Force Base, Ohio by the Raytheon Corporation [3]. Many characteristics of this laser are unknown and few studies for optimization of the system have been completed. Several aspects of the laser's operation are not well understood and previous experimental investigations appear to contradict established theory.

## Problem Definition

This investigation will characterize the performance of this HF-pumped $CO_2$ laser system in an attempt to maximize

its performance, clarify the priciples of operation, reproduce the work of reference [3], and study discrepancies between theory and prior experimental results. Output power, beam quality, and stability of the HF laser will be examined. The $CO_2$ lasing system will be studied to maximize output power. In particular, optical pumping and the effect of HF laser frequency on the $CO_2$ output power will be studied and the results compared with previous investigations and theoretical predictions. HF and $CO_2$ power pulse shapes will be experimentally observed and explained in terms of the kinetics of the HF reaction and the optical pumping scheme.

In the Raytheon study, no significant variation in the $CO_2$ output power was observed with changes in the HF laser frequency over a 300 MHz range [3:64-65]. A substantial variation would be expected on theoretical grounds, however. The main effort of this thesis will be to explain this discrepancy between theory and experiment.

Presentation

Background theory on the operation of the HF pump laser and on the optically pumped $CO_2$ laser will be presented in Chapter II. A kinetic model of the HF laser will be established. A model of the effect of HF frequency on $CO_2$ power will also be established. Chapter III will describe the HF and $CO_2$ lasers, as well as the experimental set-up for studying the frequency - power relation.

Finally, Chapter IV will present the results of characterizing the HF pump laser, studying the optically-pumped $CO_2$ laser, and of the power-frequency experiment. Conclusions concerning the laser system and the frequency effect will be drawn. Recommendations for improvement of the lasing system and for future studies are then made.

## Background Theory

Three main topics will be presented in this chapter: (1) spectroscopy of the HF laser, (2) a kinetic model of the $SF_6 + H_2$ in the electric discharge, with a derivation of the population inversion and power pulse shape, and (3) the theory of the $CO_2$ laser and the optical pumping scheme, including a derivation of the dependence of $CO_2$ output power on HF frequency.

### HF Laser Spectroscopy

An HF chemical laser was first demonstrated by Kompa and Pimentel with lasing from the $v=2$ to $v=1$ vibrational energy levels [4]. The first cw HF laser was reported by Spencer et al [5]. $SF_6$ was used as a fluorine donor and lasing was observed for three different rotational transitions within the $v=2$ to $v=1$ band. Electric discharge initiated HF chemical lasers were also demonstrated early [6,7]. Since then a number of cw and pulsed HF lasers using $SF_6$ and $H_2$ have been demonstrated [8-17]. Electric discharge, electron beams, electric arcs, and $N_2$-$SF_6$ collisions at high temperature have been used to dissociate $SF_6$ to produce atomic fluorine. It is an electric discharge, $SF_6$ type HF laser that is used in this study.

The HF chemical laser produces vibrationally excited HF molecules by direct reaction of hydrogen with fluorine. A chain reaction can be established and thus high efficiencies

are obtainable. The optical gain of HF lasers is high and can reach 100% per centimeter in pulsed operation [18]. Large amounts of energy are released during the chemical reaction and many vibrational levels can be populated. The cascading of transitions from upper vibrational levels to the ground state can yield a large number of lasing lines in a single system. Forty different lines for HF lasing in the 2.6 to 3.4 micron range have been summarized in reference [19:404].

HF lasers operate on transitions between vibrational-rotational levels of the HF molecule. The vibrational energy diagram for HF is shown in figure 1. A set of rotational energy levels is associated with each vibrational energy level. The notation $P_{\upsilon}(J)$ denotes the transition $\upsilon=\upsilon_1$, $J=J_1-1$ to $\upsilon=\upsilon-1$, $J=J_1$ . The $P_2(6)$ transition is shown in figure 1 and is used to optically pump the isotope $^{12}C^{18}O_2$. The frequency of the $P_2(6)$ transition has been measured by several authors [6,20-23]. The best experimental value is $\bar{\nu}=3531.3\pm.12\ CM^{-1}$ [6]. Buchwald reports a value of $\bar{\nu}=3531.175\ CM^{-1}$ based on the absoption of the $P_2(6)$ transition in $^{12}C^{18}O_2$ [23]. The wavelength is

$$\lambda=\frac{1}{\bar{\nu}}=2.8319\ \mu m \qquad (1)$$

The linewidth of the HF $P_2(6)$ line is important, for it will determine the range over which the HF laser can be tuned and the amount of HF power absorbed by the $CO_2$ gas.

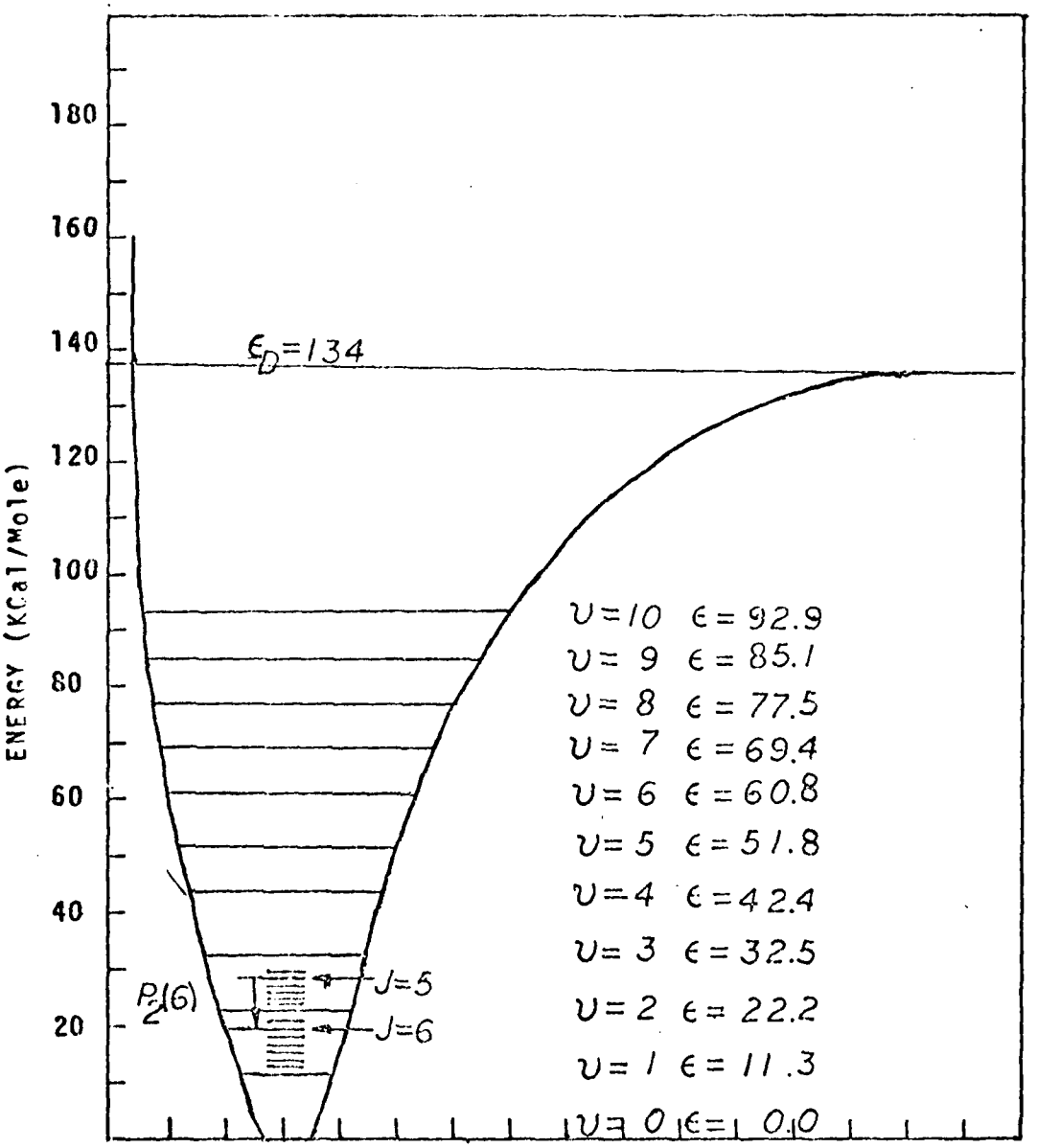


Figure 1.
Energy Level Diagram for HF
"Morse-type" Potential

The three main broadening mechanisms are natural, collisional, and Doppler.

The natural linewidth (FWHM) is

$$\Delta \nu_N = \frac{1}{2\pi\tau_R} \tag{2}$$

where $\tau_R$ is the radiative lifetime of the upper laser level [24:57]. Peterson has measured the natural linewidth for the $P_2(J)$ transitions as 3 MHz [25]. The $P_2(6)$ transition will be assumed to have a similar linewidth. Collisional and Doppler broadening will be shown to be much greater than 3 MHz and natural broadening will be neglected.

Collisional broadening arises from collisions between the active molecule (HF) and all other molecules. Its magnitude depends on the physical properties of the collision partners and on their partial pressures. The linewidth is

$$\Delta \nu_C = \frac{1}{\pi} \sum_B 2\eta_B \sigma_{AB} \sqrt{\frac{2KT}{\pi}\left(\frac{1}{M_A} \quad \frac{1}{M_B}\right)} \tag{3}$$

where

$$\sigma_{AB} = \pi\left(\frac{D_A + D_B}{2}\right)^2 \tag{4}$$

is the collisional crossection, $D_A$ and $D_B$ are the molecular diameters of particles of type A (HF) and type B (HF collision partners), $M_A$ and $M_B$ are the masses of the particles, $\eta_B$ is the number density of type B particles, and $T$ is the absolute temperature [34]. The summation is taken over all collision partners, B, including the self collisions with other type A particles.

To evaluate this expression for the HF laser, the

following analysis is performed:

Introduce the ideal gas law and total pressure

$$P_B = n_B K T \qquad P = \sum_B P_B \tag{5,6}$$

and

$$n_B = \frac{P_B}{KT} = \left(\frac{P_B}{P}\right)\frac{P}{KT} \tag{7}$$

Substitute equation (7) into equation (3):

$$\Delta\nu_C = \frac{1}{\pi}\sum_B 2\left(\frac{P_B}{P}\right)\frac{P}{KT}\sigma_{AB}\sqrt{\frac{2KT}{\pi}\left(\frac{1}{M_A}+\frac{1}{M_B}\right)}$$

$$= \frac{2}{\pi}\sqrt{\frac{2}{\pi KT}}\,P\sum_B\left(\frac{P_B}{P}\right)\sigma_{AB}\sqrt{\left(\frac{1}{M_A}+\frac{1}{M_B}\right)} \tag{8}$$

Let $P$ be in torr, atomic radii in angstroms, and mass in kg/kgmole, then, at $T = 300^\circ K$:

$$\Delta\nu_C = (.225 MHZ)P\sum_B\left(\frac{P_B}{P}\right)\frac{\pi}{4}\left(D_A + D_B\right)^2\sqrt{\frac{1}{M_A}+\frac{1}{M_B}} \tag{9}$$

To evaluate this equation for the HF laser used in this study, take $P = 80$ torr and a gas mixture of $SF_6:H_2 = 4:1$. The partial pressure of HF is set to zero. The atomic diameters are

$$D_{HF} = 4.3\,\dot{A} \quad D_{H_2} = 2.7\,\dot{A} \quad D_{SF_6} = 4.4\,\dot{A}$$

from references [27,28] Then,

$$\Delta\nu_C = 322\ MHZ \tag{10}$$

Doppler broadening arises from the distribution of particle velocities and the linewidth is

$$\Delta\nu_D = \frac{2}{\lambda_o}\sqrt{\frac{2KT\ln 2}{M}} \tag{11}$$

where $\lambda_o$ is the line-center wavelength, $T$ is absolute temperature, and $M$ is the mass of the active molecule. For the $P_2(6)$ transition in HF at 300°K, $\Delta\nu_D = 294 MHZ$.

The effects of collisional and Doppler broadening can be convolved to give a total lineshape with the use of a Voigt profile. Assuming that collisional broadening is independent of particle velocity, the total lineshape at any wavelength is simply the convolution of the Lorentzian (collisional) and Gaussian (Doppler) lineshapes. The total lineshape is given by the summation over all frequency:

$$G(\lambda) = G(\lambda_o)\frac{\zeta}{\pi}\int_{-\infty}^{\infty}\frac{e^{-\chi^2}}{\zeta^2+(\varphi-\chi)^2}\,d\chi \qquad (12)$$

where $G(\lambda)$ is the total gain lineshape factor as a function of wavelength, $\lambda$ , $\lambda_o$ is the line-center wavelength,

$$\zeta = \frac{\Delta\nu_C}{\Delta\nu_D}\sqrt{\ln 2} \qquad (13)$$

$$\varphi = \frac{(\lambda-\lambda_o)}{\lambda^2}\frac{c}{\Delta\nu_D}2\sqrt{\ln 2} \qquad (14)$$

$$\chi = \frac{(\lambda'-\lambda_o)}{\lambda^2}\frac{c}{\Delta\nu_D}2\sqrt{\ln 2} \qquad (15)$$

and $\lambda'$ is the variable wavelength of integration [29:128].

This integral is the Voigt integral and has been evaluated numerically [30]. For $\frac{\Delta\nu_D}{\Delta\nu_C} = \frac{294}{322} = .913$ , the linewidth (FWHM) is 506 MHz, $\Delta\nu_T = 506 MHZ$ .

Several studies of line broadening in HF lasers have been completed [31-32]. These studies have dealt mainly with the $P_1(J)$ transitions and HF - HF collisions. Broadening of the $\upsilon=2$ to $\upsilon=1$ transition due to HF - HF collisions is 7.9 MHz/Torr HF [31:1575]. Collisional broadening of the

$P_1(5)$ transition at 50 torr and 100°C has been measured as 672 MHz [32:1117]. No studies of the $P_2(6)$ transition with $SF_6$ collision partners were found. The value $\Delta\nu_T = 506 MHZ$ will be used in this study.

Axial modes in a laser are given by

$$\nu_q = \frac{qC}{2\eta L} \tag{16}$$

and the free spectral range by

$$\Delta\nu_q = \frac{C}{2\eta L} \tag{17}$$

where $L$ is cavity length, $\eta$ is the index of refraction of the lasing medium, and $C$ is the speed of light. $q$ is an integer specifying the axial mode number. For $\eta L = .56 M$ (see the experimental section for a description of the optical cavity), $\Delta\nu_q = 268 MHZ$. Note that $\frac{\Delta\nu_T}{\Delta\nu_q} = 1.89$ and thus, one or two axial modes will exist depending on the exact value of $L$. The frequency of the laser can be changed by varying the cavity length. The relation between frequency change and length change is

$$\delta\nu_q = -\frac{qC}{2\eta L^2}\delta L = -\frac{C}{\lambda L}\delta L \tag{18}$$

To vary the laser frequency across its full width of 506 MHz, the length of the cavity must be varied by 2.6 μm.

This length change is easily achieved with a piezo-electric crystal. The converse piezo-electric effect states an applied electric field produces a proportional strain in the crystal

$$S = \frac{\Delta L}{L} = \xi E \tag{19}$$

where $S$ is strain, $\xi$ is the piezo-electric constant, and

$\underline{E}$ is the electric field. The magnitude of $\xi$ for many piezo-electric materials is sufficient to provide a 2.6 μm deflection under the application of a 1 KV voltage. A $BaTiO_3$ crystal was used to vary the HF laser frequency and is described in the experimental section.

One last parameter is required to specify the energy levels and transitions. The transition rate between energy levels affects the population inversion and output power.

These transition rates are given by the Einstein coefficients. Take the following two level system:

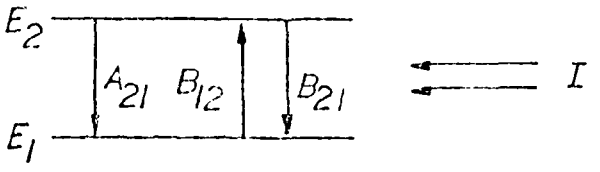


$E_2$ is the upper energy level and $E_1$ is the lower level, $I$ is the incident photon intensity and $A_{21}, B_{12}, B_{21}$ are the Einstein coefficients defined as

$A_{21}$ = the probability of a molecule spontaneously decaying from the upper energy level to the lower level per unit time. $\tau = 1/A_{21}$, the radiative lifetime from the upper to lower energy level.

$B_{12}I$ ($B_{21}I$)=the probability per unit time of a molecule being stimulated to transition to the other energy level by the incident photon intensity, $I$.

The Einstein coefficients are related by

$$A_{21} = \frac{2hC}{\lambda^3} B_{21} = \frac{2hC}{\lambda^3} B_{12} \qquad (20)$$

[34:2-18]

The Einstein coefficient, $B_{21}$, for the $P_2(6)$ transition in HF is $1.372 \times 10^{14}$ cm$^2$/J sec [19:483]. The radiative lifetime is then .4 seconds.

The spectroscopy of the HF lasing transition has been established. The mechanism for establishing the population inversion will now be examined.

Kinetic Model of $SF_6 + H_2$ in the Electric Discharge

HF chemical lasers establish a population inversion of the vibrational-rotational levels of HF through chemical reactions involving H, $H_2$, F, and $F_2$. The pumping processes are chemical reactions whose products are vibrationally excited HF molecules. The two major reactions are

$$F + H_2 \longrightarrow HF(v) + H \quad \Delta H = -31.6 \frac{KCAL}{MOLE} \tag{21}$$

$$H + F_2 \longrightarrow HF(v) + F \quad \Delta H = -98.0 \frac{KCAL}{MOLE} \tag{22}$$

[35]

Reaction (21) is termed the cold reaction, due to its lower $\Delta H$. Population of the $v=0$ to $v=3$ levels are possible, with the $v=2$ state preferred:

$$F + H_2 \longrightarrow HF(0) + H + 31.6\ KCAL/MOLE$$
$$K_0 = 1.2 \times 10^{13} \times 10^{-350/T}\ CM^3/MOLE\text{-}SEC \tag{23}$$

$$F + H_2 \longrightarrow HF(1) + H + 20.4\ KCAL/MOLE$$
$$K_1 = 2.4 \times 10^{13} \times 10^{-350/T}\ CM^3/MOLE\text{-}SEC \tag{24}$$

$$F + H_2 \longrightarrow HF(2) + H + 9.6\ KCAL/MOLE$$
$$K_2 = 8.2 \times 10^{13} \times 10^{-350/T}\ CM^3/MOLE\text{-}SEC \tag{25}$$

cortical processes in the two cases which reflect the accompanying psychic events are quite different. It would be erroneous to conclude, however, that the ergotropic downward discharges are not subject to adaptive changes. That fundamentally different types of ergotropic discharges occur is evident from the increased excretion of noradrenaline (without that of adrenaline) and vice versa. Moreover, adjustments take place even within the autonomic-somatic components of the ergotropic downward discharge, as illustrated by the fundamental differences in the rates of excretion of noradrenaline and adrenaline in acute and chronic states of exposure to cold and in the absence of shivering in the cold-adapted organism.

# VIII

## *Internal Secretions and the Ergotropic and Trophotropic Systems*

THAT increased ergotropic activity enhances the secretion of adrenomedullary hormones as reviewed in the preceding chapter is but one example of ergotropic-hormonal relations. The reader will remember that conditioning and other forms of stress associated with augmented ergotropic discharges were shown to cause an increased secretion of adrenocortical steroids (Chapter III). These and numerous related investigations constitute an important part of neuroendocrinology, the discussion of which is obviously beyond the scope of this book. But in order to illustrate further the dependence of internal secretions on the ergotropic and trophotropic systems and vice versa, a brief survey of the influence of hypothalamus on the activity of several endocrine glands is presented in this chapter.

### 1. THE THYROID GLAND*

Clinical observations on Graves' disease and early physiological studies on prolonged stimulation of the cervical sympathetic nerves suggested but did not prove an influence of the ergotropic system on the activity of the thyroid gland. However, recent work involving the study of hypothalamic stimulations and lesions has finally established this relation.

The basic facts may be summarized as follows. In animals previously injected with radioactive $I^{131}$ the difference in radioactivity between the venous and the arterial blood of the thyroid gland increases on stimulation of the anterior hypothalamus, the median eminence, or the tuber cinereum anterior to the median eminence, whereas stimulation of other hypothalamic sites is without effect (143). These results can be matched by the injection of thyrotropin (TSH). Furthermore, unanesthetized rabbits provided with a wire coil ending in a hypothalamic electrode in which a current is induced through a large primary coil (located outside the cage) likewise show an increase in thyroid activity on stimulation: radioactive $I^{131}$ is released in increased amounts from the thyroid gland while the plasma protein-bound $I^{131}$ ($PBI^{131}$) rises (429). In the rat, multiple

*For the literature see 114, 186, 642, 818, and 932.

$$F + H_2 \longrightarrow HF(3) + H + .8 \text{ KCAL/MOLE}$$
$$K = 4.1 \times 10^{13} \times 10^{-350/T} \text{ CM}^3\text{/MOLE-SEC} \quad (26)\ [36]$$

Reaction (22), the hot reaction, populates the $V=0$ to $V=12$ states, with the $V=5$ or 6 state preferred [19:591]. Note that the set of reactions (21) and (22) form a chain mechanism. As a result, efficiency based on output power versus electrical input can be substantially greater than 100%. The length of the average chain has been estimated as 20 cycles [14]. Systems operating on both reactions should have larger output powers than those utilizing only one reaction.

To initiate reaction (21) and/or (22), donors for F, $F_2$, H, and $H_2$ must be provided. As noted earlier, $SF_6$ and $H_2$ have been used in a number of operating HF lasers and are used in this Raytheon HF laser.

$H_2$ gas is readily available and can be dissociated to provide H atoms. If only $H_2$ were provided with no dissociation, both reaction (21) and (22) could still operate, since hydrogen is produced in reaction (21).

The complication in the kinetics arises from the $SF_6$ donor for fluorine. $SF_6$ is used because it is inert and more easily handled than fluorine gas. Before examining the processes for the production of F and $F_2$ from $SF_6$, the structure and properties of $SF_6$ should be examined.

Sulfur hexafluoride ($SF_6$) has an octahedral structure

with six σ-bonds between fluorine atoms and the sulfur atom. Fluorine has one empty p-orbital ($1s^2 2s^2 2p^5$) and sulfur has six electrons in its outer shell ($1s^2 2s^2 2p^6 3s^2 3p^4$). The six fluorine atoms each share one of the outer electrons with the sulfur atom to form $d^2sp^3$ hybrid orbitals [28:99]. The S - F bond energy is slightly less than 78 kcal/mole (3.3 eV/molecule) and the bond length is approximately 1.4 angstroms [37:534-539,38:F202].

$SF_6$ is very stable and reacts only under extreme conditions. This HF laser uses an electric discharge (12kV, 350 Amps) to produce the fluorine from $SF_6$. $H_2$ is also dissociated in the discharge.

The energy of the electrons in the discharge is important to the nature of $e^-$ - $SF_6$ reactions. An estimation of electron energies can be obtained with the model of figure 2.

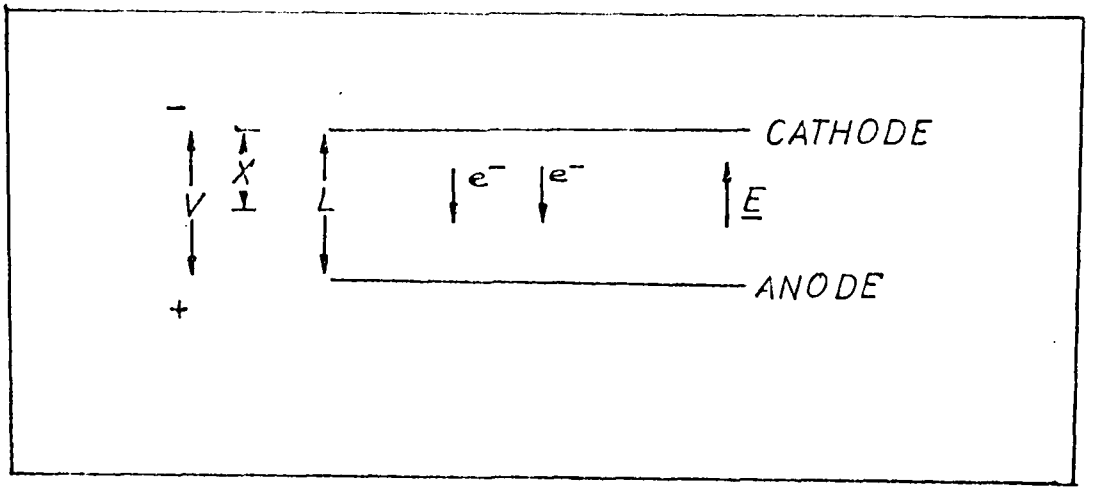


Figure 2.
ELECTRON DISCHARGE MODEL

The electrons at the cathode have a potential energy

of $eV$, where $e$ is the charge of an electron and $V$ is the voltage applied across the cathode/anode structure. For a uniform electric field, this potential energy will vary linearly across the gap to zero at the anode. From energy conservation, the decrease in potential energy of an electron as it moves to the anode is equal to the increase in the electron's kinetic energy. The electron is originally at rest and the kinetic energy of an electron at distance $X$ from the cathode is

$$E = eV\frac{X}{L} \tag{27}$$

The average kinetic energy at collision is then

$$\langle E \rangle = eV\frac{\langle X \rangle}{L} = eV\frac{\Lambda}{L} \tag{28}$$

where $\Lambda$ is the average distance an electron will travel before collision with a gas molecule, or the electron's mean free path. If it is assumed that an electron gives all its energy to the gas molecule upon collision, then the average electron energy throughout the gas, in electron volts, will be

$$\langle E \rangle = \frac{\Lambda}{L} 12\,KeV \tag{29}$$

for a 12 kV applied voltage. $L$ is about 1 cm.

A very rough estimate of the mean free path can be obtained from a hard sphere model of collisions

$$\Lambda = \frac{4}{\pi n d^2} \tag{30}$$

where $n$ is the number density of $SF_6$, $d$ is the diameter

of $SF_6$ and the equation is valid for light-heavy particle interactions. Taking $d = 2.8\text{Å}$ (twice the S-F bond length) and using the ideal gas equation for number density

$$n = \frac{P}{KT} = \frac{80\,(760\,TORR)\left(\frac{1ATM}{760TORR}\right)\left(\frac{10^5 N/M^2}{1.987ATM}\right)TORR}{(1.38\times10^{-23})(300)JOULE} \qquad (31)$$

Then, $n = 2.6\times10^{24}\,1/M^3$ and $\Lambda = 6.4\mu m$.

This estimate is crude, for it completely neglects the electric field interaction. A more accurate value for $\Lambda$ is obtained from a measurement of the $e^-$ - $SF_6$ crossection. This crossection has been measured as $\sigma = 2.2\times10^{-19}\,m^2$. Thus,

$$\Lambda = \frac{1}{\sigma n} = 1.79\,\mu m. \qquad (32)$$

This slightly smaller mean free path will be used for further calculations.

The average electron energy from equation (29) is

$$E = \frac{\Lambda}{L}12keV = \left(\frac{1.79\times10^{-6}}{.01}\right)12keV = 2.2\,eV \qquad (33)$$

The average electron velocity is about $10^6$ m/sec.

The mean free path is small compared to the anode-cathode separation and the elctrons will suffer many collisions before clearing the discharge volume. The large number of electron collisions and low average energy suggests some sense of equilibrium may be obtained, and the electrons could be characterized by a temperature $T$, such that

$$\langle E \rangle = \frac{3}{2}KT \qquad (34)$$

The temperature at 2.2 eV is then 25,500 °K.

The actual distribution of electron energies is potentially

complex. There exists a large electric field, accelerating the electrons. There also exists a number of collision partners that could selectively depopulate particular energy electrons from the distribution. A steady state solution of the Boltzman equation for a system with an 18 kV/cm electric field was computed [41] and modified for an $SF_6$ -$H_2$ mixture [42]. Results indicate a distribution that does not vary from a Maxwellian distribution by more than a factor of two over the 0 - 50 eV energy range. Thus, a Maxwellian distribution of electron energies will be assumed , with an average energy of 2.2 eV or temperature of 25,500°K.

A number of authors have investigated the kinetics of $SF_6 + e^-$ [14, 43-45]. Simply from the structure of $SF_6$ , it would be expected that only atomic fluorine would be produced. To produce $F_2$ , two , adjacent S-F bonds would need to be broken and the F-F bond created. The production of $F_2$ is much more likely from the process

$$F + F + M \longrightarrow F_2 + M \qquad (35)$$

and will be discussed later.

The production of atomic fluorine is based on the mechanism

$$SF_6 + e^- \longrightarrow SF_6^{-*} \begin{cases} \longrightarrow SF_6^- \\ \longrightarrow SF_5^- + F \end{cases} \qquad \begin{matrix} (36) \\ [43] \end{matrix}$$

The low energy, "thermalized" electrons attach to the $SF_6$ molecule to produce an excited state $SF_6^*$, which decays very rapidly to either $SF_6^-$ or $SF_5^-$ + F. Since the second reaction

rates are so rapid, the final products may be considered the products of $SF_6 + e^-$ .

Bashkin reports major flourine production from the reactions

$$SF_6 + e^- \longrightarrow SF_5^+ + F + 2e^- \quad (37)$$

$$SF_6 + e^- \longrightarrow SF_5 + F + e^- \quad (38)$$

as well. These reactions have been investigated by Ahearn [46] and Assundi [47]. The reaction

$$SF_6 + e^- \longrightarrow SF_5 + F^- \quad (39)$$

is described by Curran [48] and included in a model of $SF_6 + H_2$ in an electric discharge developed by Lyman [42]. In this article by Lyman, pulse shapes for an $SF_6 + H_2$ electric discharge laser with a μsec duration have been theoretically computed.

After these processes are initiated, further fluorine production from a reaction proposed by McGeehan [45] is possible:

$$SF_5^- + SF_6 \longrightarrow SF_4 + F^- + SF_6 \quad (40)$$

This reaction depends greatly on the ratio of electric field to number density (a measure of average electron energy) and is only important if $E/n \geq 3 \times 10^{-15}$ VOLT-CM$^2$ . The Raytheon laser has a 12 kV voltage applied across a 1 cm gap with 80 torr total pressure, and thus

$$E/n = 2 \times 10^{-15} \text{ VOLT-CM}^2 \quad (41)$$

The production of $F_2$ from reaction (40) will be neglected.

Reactions such as

$$SF_6 + M \longrightarrow SF_5 + F + M \qquad (42)$$

and

$$SF_5 + M \longrightarrow SF_4 + F + M \qquad (43)$$

have such high activation energies ( 76 kCal/mole and 66kCal/mole) that they may be neglected. $SF_6$ may also be collisionally dissociated to produce ground state HF by

$$SF_6 + H \longrightarrow SF_5 + HF \qquad (44)$$

This reaction will be discussed later in conjunction with the pumping reactions.

Hydrogen gas is also dissociated in the electric discharge. Collisonal dissociation is again small, due to the high activation energy. Hydrogen dissociation is given by the reaction

$$H_2 + e^- \longrightarrow H + H + e^- \qquad (45)$$

Hydrogen may also be ionized by the electrons:

$$H_2 + e^- \longrightarrow H_2^+ + 2e^- \qquad (46)$$

$$H + e^- \longrightarrow H^+ + 2e^- \qquad (47)$$

Charge transfer such as

$$A^- + B \longrightarrow A + B^- \quad A,B: ANY\ SPECIE \qquad (48)$$

can alter the concentrations $H_2^+$, $H^+$, F, $F^-$, and other species. The effect of these charge transfer equations will be addressed after presenting the pumping, recombination, and depopulating processes.

The pumping reactions have been presented in reactions (21) and (22). Several additional sources of HF should be considered. The decomposition of $SF_6$ by H to produce HF by reaction (44) was studied by Fenimore [49] and lasing with the reaction

$$XF_6 + H \longrightarrow HF + XF_5 \qquad X = Mo, U \tag{49}$$

important to the production of HF was studied by Dolgave [75]. The rate constant for reaction (44) is about $10^{20}$ smaller than the rates for reactions (21) and (22) and the reaction may be completely neglected. (See Appendix A for rate constants)

The direct production of HF by

$$H + F + M \longrightarrow HF + M \tag{50}$$

is a moderately slow reaction, with a rate constant on the same order as for reaction (35) and may be important to the production of ground state HF. Reaction (50) will be analyzed in conjunction with the recombination of fluorine, reaction (35).

The importance of the hot reaction (22) depends on the quantity of diatomic fluorine available for reaction. Many $SF_6 + H_2$, electric discharge experiments indicate reaction (22) is not important [5,8,9,14,16,20]. In such cases, no vibrational transitions from levels higher than $v=3$ are observed and power is relatively low. Bashkin observed an increase in power by a factor of 20 when $F_2$ was added to the $SF_6 + H_2$ mixture under conditions very similar to this investigation [14]. It might be expected that the production of $F_2$ in this Raytheon laser is also small.

To establish the rate of production of $F_2$ , reaction (35) must be examined, for it is the sole source of $F_2$.

The rate of formation of products can be charcterized by the time interval required to reduce the concentration of reactants to a fixed percentage of the initial concentration, say .5 or .37. By comparing the magnitudes of these characteristic times to the gas flow rate, discharge pulse width, and other reactions, the importance of each reaction can be established. To make these comparisons, the gas flow rate and discharge duration must be examined.

The most important features of the HF laser in determining the flow rate are the discharge dimensions and the volume capacity of the gas recirculating fans. The gas flow velocity is about 250 ft/sec and the discharge structure's width is .166 inch (See experimental section). The time interval during which the products remain in the cavity is

$$T = L/U = 55\mu S \quad U = 250 FT/S \quad L = .166 IN. \quad (51)$$

The effects of thermally caused pressure waves as described in the experimental section increase this time by a factor of 2-5, or to about 200 μsec. Reactions with characteristic times greater than 200 μsec may be neglected.

Another important factor of the laser design is the time width of the electric discharge, because it will determine the time interval during which atomic fluorine is produced.

This pulse width is about 100 nsec. The cold reaction is fast and has acharacteristic time of about 100 nsec (See Appendix A). Thus, atomic fluorine is produced and consumed on a time scale of 100 nsec. After this time, little excited HF is produced. Since the HF output power pulse is the quantity of interest, only those reactions with characteristic times on the order of 100 nsec need be considered.

With this information, all the reactions of the $SF_6$ and $H_2$ system can be analyzed. An example calculation of characteristic times for the cold reaction and recombination of fluorine will be presented here. The characteristic times for the remainder of the reactions is presented in Appendix A.

The reaction

$$F + F + M \longrightarrow F_2 + M \tag{35}$$

implies the rate equation

$$\frac{d[F]}{dt} = -K_1[F]^2[M] \tag{52}$$

where $[F]$ and $[M]$ are the concentrations of fluorine and the arbitrary collision partner $M$ .

The characteristic time for the reaction will be taken as the time required for 63% of the reactants to be consumed. This percentage is used to facilitate the comparisons of characteristic times to the bimolecular reactions whose concentrations decay exponentially in time. An expression for this time is established by considering the concentration of M constant:

$$\int d[F]/[F]^2 = -K_1[M]\int dt \tag{53}$$

$$-2\left(\frac{1}{[F]} - \frac{1}{[F_0]}\right) = -K_1[M]t \tag{54}$$

$t = \tau_1$ for $[F] = .37[F_0]$. $[F_0]$ is the concentration of F at t=0. Thus,

$$\tau_1 = \frac{3.4}{K_1[M][F_0]} \tag{55}$$

Likewise, the characteristic time for the cold reaction

$$F + H_2 \longrightarrow HF + H \tag{21}$$

is obtained by considering the rate equation

$$\frac{d[F]}{dt} = -K_2[H_2][F] \tag{56}$$

$$\int \frac{d[F]}{[F]} = -K_2[H_2]\int dt \tag{57}$$

$$[F] = [F_0]\, e^{-K_2[H_2]t} \tag{58}$$

and

$$\tau = \frac{1}{K_2[H_2]} \tag{59}$$

To evaluate these characteristic times, the rate constants presented in the appendix are needed. For the cold reaction $K_2 = 10^{13}\ CM^3/MOLE\text{-}SEC$ and for the fluorine recombination $K_1 = 10^{16} CM^3/MOLE\text{-}SEC$. The initial concentration of $H_2$ is $(P = 18\ TORR)$

$$[H_2] = \frac{P}{KT} = 5.8\times 10^{23}\frac{1}{M^3} \cong 10^{6}\frac{MOLE}{CM^3} \tag{60}$$

Then $\tau_2 = 100NS$, as quoted before. The exact concentration of $F_0$ depends on the electron attachment reactions. An upper limit for $F_0$ would certainly be the initial concentration of $SF_6$, since only one flourine atom is produced from each $SF_6$ molecule. Then, the characteristic time for flourine

recombination is 17 μsec or greater for a 4:1 $SF_6$ : $H_2$ mixture. Since $\tau_1 \gg \tau_2$ , most of the atomic fluorine will be consumed by the cold reaction and the recombination of fluorine may be neglected. Note that fluorine atoms would recombine during the time they remain in the cavity ( 200μsec) if they did not react in reaction (21).

Similar arguments for the recombination process (50) indicates it too may be neglected. The characteristic time is 20 μsec.

A number of process can reduce the concentration of excited HF by depopulation or recombination. These reactions include:

$$H + H + M \longrightarrow H_2 + M \quad (61)$$

$$HF(v) + H \longrightarrow H_2 + F \quad (62)$$

$$HF(v) + M \longrightarrow H + F + M \quad (63)$$

$$HF(v) + M \longrightarrow HF(v-1) + M \quad (64)$$

$$HF(v) + HF(v') \longrightarrow HF(v-1) + HF(v'+1) \quad (65)$$

$$HF(v) + H_2(v') \longrightarrow HF(v+1) + H_2(v'-1) \quad (66)$$

The laser is designed to convect the reaction products away from the optical cavity before processes (61-66) affect the laser output power. The same characteristic time analysis for these reactions is completed in Appendix A. The only significant reactions leading to excited HF depopulation are:

$$HF(v) + F \longrightarrow HF(v-1) + F \quad (67)$$

$$HF(v) + H \longrightarrow HF(v') + H \quad (68)$$

The reaction rates for the charge transfer equations are very fast. The ion concentration is very low, however. This ion concentration is specified by the discharge current of 350 Amps:

$$I = dq/dt \qquad q = I\Delta t = (350)(100 \times 10^{-9}) \text{ COUL.} \tag{69-70}$$

The number of charges in the $8cm^3$ volume is then

$$n_{e^-} = q/e = 4.4 \times 10^{-11} \frac{MOLES}{CM^3} \tag{71}$$

The total production of positive ions is of the same order as the electron concentration. If the concentration of any ion is taken as $10^{-10}$ moles/$cm^3$, the characteristic time is

$$\tau = \frac{1}{K n_{e^-}} \approx 1 \text{ mS} \tag{72}$$

This time interval is four orders of magnitude greater than the discharge pulse width of 100 nsec. Thus, charge transfer depending on an ion concentration may be neglected. The reaction

$$F^- + M \longrightarrow F + M^- \tag{73}$$

may be significant, however. Here

$$\tau = \frac{1}{K[M]} = 20 \text{ nS} \tag{74}$$

which is a very short characteristic time. This is the only charge transfer equation that will be considered.

The system of kinetic equations, or mechanism, for the production of vibrationally excited HF that results from this complete presentation is:

Initiation

$$SF_6 + e^- \longrightarrow SF_6^- \qquad K_1$$

$$\longrightarrow SF_5^- + F \qquad K_2 \qquad (36)$$

$$\longrightarrow SF_5^+ + F + 2e^- \qquad K_3 \qquad (37)$$

$$\longrightarrow SF_5 + F + e^- \qquad K_4 \qquad (38)$$

$$\longrightarrow SF_5 + F^- \qquad K_5 \qquad (39)$$

$$H_2 + e^- \longrightarrow H + H + e^- \qquad K_6 \qquad (45)$$

$$\longrightarrow H_2^+ + 2e^- \qquad K_7 \qquad (46)$$

$$H + e^- \longrightarrow H^+ + 2e^- \qquad K_8 \qquad (47)$$

Charge Transfer

$$F^- + M \longrightarrow F + M^- \qquad K_9(M) \qquad (73)$$

$M$ = ALL NUETRAL SPECIES

Cold Reaction

$$F + H_2 \longrightarrow HF(v) + H \qquad K_{10}(v) \qquad (21)$$

Deactivation

$$HF(v) + F \longrightarrow HF(v-1) + F \qquad K_{11}(v) \qquad (67)$$

$$HF(v) + H \longrightarrow HF(v') + H \qquad K_{12}(v,v') \qquad (68)$$

The system of rate equations modeling the discharge is

$$\frac{d}{dt}[SF_6] = -(K_1+K_2+K_3+K_4+K_5)n_e[SF_6] \qquad (75)$$

$$\frac{d}{dt}[H_2] = -K_6 n_e[H_2] - \sum_v K_{10}(v)[F][H_2] \qquad (76)$$

$$\frac{d}{dt}[H] = 2K_6[H_2]n_e - K_8 n_e[H] + \sum_v K_{10}(v)[F][H_2] \qquad (77)$$

$$\frac{d}{dt}[F] = +(K_2+K_3+K_4)n_e[SF_6] + \sum_M K_9(M)[F^-][M] - \sum_v K_{10}(v)[F][H_2] \qquad (78)$$

$$\frac{d}{dt}[F^-] = +K_5 n_e[SF_6] - \sum_M K_9(M)[M][F^-] \qquad (79)$$

$$\frac{d}{dt}[HF](v) = +K_{10}(v)[F][H_2] - K_{11}(v)[HF(v)][F] \qquad (80)$$

$$+K_{11}(v+1)[HF(v+1)][F] - \sum_{v'<v} K_{12}(v,v')[HF(v)][H]$$

$$+\sum_{v'<v} K_{12}(v',v)[H][HF(v')]$$

with the initial values

$$[H]\Big|_0 = [F]\Big|_0 = [F^*]\Big|_0 = [HF]\Big|_0 = 0 \; ; \; [N_2]\Big|_0 = 4[H_2]\Big|_0 = 4\times 10^{19}\ \frac{\text{molecules}}{cm^3} \qquad (81)$$

The current forcing function is

$$\eta_e = \frac{1}{e}\int_{t_1}^{t_2} I(t)\,dt \qquad (82)$$

The current pulse is given in Appendix B and is taken from the observations of the Raytheon study [3:36].

The limits of integration on the current forcing term are taken as $t_2 - t_1 = 20\,NS$. The average electron energy at collision is, from equation (33), 2.2 eV, and the velocity corresponding to this energy is 8.8 x $10^5$ m/s. The electron's energy increases linearly after each collision; the average energy is 1 eV and the average velocity is 6.2 x $10^5$ m/s. The electrons take 16 nsec to traverse the cathode/anode gap. The system of rate equations is solved numerically in Appendix B with a step-by-step integration method. A 20 nsec time interval is used for this integration as well.

The rate constants $K_1 - K_{10}$ are listed in Appendix A.

Optical processes have not yet been considered. Spontaneous emission may be neglected, due to the long radiative lifetime of HF (.4Sec) (See p12). Stimulated emission is certainly of prime importance and does affect the population of excited HF levels. The stimulated processes are

$$\varphi + HF(v) \longrightarrow HF(v) + \varphi + \varphi \qquad K_{13} \qquad (83)$$

$$\varphi + HF(v-1) \longrightarrow HF(v) \qquad K_{-13} \qquad (84)$$

where $\varphi$ is the symbol for photons of energy $h\nu = hC/2.8\mu M$. The number density of photons is given by the implied rate equation

$$\frac{d\eta_\varphi}{dt} = K_{13}\eta_\varphi[HF(v)] - K_{-13}\eta_\varphi[HF(v-1)] \quad (85)$$

The reactions (83) and (84) would affect the rate equation (80), adding a term of

$$-K_{13}\eta_\varphi[HF(v)] + K_{-13}\eta_\varphi[HF(v-1)] \quad (86)$$

The rate constants for reactions (83) and (84) are calculated in Appendix A and are related to the Einstein coefficent of page 12 by

$$K_{13} = K_{-13} = Ch\nu B_{21} = 1.2\times10^{-4}\ \frac{CM^3}{SEC\text{-}PARTIC} \quad (87)$$

The characteristic time for the term (86) is then

$$\tau = \frac{1}{\eta_\varphi K_{13}} \quad (88)$$

where

$$\eta_\varphi = \frac{ENERGY\ PULSE/h\nu}{BEAM\ VOLUME} = \frac{E_p/h\nu}{\pi W^2 C t_p} = 6.5\times10^{11}\ \frac{1}{CM^3} \quad (89)$$

and then, $\tau = 12\ NSEC.$

Rather than include the reactions (83) and (84) in the system of equations on page 26, the model will be simplified by assuming thatstimulated emission is very fast compared to the pulse width $12\ NSEC \ll 100\ NSEC$. With this assumption, all the excited HF molecules in the upper laser level, $N_2$, created during the integration interval of 20 nsec will be stimulated to emit a photon.

Once a photon is created, it leaves the optical cavity very quickly, due to low mirror reflectivity. The photon

lifetime is given by

$$\tau_c = \frac{1}{c\left(\alpha_o + \frac{1}{2L} \ln \frac{1}{R}\right)} \qquad (90)$$
[50:79]

where $\alpha_o$ is the distributive loss coefficient, $L$ is the cavity length, and $R$ is the output mirror reflectivity. Assuming $\alpha_o = 0$ and evaluating equation (90) for the Raytheon laser ($L = .56M$, $R = 30\%$), $\tau_c = 3.1 NSEC$.

Therefore, most of the photons created in the 20 nsec integration interval will leave the cavity. The output power is then

$$P = [HF(2)]V \frac{h\nu}{\Delta t} \qquad \Delta t = 20\,NSEC \qquad (91)$$

where $[HF(2)]V$ is the total number of $v=2$ HF molecules created in the 20 nsec interval.

The solution to the system of differential equations on page 26 with these assumptions on the optical processes is detailed in Appendix B. Several of the equations can be decoupled from the rest of the system and solved directly. The remaining equations form two sets; one involving $H_2$, H, F, and $F^-$, and the second involving the vibrational levels of HF and the output power. These two sets are solved numerically by a step-by-step integration method. The resultant power pulse shape is plotted in figure 3.

The HF pump laser has been discussed in these first two sections. The final section of this chapter will analyze the optical pumping and $CO_2$ laser.

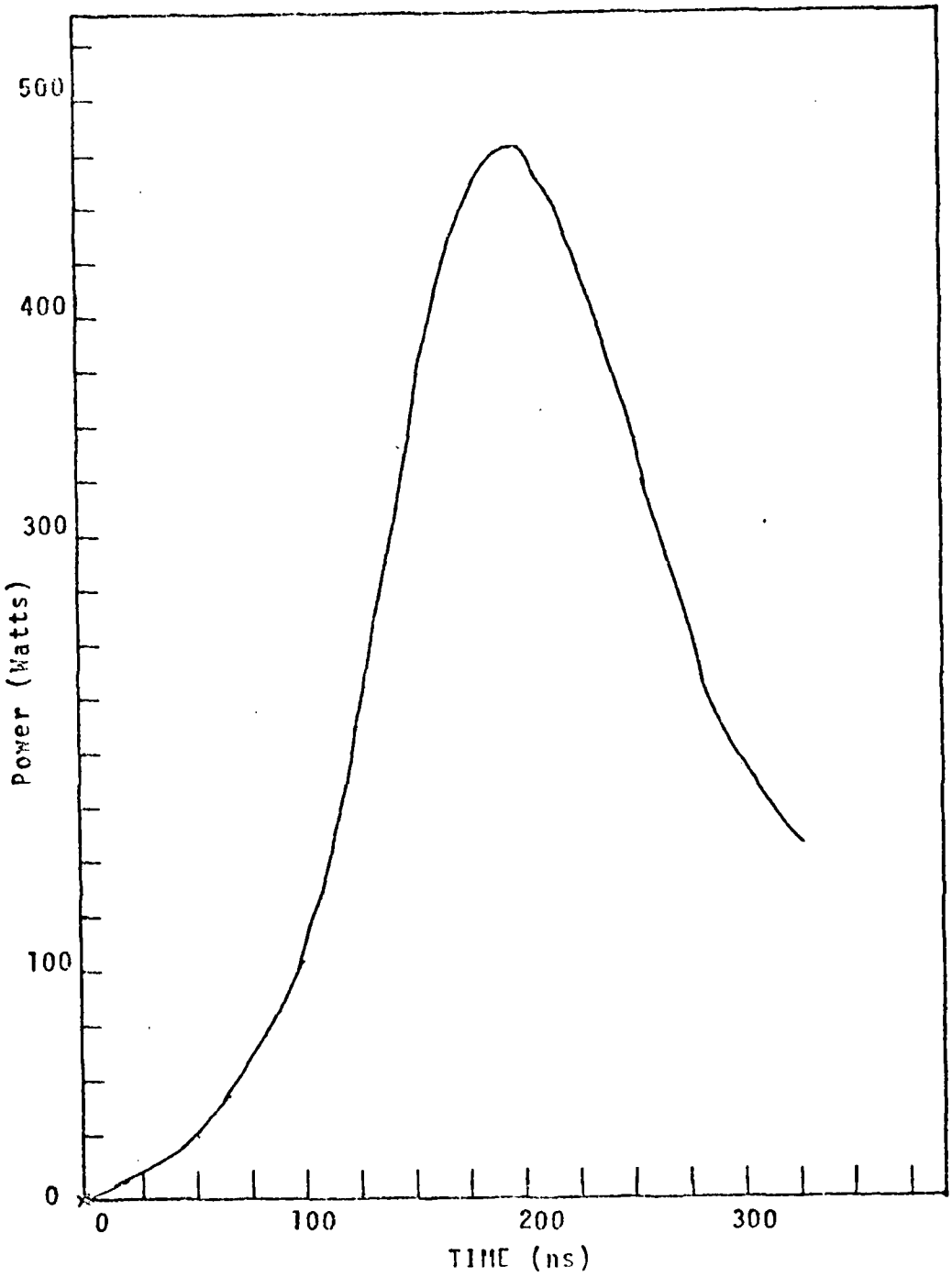


Figure 3.
Predicted HF Power Pulse Shape

## Optical Pumping and the $CO_2$ Laser

Various pumping techniques may be used to establish a population inversion within a lasing medium. Optical pumping, using a high energy IR laser to pump a second laser medium, can be advantageous. Most of the energy can be efficiently coupled into the lasing medium. No pumping of the lower laser level occurs, due to the narrow energy band of the pump. Optical pumping in this case is used to convert a laser beam to a longer wavelength.

Several types of optical pumping are possible [51,2]. Figure 4 illustrates five different optical pumping schemes.

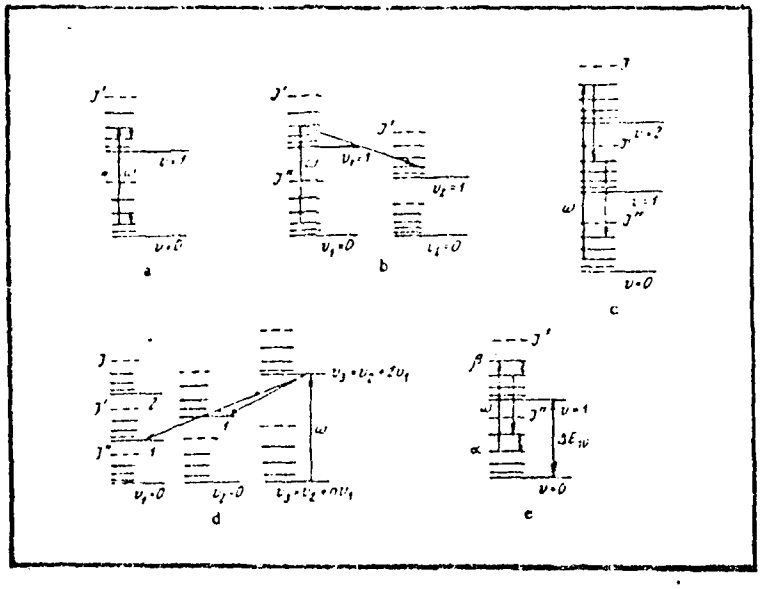

Figure 4.

Optical Pumping Schemes [51]

Diagrams a,c, and e illustrate pumping and lasing occuring on the same fundamental band. One example is to pump on an R transition and lase on a P transition. Diagram b shows pumping to a fundamental level and lasing within a difference

band to a lower level. Finally, diagram d illustrates pumping to a combined vibrational level of the molecule ( such as 101 in $CO_2$ ) and lasing on a hot band.

A number of lasers based on these processes have been demonstrated [2,52]. Investigations of HF pumped media [2,52] and optical pumping of $CO_2$ [53-56,25] have been performed. Raytheon searched for a laser source at 4.3 - 5 μm compatible with the HF/DF laser design and found no "priciple" laser source [3:56]. Isotopic species of $CO_2$ [2,23] and $N_2O$ [2,52] appeared to satisfy the requirements for optical pumping by the HF laser and were investigated [3:56-57]. No lasing was achieved with $N_2O$, but three isotopes of $CO_2$, including $^{12}C^{18}O_2$, did establish lasing. One other HF pumped $CO_2$ laser has been reported [23].

The isotope $^{12}C^{18}O_2$ was used in this experiment and the HF $P_2(6)$ transition was used to pump the $CO_2$ 101 vibrational level. An inversion is created between the 101 and 100 levels and is of the type of optical pumping shown in figure 4d. The 001 $CO_2$ level is nearly resonant with the lasing transition and some self absorption will occur. The lower laser level decays mainly to the 010 vibrational level.

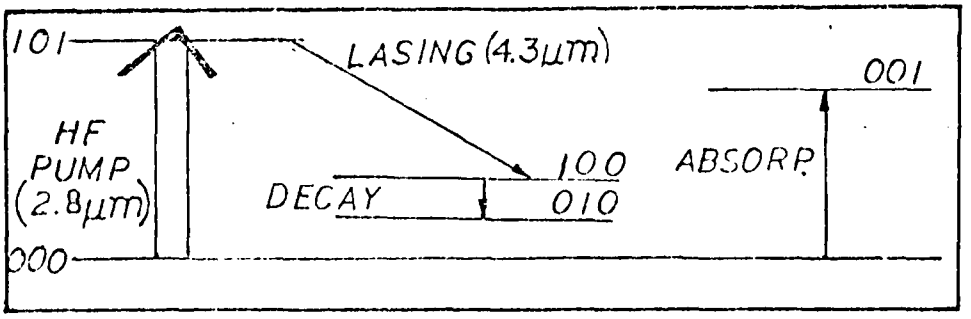


Figure 5
$CO_2$ Energy Level Diagram

A first order calculation of transition frequencies can be made from the fundamental vibrational modes:

$$\bar{\nu} = (v_1 + 1/2)\bar{\nu}_1 + (v_2 + 1/2)\bar{\nu}_2 + (v_3 + 1/2)\bar{\nu}_3 \qquad (92)$$

$\bar{\nu}_1 = 1330.0\ CM^{-1}$ SYMMETRIC

$\bar{\nu}_2 = 667.3\ CM^{-1}$ ANGLE BEND

$\bar{\nu}_3 = 2349.3\ CM^{-1}$ ANTI-SYMM

[57]

From equation (92) the transitions are:

$000 - 101$

$$\Delta\bar{\nu} = \bar{\nu}_{101} - \bar{\nu}_{000} = \bar{\nu}_1 + \bar{\nu}_3 = 3679.3\ CM^{-1} \qquad (93)$$

$101 - 100$

$$\Delta\bar{\nu} = \bar{\nu}_{101} - \bar{\nu}_{100} = \bar{\nu}_3 = 2349.3\ CM^{-1} \qquad (94)$$

$001 - 000$

$$\Delta\bar{\nu} = \bar{\nu}_{001} - \bar{\nu}_{000} = \bar{\nu}_3 = 2349.3\ CM^{-1} \qquad (95)$$

Due to the requirement for nearly resonant pumping, a much more exact spectroscopic study is required. Rotational levels must be considered and more precise, experimental measurements of the energy levels are needed.

A first calculation of rotational levels, shows a large seperation between adjacent $J$ levels:

$$E_J = \beta J(J+1)hc \qquad \Delta J = \pm 1 \qquad (96)$$

$$\Delta E = E_{J+1} - E_J = 2\beta(J+1)hc \qquad (97)$$

The seperation between lines is

$$\Delta E' \quad \Delta E = 2\beta \qquad \beta \approx .387\ CM^{-1} \quad [76] \qquad (98)$$

and, then

$$\Delta E' - \Delta E = .774\ CM^{-1} \qquad \Delta\nu = C(.774) = 23.2\ GHZ \qquad (99)$$

The exact rotational-vibration transitions are given in figure 6

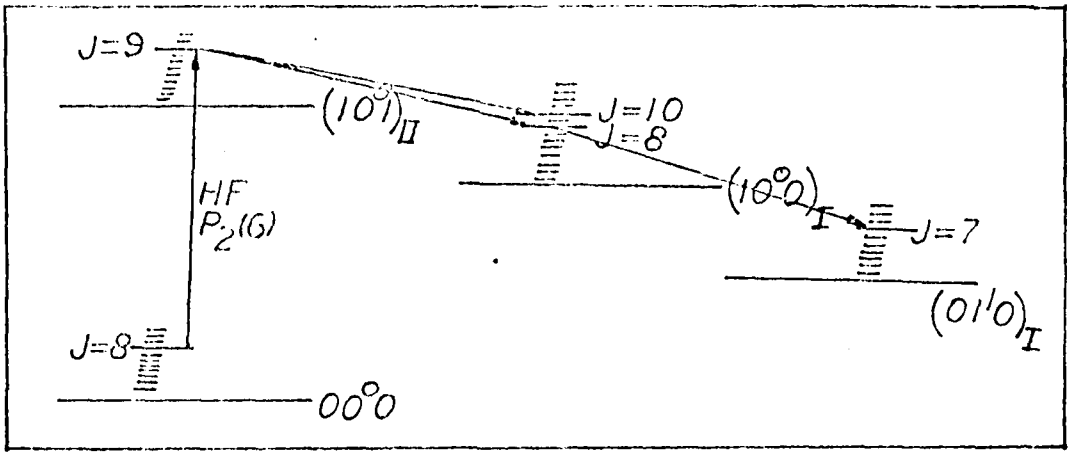


Figure 6.

$^{12}C^{18}O_2$ Energy Level Diagram[22]

It is important to note the degeneracy of the angle bend mode, denoted by the angular momentum quantum number superscript, and the nuclear spin, denoted by the subscipt, to obtain the very exact transition frequencies required.

Many studies of the 10.6 μm band of $CO_2$ are available as a result of high energy $CO_2$ laser research [58,59], but less data is available for the 2.8 - 4.3 μm region, particularly for certain isotopes of $CO_2$. The 2.8 μm band for $^{12}C^{16}O_2$, $^{13}C^{16}O_2$, and $^{12}C^{16}O^{18}O$ are known to an accuracy of .005 $cm^{-1}$ [60] and for $^{12}C^{18}O_2$ to .03 $cm^{-1}$ [61]. Such accuracy is inadequate to compare the seperation of the $P_2(6)$ HF line and the $(00^{\circ}0) - (10^{\circ}1)_{II}$ $CO_2$ transition. Buchwald gives a seperation between the HF $P_2(6)$ line and the $CO_2$ absorption transition of $\Delta\bar{\nu} = .007\ CM^{-1}$, based on direct laser pumping observations [23]. This yields $\Delta\nu = \Delta\bar{\nu}(C) = 210\ MHZ$.

Note that this seperation is much less than the 23 GHz between rotational levels of $CO_2$ and thus only one rotational level need be considered.

Finally, a study of line broadening is required. Collisional broadening is given by equation (9)

$$\Delta\nu_C = (.225\,MHZ)\,P\sum_B \left(\frac{P_B}{P}\right)\frac{\pi}{4}\left(D_A + D_B\right)^2\sqrt{\frac{1}{M_A}+\frac{1}{M_A}} \qquad (9)$$

For pure $^{12}C^{18}O_2$ at 7 torr total pressure and 300°K and using the C-O bond length of 1.2 angstroms to give a 2.4 angstrom diameter for $CO_2$ ,then

$$\Delta\nu_C = 5.82\,MHZ \qquad (100)$$

[38:F202]

Doppler broadening is given by equation (11)

$$\Delta\nu_D = \frac{2}{\lambda_o}\sqrt{\frac{2KT\ln 2}{M}} \qquad (11)$$

and at 300°K for $^{12}C^{18}O_2$ at 2.8 μm, and 4.3 μm,

$$\Delta\nu_{D_{2.8\mu m}} = 192\,MHZ \qquad \Delta\nu_{D_{4.3\mu m}} = 125\,MHZ \qquad (101)$$

The total linewidth, $\Delta\nu_T$ , based on the Voigt Profile as given by equation (12), is for $\frac{\Delta\nu_D}{\Delta\nu_C} = \frac{192MHZ}{5.82MHZ}$

$$\Delta\nu_{T_{2.8\mu m}} \cong 196\,MHZ \qquad \Delta\nu_{T_{4.3\mu m}} \cong 129\,MHZ \qquad (102)$$

The $CO_2$ transition for absorption and the HF $P_2(6)$ transition are shown in figure 7.

As the HF frequency is increased, more of the HF pulse is absorbed, a greater $CO_2$ population inversion is created and a greater output power should be obtained. In this rough way, $CO_2$ power should depend on HF frequency. Two calculations of this dependence follow. The first is based

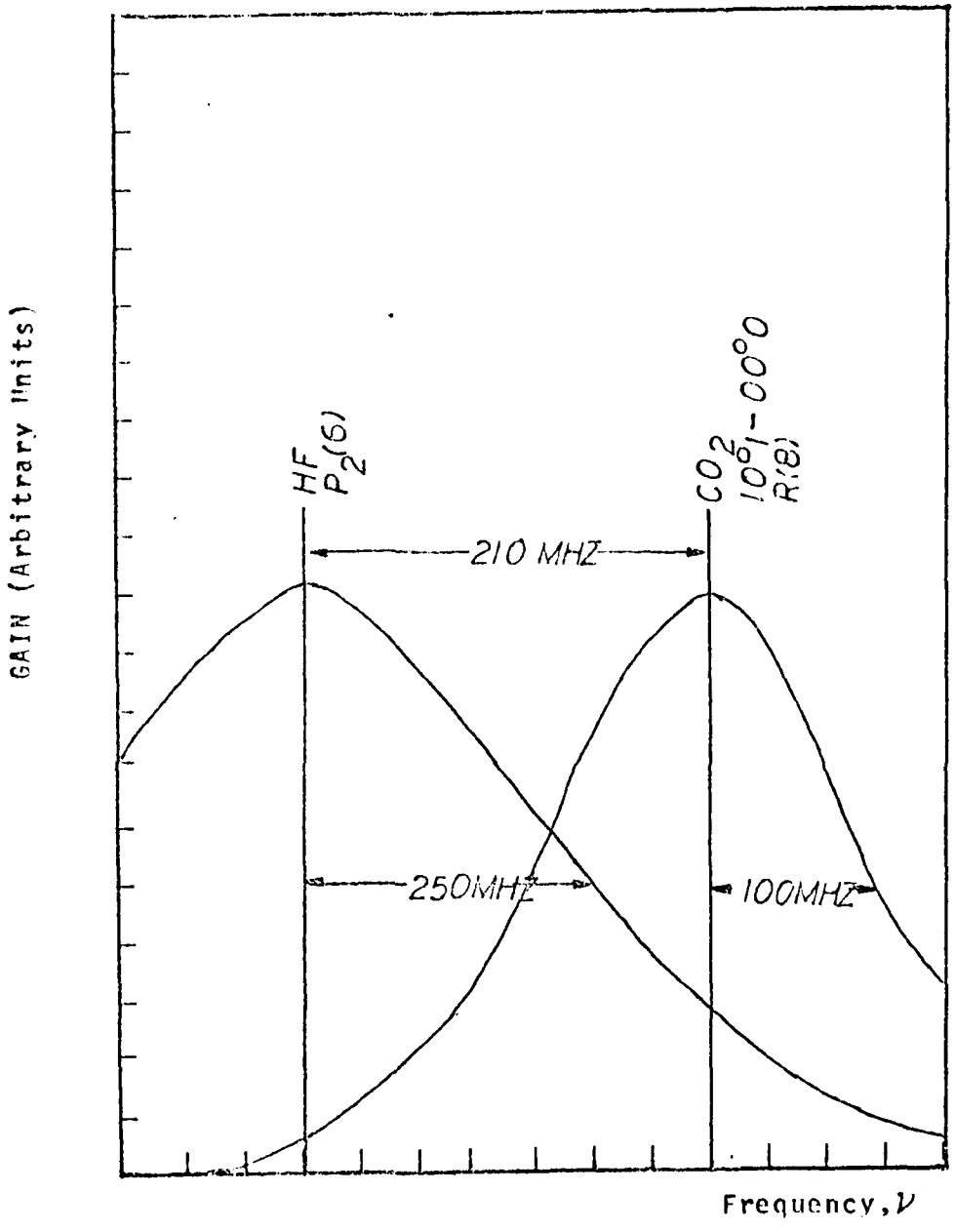


Figure 7.

HF and $CO_2$ Line Broadening

on figure 7. The second is based on a derivation of the $CO_2$ gain curve and its dependence on HF frequency.

First Calculation

The $CO_2$ absorption curve is Doppler broadened and the lineshape function is

$$G(\nu)=\frac{1}{\pi}\sqrt{\frac{\ln 2}{\pi}}EXP\left(-4\ln 2\frac{(\nu-\nu_o)^2}{(\Delta\nu_T)^2}\right) \quad (103)$$

$$\Delta\nu_T=200\,MHZ \quad [24:167]$$

where

$$\nu_o=c/\lambda \;;\quad \lambda=2.8\mu m \quad (104)$$

and let

$$\delta=\nu-\nu_o \;;\quad \delta\ IN\ 100MHZ \quad (105)$$

Then

$$G(\delta)=(7.8\times10^{-10}\,SEC)FXP-\left(\frac{\delta}{1.2}\right)^2=T_1EXP-\left(\frac{\delta}{1.2}\right)^2 \quad (106)$$

The absorption coefficient is related to this lineshape function by

$$\alpha(\delta)=\frac{h\nu B_{12}}{4\pi}\left(n_1-\frac{g_1}{g_2}n_2\right)G(\delta) \quad (107)$$

where $\nu\approx\nu_o$, $n_1$ and $n_2$ are the number densities of molecules in the lower and upper $CO_2$ laser levels, $B_{12}$ is the stimulated Einstein coefficient, and $\alpha$ is the absorption coefficient as in Beer's Law

$$I=I_o e^{-\alpha Z} \quad (108)$$

Since the number of photons incident is proportional to the incident intensity, $I$, then

$$N_\varphi=N_{\varphi_o}e^{-\alpha Z} \quad (109)$$

where $N_\varphi$ is the number of photons remaining in the HF pump

beam as a function of the propogation distance, $Z$, and $N_{\varphi_0}$ is the number of incident photons.

The number of photons absorbed, $N_{\varphi_0} - N_{\varphi}$, is identical to the number of $CO_2$ molecules pumped to the 101 energy level:

$$N_2 = N_{\varphi_0} - N_{\varphi} = N_{\varphi_0}(1 - e^{-\alpha Z}) \tag{110}$$

The incident photon number is estimated assuming a uniform number of photons in time: .

$$N_{\varphi_0} = \frac{PULSE\ ENERGY}{h\nu} = \frac{150\,mJ}{7.1\times10^{-20}J} = 2.2\times10^{15} \tag{111}$$

If a small total absorption is assumed, then there will exist a uniform population inversion within the length of the $CO_2$ gas cell ($L = 33CM$) and the population inversion $\eta_1 - \frac{g_1}{g_2}\eta_2 \approx \eta_1$ . A characteristic time can then be defined as

$$1/T' = \frac{h\nu}{4\pi} B_{12}\left(\eta_1 - \frac{g_1}{g_2}\eta_2\right)\Delta Z \tag{112}$$

$$= \frac{hc}{4\pi\lambda}\eta_1 L B_{12} \tag{113}$$

$$= \left(\frac{hc}{4\pi\lambda}\right)\left(\frac{PL}{KT}\right)B_{12} \tag{114}$$

where

$$\left(\frac{hc}{4\pi\lambda}\right) = 5.56\times10^{-21}\,JOULES \tag{115}$$

$$\left(\frac{PL}{KT}\right) = (1.05\times10^{22})P_{TORR}\ \frac{1}{M^2} \tag{116}$$

and from [62]; $A_{21} = .63S^{-1}$ and from eq (20), $B_{12} = 3.5\times10^{7}\frac{M^2}{J-S}$ .

The characteristic time is then

$$T' = 7.0\times10^{-11}\,SEC\ \ AT\ 7\ TORR \tag{117}$$

From equation (107) and (110), the 101 level population is

$$N_2 = N_{\varphi_0}\left[1 - EXP\left(\frac{-T}{\tau}EXP-\left(\frac{\delta}{1.2}\right)^2\right)\right] \quad (118)$$

Assuming no losses, the pulse energy is

$$E = h\nu N_{\varphi_0}\left[1 - EXP\left(\frac{-T}{\tau}EXP-\left(\frac{\delta}{1.2}\right)^2\right)\right] \quad (119)$$

or

$$E = 102\mu J\left[1 - EXP\left(-1.59P_{TORR}EXP-\left(\frac{\delta}{1.2}\right)^2\right)\right] \quad (120)$$

The absorption, from equation (109) is

$$N_\varphi = N_{\varphi_0}\left[EXP\left(-1.59P_{TORR}EXP-\left(\frac{\delta}{1.2}\right)^2\right)\right] \quad (121)$$

or

$$\frac{L}{L}\ln\frac{N_{\varphi_0}}{N_\varphi} = .0023CM^{-1}P_{TORR} \quad (122)$$

HF power was assumed not to vary with HF frequency in this derivation. The HF transition has a large collisional, or homogeneous, broadening. For a cw, homogeneously broadened laser, the gain is "pegged" at the threshold level. Under such conditions, $\gamma = \gamma_{TH}$ , and the power is held relatively constant with changes in frequency. The time interval before the gain returns to threshold level is basically the time required to reach a steady state solution of the laser rate equations. This is a relatively fast process and is basically determined by the photon lifetime. From equation (90) the photon lifetime is 3.1 nsec. Since the pulse time of 100 nsec is much longer than this lifetime, it may be assumed that HF power does not vary significantly with HF frequency.

A plot of $CO_2$ absorption versus $CO_2$ pressure (eq 122) is given in figure 8 and $CO_2$ power versus HF frequency in figure 9.

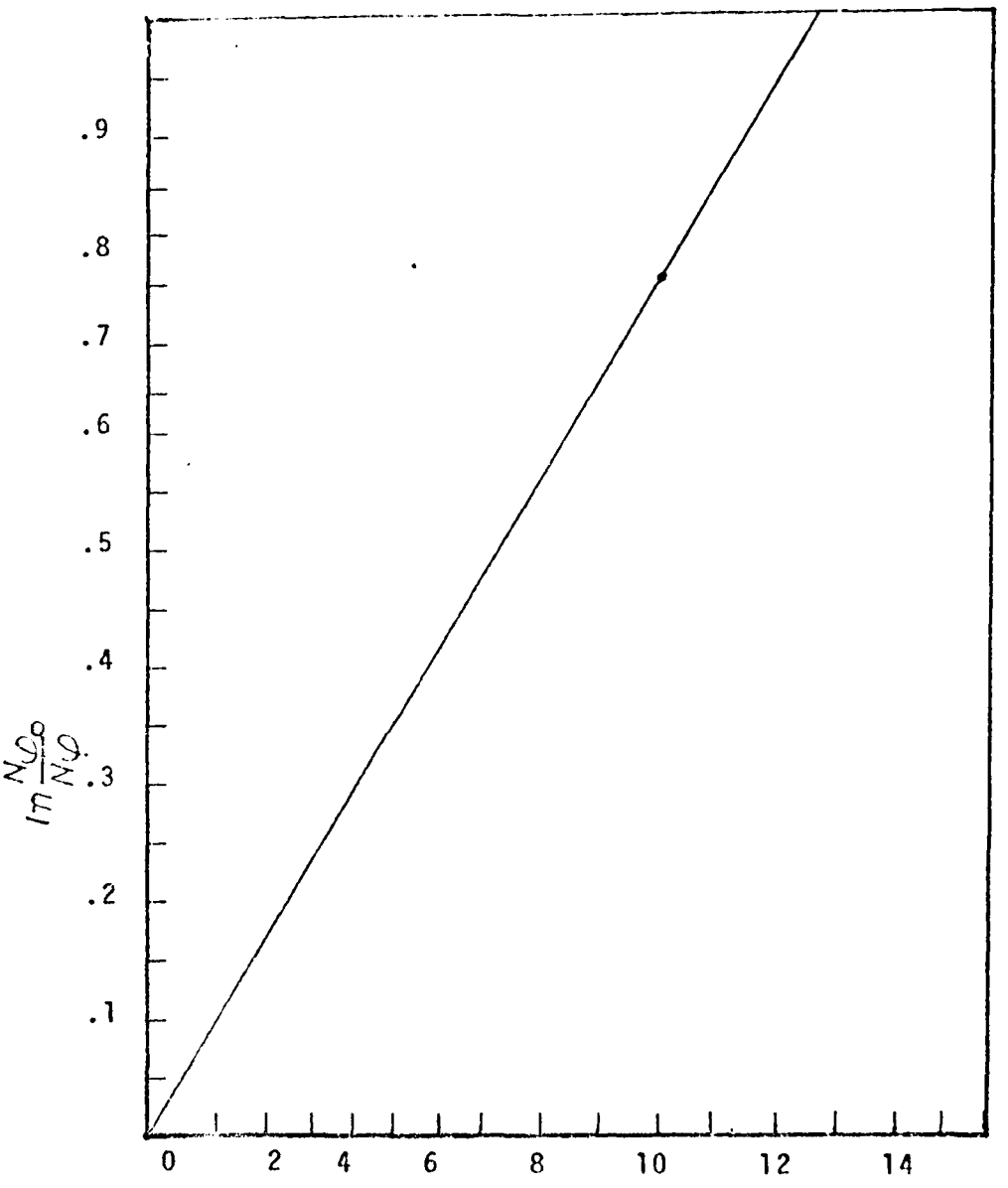


Figure 8.

$CO_2$ Absorption versus $CO_2$ Pressure

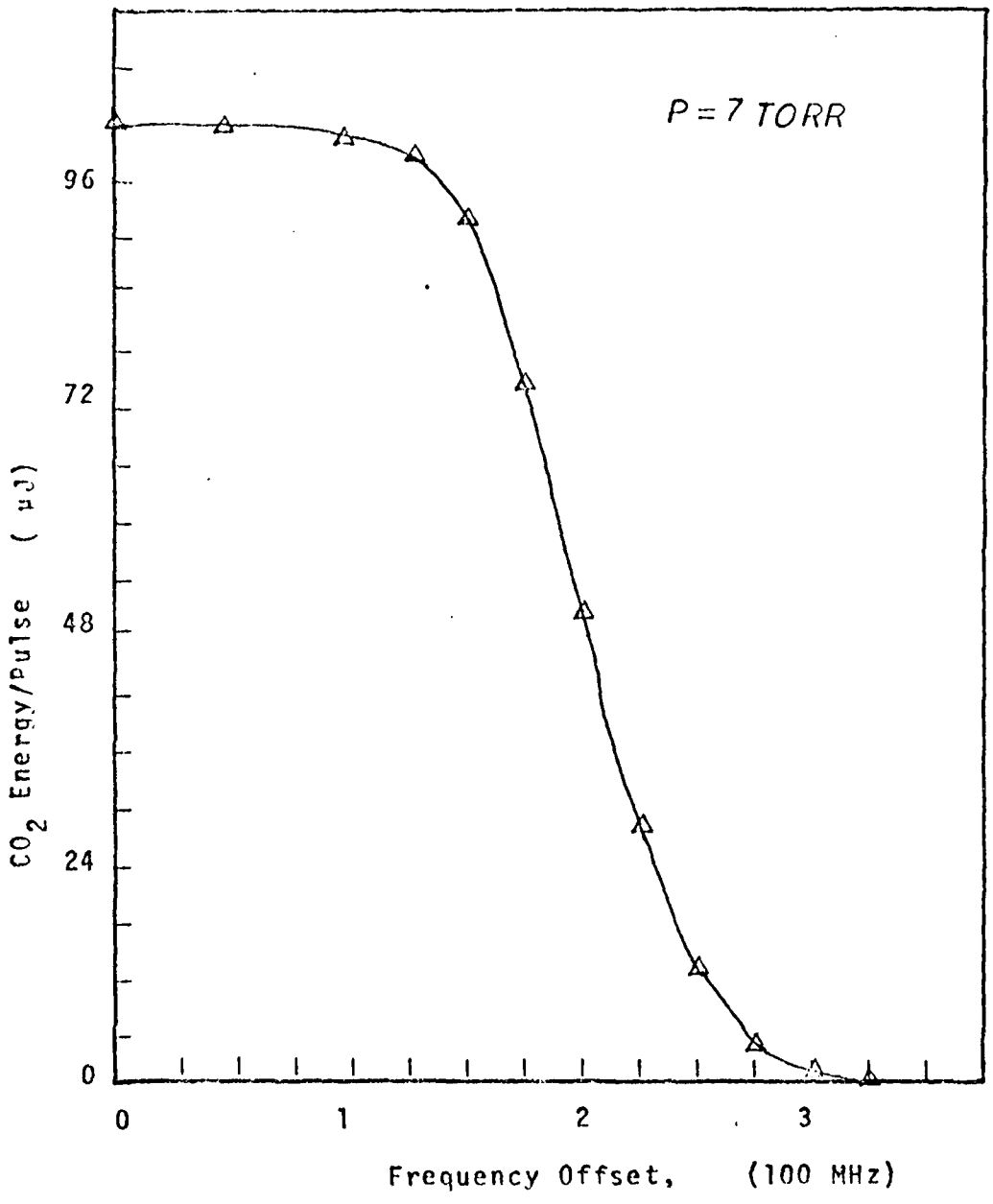


Figure 9.

$CO_2$ Power versus HF Frequency

Several general remarks concerning these theoretical results can be made. First, $CO_2$ power is very sensitive to the offset frequency, $\delta$ = HF frequency - $CO_2$ line-center, and is a maximum for zero offset. Pumping directly on the $CO_2$ linecenter is most efficient and efficiency drops off rapidly with offset frequency, as expected.

Secondly, power increases with increasing $CO_2$ pressure. This is reasonable, for the number of absorbers is increasing and thus output power increases. Note that the increase in power is not a result of increased linebroadening, because the transition is Doppler broadened. This second effect would be important above 70 torr, or so. In such cases the model would require revision to include collisional broadening.

The theory does not predict a maximum operating pressure, but rather power increases continuously with pressure. This is clearly not physical. The model assumed small total absorption, but as pressure increases so does total absorption. The small absorption assumption fails at high pressures. Even at 1 torr, 80% of the HF beam is absorbed.

Finally power increases with increasing $T_1$ , or increased Doppler broadening, as expected. $T'$ is basically a constant of the transition in question. The actual output power is rather sensitive to inaccuracy in this number, however.

This calculation of $CO_2$ power as a function of HF frequency has neglected the effects of coherent pumping. Two photon processes can affect the gain spectrum [63,64] and saturation [65-67] of laser excited lasers. In the

Raytheon study, the $CO_2$ gain curve was derived including these effects and evaluated for different HF frequencies [3:63-66].

Second Calculation

This derivation is based on the work of Feld and Javan, who studied the line shape of a Doppler broadened transition in the presence of a laser field resonating with a second doppler broadened transition sharing a common energy level [64]. The derivation is valid for two Doppler broadened transitions if one of the fields fully saturates its transition and the second field is weak. The intense field must be detuned from linecenter and the difference between transition frequencies greater than the natural linewidth of the medium.

The three level system is as shown in figure 4d, and in terms of the $CO_2$ energy levels is as shown in figure 10.

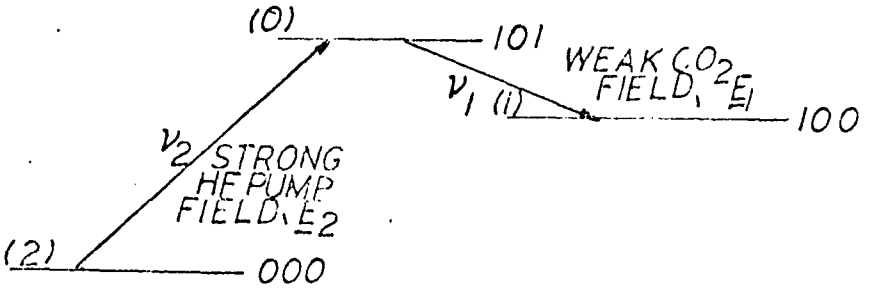


Figure 10.

Three Level $CO_2$ Model

The three level system consists of the strong HF pump field resonant with the 000 - 101 $CO_2$ transition and the lasing transition (weak field) is the 101 - 100 transition, with the shared level being the 101 level.

A single, inhomogeneously broadened gain curve will

demonstrate hole burning in the presence of a laser field. That is, molecules with a velocity such that their doppler shifted observed frequency matches the laser frequency, will be selectively depopulated from the upper laser level. A second transition sharing one of these selectively depopulated energy levels has its own doppler curve altered. The gain of the first transition is

$$\gamma_1 = \sigma_1 \Delta_1 = \sigma_1 (N_0 - N_1) \tag{123}$$

and of the second transition is

$$\gamma = \sigma_2 \Delta_2 = \sigma_2 (N_0 - N_1) \tag{124}$$

where $\gamma$ is the gain coefficient, $\sigma$ the absorption crossection and $N_i$ the total population of the $i^{th}$ energy level. Thus, holeburing in one gain curve affects $N_0$ which in turn affects the second transition's gain.

The gain curve for a single, hole-burned doppler transition is symmetric, but this need not be the case for the coupled transition. This assymetry will produce a directional dependance on gain. A beam of radiation from the second transition will be more intense when it propogates with the pump beam than when propogating in the opposite direction. This issue will be discussed again in conjunction with the amplified spontaneous emission nature of the $CO_2$ cavity.

There are actually two distinct processes that affect the shape of the gain curve of the weak field. First, there is the single quantum affect already discussed in which one field affects the rate of stimulated emission in the second field. The second process involves the exchange of a photon

with each of the fields and is a two photon process. Both of these processes can be analyzed by establishing the transition rates with a semi-classical, perturbational approach.

This derivation involves ten major steps:

(1) Express the electric fields classically with the appropriate frequencies, $\nu_2$ for HF and $\nu_1$ for the 4.3 μm $CO_2$ transition.

(2) Transform to a coordinate frame at rest with respect to the particles of velocity $U$ . Frequencies must be transformed according to the doppler effect, $\nu = \nu_0(1 + U/C)$

(3) Express the Hamiltonian as the sum of the strong field and weak perturbing field potentials,
$H = H_0 - \mu_2 E_2 + V$
where $V = -\mu_1 E_1$ is the perturbing potential of the weak field $E_1$ , $E_2$ is the strong field, and $\mu$ is the dipole moment.

(4) Expand the wavefunction, $\Psi(\Omega,t)$, in terms of the stationary states, $\Psi(\Omega,t) = \sum_n C_n(t)\,\psi_n(\Omega)$

(5) Apply the time-dependent Schrodinger Wave Equation to $\Psi(\Omega,t)$, $H\Psi = i\hbar \frac{\partial \Psi}{\partial t}$

(6) Integrate over all space and transform to the Heisenberg interaction picture $(C_n \to d_n)$

(7) Establish the equations of motion in terms of the time derivatives of the wavefunction expansion coefficients $(d_n)$ and add term appropriate for spontaneous decay, $1/T_i$ .

$$\dot{d}_i = \sum_j b_{ij} d_j \; ; \; b_{ij} = a_{ij} EXP\left[\left(\frac{1}{\hbar}\right)\left(\frac{1}{T_i} - \frac{1}{T_j}\right)\right]$$

$$a_{ij} = -\frac{i}{\hbar}\langle i | -er | j \rangle EXP\left[\left(\frac{E_i - E_j}{\hbar}\right) t\right](E_1 + E_2)$$

(8) Solve the system of equations with a perturbational method

(9) Calculate the transition rates, given by $|d_i|^2$
Total power is $P = n_2 J_{21} + n_0 J_{01} - n_1(J_{10} + J_{12})$ where $n_i$ is the population of level $i$ and $J_{ij}$ is the transition rate.

(10) Take an ensemble average of velocities, directly related to the frequency by the doppler effect,

Then, gain is

$$G(\nu_1) = \frac{1}{\pi}\frac{\nu_{01}}{C}\eta_2\frac{\mu_1^2}{H}\frac{\mu_2^2E^2}{4h^2}\,IM\left\{\int_{-\infty}^{\infty}\left[\frac{1}{\sqrt{2KT/M}}\,EXP-\left(\frac{U^2}{2KT/M}\right)\right]\times\right.$$

$$\left[\frac{\frac{\nu_2}{2}\left(1-\frac{U}{C}\right)-\nu_{02}+\frac{1}{2\pi T_{20}}+2\frac{T_0}{T_{20}}\left(\frac{\nu_2}{2}\left(1-\frac{U}{C}\right)-\nu_{02}-\nu_1\left(1-\epsilon\frac{U}{C}\right)+\nu_{01}-\frac{1}{2\pi T_{21}}\right)}{\left(\frac{\nu_2}{2}\left(1-\frac{U}{C}\right)-\nu_{02}\right)^2+\frac{1}{4\pi^2T_{20}}+\frac{\mu_2^2E^2}{4\pi^2h^2}\frac{T_0T_2}{T_{20}^2}}\right]\times$$

$$\left.\left[\frac{dU}{\left(\frac{\mu_2^2E^2}{16\pi^2h^2}\right)-\left(\nu_1\left(1-\epsilon\frac{U}{C}\right)-\nu_{01}-\frac{1}{2\pi T_{10}}\right)\left(\frac{\nu_2}{2}\left(1-\frac{U}{C}\right)-\nu_{02}-\nu_1\left(1-\epsilon\frac{U}{C}\right)+\nu_{01}-\frac{1}{2\pi T_{21}}\right)}\right]\right\}$$

(125)

Where,

$M = 48$ AMU; MOLECULAR WEIGHT OF $CO_2$
$K$ = BOLTMAN CONSTANT; $h$ = PLANCK CONSTANT
$T$ = ABSOLUTE TEMP.; $C = 3\times10^8$ M/S
$\eta_2$ = $CO_2$ GROUND STATE NUMBER DENSITY

$\nu_{01}$ = $CO_2$ 101 − 100 LINECENTER FREQ.
$\nu_{02}$ = $CO_2$ 000–101 LINECENTER FREQ.

$T_0$ = SPONT. DECAY TIME FROM 101
$T_1$ = " " " " 100
$T_2$ = " " " " 000
$T_{10}$ = POLARIZATION DECAY 100–100
$T_{20}$ = " " " 101–000
$T_{21}$ = RAMAN COHERENCE DECAY 000–100
$\epsilon = \pm 1$ (CO-/COUNTER- PROPOGATION)

This expression for gain was evaluated numerically in reference [3] under various conditions. Of particular interest are the results for HF power = 100 kW/cm$^2$ ( .7 mJ per pulse coupled into a 3mm diameter tube), $CO_2$ pressure = 10 torr, and three different HF pump frequencies [3:66]. The results for these conditions are given in figure 11.

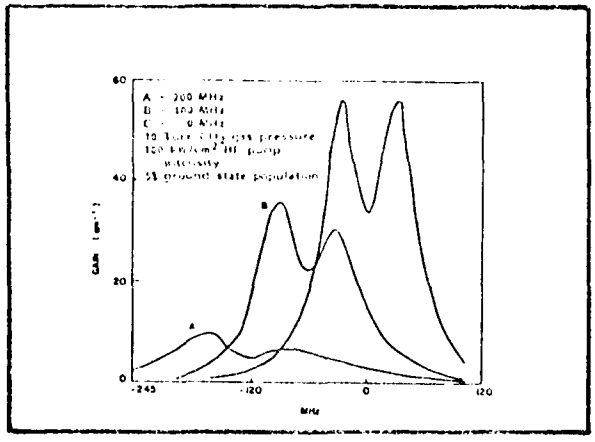


Figure 11.
$CO_2$ Gain for 3 HF Pump Frequencies [3:65]

From these curves, $CO_2$ output power as function of frequency can be established. First, the nature of the $CO_2$ cavity will be addressed.

The $CO_2$ laser is simply a pyrex cell with $CaF_2$ windows; no mirrors are used and sufficient gain is established in a single pass to produce lasing. That is, the $CO_2$ laser operates in an amplified spontaneous emission mode (ASE). Typical ASE operation does not exhibit a preference for forward or backward propogating beams. The HF pumped $CO_2$ laser has a forward to backward power ratio of 12, however [3:73].

This ratio is partially explained by the previous arguments concerning the coupling of the two doppler curves. The

optical pumping also establishes a population gradient within the cell due to the variable intensity of the HF beam as it propogates through the $CO_2$ gas. The HF beam also requires a finite time to pass through the cell and the population inversion at one end is established before it is at the other end. A detailed rate equation investigation would be required to explain the details and size of the forward to backward power ratio.

Such a directional nature to gain is often associated with superradiance [68-70]. It is probable that this system is not superradiant and simply operates in an ASE mode. The Raytheon report states the $CO_2$ laser operates in ASE mode without explanation [3:70]. Superradiant operation usually entails very short time scales, on the order of picoseconds. In a superradiant mode, the molecules in a volume whose dimensions are much less than the size of a wavelength are coupled and power is proportional to the number of excited states squared, rather than linearly proportional to population inversion , as in ASE. Since the same energy is available, but the pulse is much greater in magnitude, the pulse must be narrow in time [71]. The $CO_2$ pulses do not exhibit this nature, but rather, they follow the HF pump pulse rather closely [3:74]. No conclusive statement concerning superradiance can be made from the data obtained in this experimental study, but the process is probably not important.

Since the $CO_2$ laser operates without a "cavity", the determination of axial modes from the usual criterion of waves constructively interferring does not apply. Rather,

there exists a "natural" cavity length, $L$ , determined by the gain curve. The system will tend to operate at the maximum in the gain curve for ASE operation.

Now, returning to the gain curves, the $CO_2$ power as a function of HF frequency can be obtained from the maximum gain of each curve in figure 11, as shown in Table I.

Table I.

$CO_2$ Gain versus HF Frequency

| $\delta$ (100MHZ) | $\gamma$ ($CM^{-1}$) | $\gamma/\gamma(\delta=0)$ |
|---|---|---|
| 0 | 55 | 1.0 |
| 1 | 35 | .64 |
| 2 | 10 | .18 |

Power is proportional to gain. If $\gamma=\gamma^{\circ}$ and $P=P^{\circ}$ for $\delta=0$ , then $\frac{\gamma}{\gamma^{\circ}}$ or $\frac{P}{P^{\circ}}$ can be plotted as a function of HF frequency, as is shown in figure 12. A value for $P^{\circ}$ will be calculated after considering gain saturation.

In the Raytheon investigation, no variation of $CO_2$ power with changes in HF frequency were observed. Saturation was suggested as a possible explanation [3:75]. Saturation in two senses can be considered. First, a total inversion is possible for very high pump energies. If one-half of the $CO_2$ molecules are raised from the 000 state to the 101 state, then absorption goes to zero. More intense HF beams

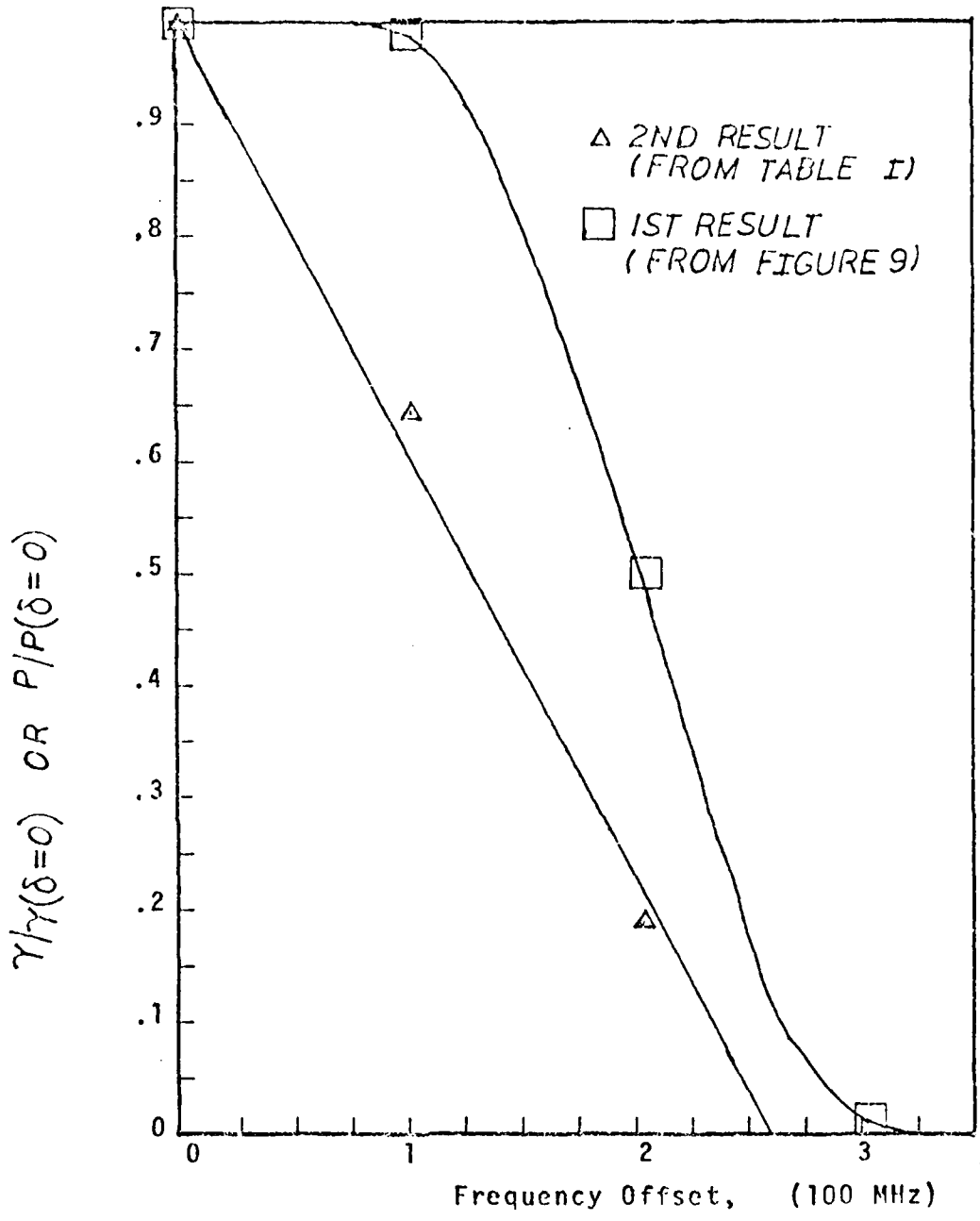


Figure 12.

$CO_2$ Gain versus HF Frequency

will simply be transmitted by the $CO_2$ gas. Secondly, the laser field created by the population inversion decreases the inversion and thus, decreases gain and power. That is, gain depends on the field intensity.

Under no circumstance is the $CO_2$ system completely inverted. Assuming a Boltzmann distribution of molecules among the rotational states of the ground vibrational level, only 5 % of the total number of $CO_2$ molecules populate the J = 8 level and are accessible for transition to the 101 vibrational level. Buchwald found the characteristic time for equilibration of the ground state rotational levels to be 90 ns-atm, or .8 ns at 7 torr [23]. This equilibration time is much shorter than the pump pulse duration of 100 ns. Many of the ground state $CO_2$ molecules will fill the J = 8 level as the HF pump pulse depletes them. Five percent of the total $CO_2$ number is a very conservative value for considering total inversion and will be used.

The number of $CO_2$ molecules available for transition are

$$.05N = .05\left(\frac{PV}{KT}\right) = 4 \times 10^{17} \qquad (126)$$

for $V = 37 CM^3$, $T = 300^{\circ}K$, $P = 7 TORR$. The incident number of HF photons is from equation (111) $22 \cdot 10^{15}$ Even if every photon is absorbed and only 5 % of the $CO_2$ molecules are available for pumping, $\frac{N_0}{.05N} = 55 \times 10^{-3}$. and a total inversion is impossible. Raytheon used a smaller cell ( 2.3 $cm^3$ ) and a higher pump energy (.8 mJ). For these conditions, $N_0/.05N = .45$ and $N_2 \sim N_1$. A total inversion

is possible if all the photons are absorbed and no equilibration of rotational levels occur. This is not the case and the system would only approach the criteria for a total inversion.

Saturation from the laser field intensity reduces the gain of the system according to

$$\gamma = \frac{\gamma_0}{1 + \frac{I_\nu}{I_S}} \tag{127}$$

[24:168]

where

$$\gamma_0 = \frac{\lambda^2 G(\nu)}{8\pi} A_{21} \Delta$$

$$I_\nu = \frac{c E^2}{2} \tag{128}$$

$$I_S = \frac{4\pi h \nu A_{21}}{G(\nu) R T_{INVERSION}} \tag{129}$$

(130)

This gain saturation relationship is strictly valid for a steady state operation. The cavity photon lifetime is very short for the $CO_2$ laser since there are no mirrors on the cavity. The arguments of page 39 can again be used to justify the use of equation (127).

To evaluate $I_S$ from equation (129), the lineshape from equation (106) and an Einstein coefficient of $A_{21} = 200 \frac{1}{S}$ [3:60] is used. Approximating the inversion lifetime, $T$, as the pulse width (100 ns),

$$I_S = 5.6 \times 10^3 \frac{J}{CM^2 S} \tag{131}$$

The HF pump intensity is

$$I_\nu = 1.3 \times 10^3 \frac{J}{CM^2 S} \tag{132}$$

A beam spot size of $\omega = .6 CM$ is used in this calculation. The $CO_2$ field intensity is some fraction of the HF intensity

$$I_{CO_2} = \beta I_{HF} \tag{118}$$

$\beta \ll 1$ and $\sim .1$ . Under these conditions the transition is not saturated.

For the Raytheon studies, $E_p = 0.8\,mJ$ and $A = \pi 1.015^2\,cm^2$ giving $I_{HF} = 1.1 \times 10^7 \frac{1}{cm^2 s}$ , and the 101 -100 transition is certainly saturated.

Now that saturation has been examined, a value of $p^o$ for page 49 and figure 12 can be calculated. From equations (131) and (132) , the relation between small signal and saturated gain is

$$\gamma = 5.6 \times 10^{-3} \gamma_o \tag{133}$$

Gain is related to inversion by

$$\gamma = \sigma \Delta \qquad \text{SEE EQ 128} \tag{134}$$

and inversion to energy per pulse, assuming no losses, by

$$E_p = h\nu \Delta V \tag{135}$$

where $\Delta$ is the population inversion per volume and $\sigma$ is the optical crossection related to transition rate by

$$\sigma = \frac{A_{21}}{8\pi} G(\nu) \tag{136}$$

Again using $G(\nu) = 7.6 \times 10^{-11} s$ and $A_{21} = 200 \frac{1}{s}$ , then

$$\Delta = 20 \times 10^{14} \; cm^{-3} \tag{137}$$

and energy is

$$E_p = 30\,\mu J \qquad p \approx 300\,W \tag{138}$$

The theory of the HF pump laser, a kinetic model for the $SF_6 + H_2$ in an electric discharge, and the theory of optical pumping and the $CO_2$ laser has been presented. To compare these predictions with the performance of the actual system, an experiment has been designed and is described in the next section.

## Experiment

This experiment was designed to characterize the performance of the HF pumped $CO_2$ laser and study the dependance of $CO_2$ power on HF frequency. First, the HF laser developed by the Raytheon Corporation [3] and the modifications made to this laser will be described. Next, the experiments to characterize the HF laser's performance are outlined. The HF pumped $CO_2$ system is then analyzed, including the coupling of the HF beam into the $CO_2$ cell. Finally, the expandmental set-up and procedure for the frequency investigation is presented.

### HF Laser Description

The molecular laser used to pump the $CO_2$ laser is an $SF_6$ + $H_2/D_2$, electric discharge, high repetition rate HF/DF laser. Only hydrogen will be used in this experiment. The laser's specifications, as presented in reference [3] are listed in figure 13.

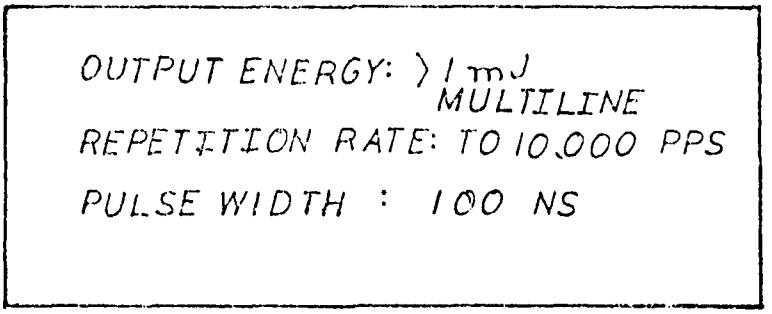


Figure 13.

HF Laser Specifications

A picture of the laser, without the high-voltage electrical conections or exhaust pump, is shown in figure 14 [3:29].

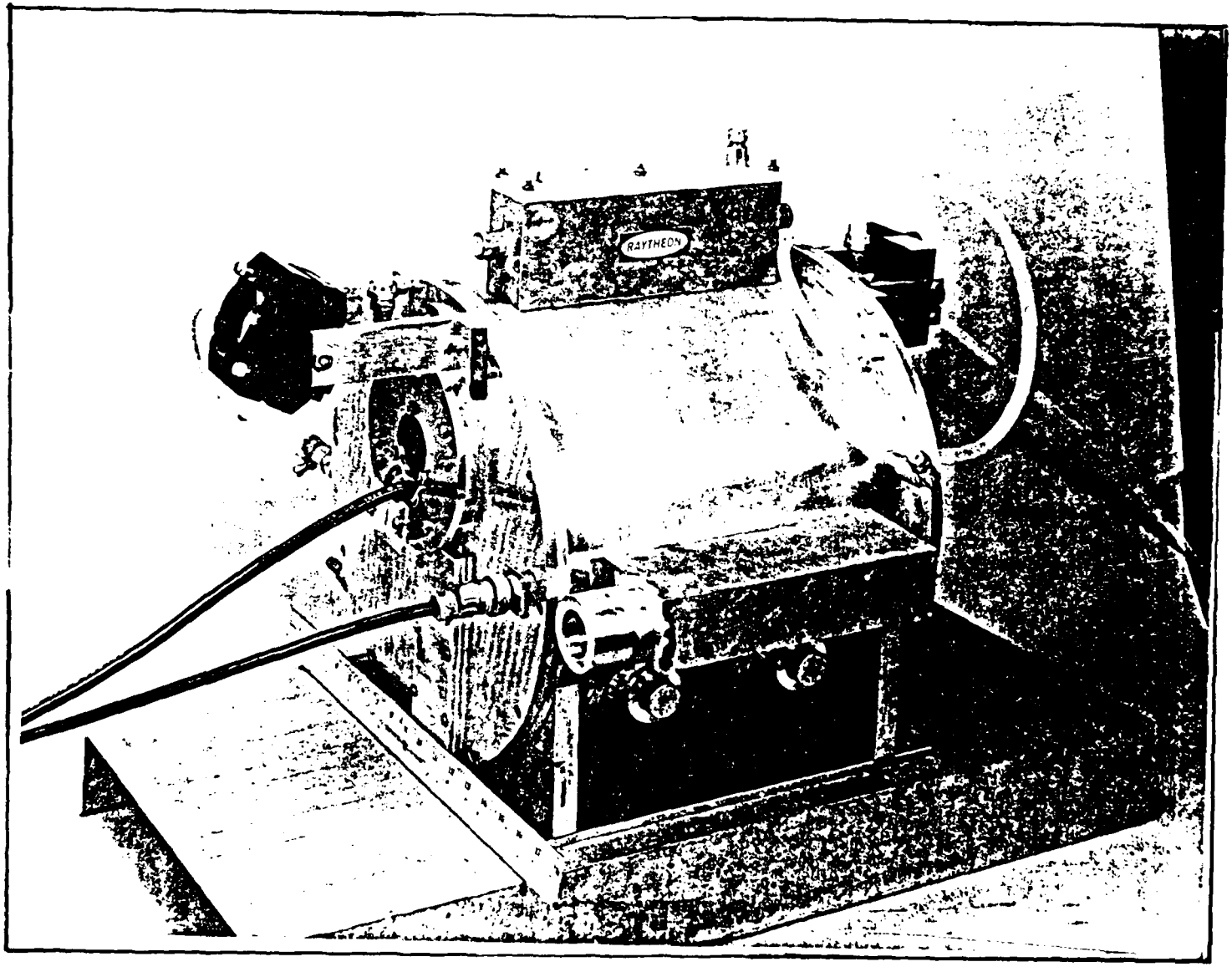


Figure 14.

$SF_6 + H_2$ Electric Discharge Laser

The cathode (8" x 1 3/4" x 3 1/2") is situated above the cylindrical body (13 1/4" x 14 1/2"dia) directly above the optical cavity (gas volume: 17 1/2" x 1 1/8" dia.). The grating (left) and output coupler (right) extend the cavity to .5 meters. The remainder of the cylinder houses the gas recirculating and cooling systems, and the thyratron.

Details of the laser and its four subsytems will be discussed in the following sections.

Optical Cavity

The reacting gases are sealed within the cylindrical laser housing. The optical path is formed by two CaF windows (1 3/8" dia.) at Brewster's angle, 55°, seperated by 17 1/2". The cavity is establishedby a copper and a germanium mirror, as shown in figure 15.

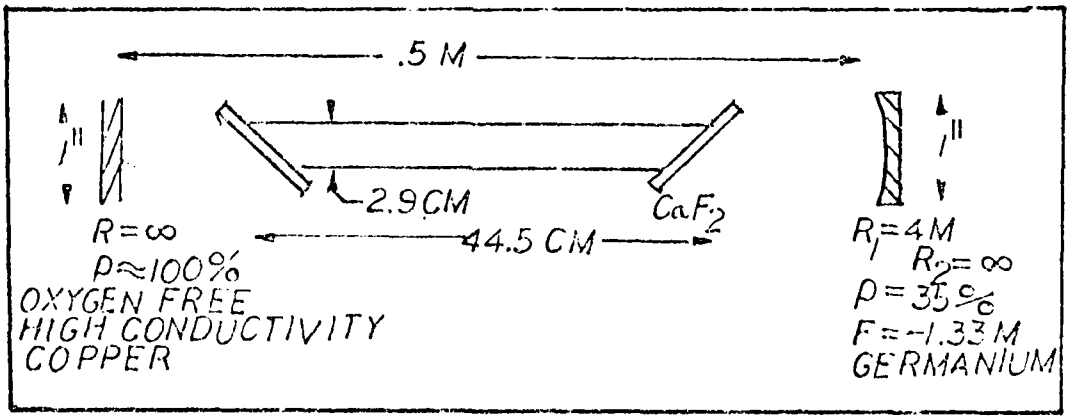


Figure 15.

HF Optical Cavity

A 300 gr/mm grating ( 1 3/4" x 1 3/4" ) can be exchanged for the copper mirror. The grating's normal is fixed at 39° to the optic axis. A 35 % output reflectivity was selected as the maximum output coupling based on the work with an HF

mini-TEA laser [3:10]. The active volume of the optical cavity is determined by the elctrodes and is described in the next section.

Electric Discharge

The electrical circuit design is dictated by the requirements for a 350 Amp, 120 ns current pulse to initiate the chemical reaction at repetition rates of up to 10 kHz. The discharge circuit is shown in figure 16 and consists of three main components; (1) the voltage supply and doubler, (2) the trigger and thyratron, and (3) the laser cathode/anode structure.

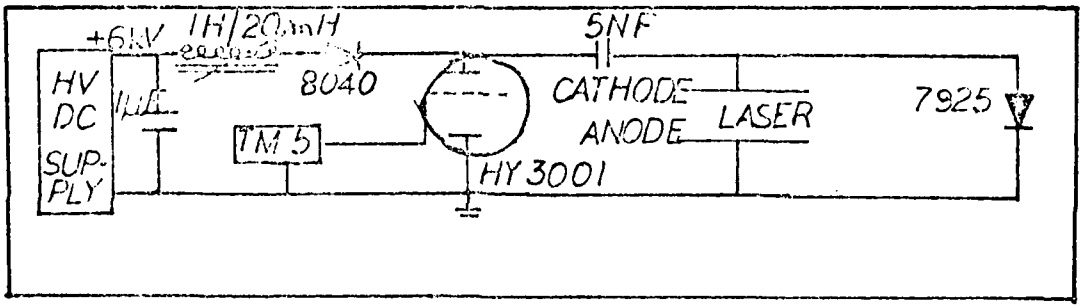


Figure 16.

HF Laser Discharge Circuit

The 6 kV supply charges the 5 nF capacitor through the diodes and inductor while the thyratron is open circuited. When the TM-5 trigger fires the thyratron, 12 kV is placed across the cathode/anode, a large current flows through the thyratron and from the anode to cathode. (Electrons flow from the cathode to the anode.)

The DC voltage supply is a 10kV, 5kW, Glow Discharge Power Supply, Electro Powerpacs Corp Model 1102. The high voltage diodes are manufactured by Solitron, but no specifications could be obtained. The saturable inductor is used to eliminate

the losses associated with resistive charging and to meet the 10kHz repetition rate requirement. The high inductance required for charging the 5 nF capacitor would also cause the thyratron to "lock-on" during discharge, but the inductor reduces its value to 20 mH at saturation and the thyratron operates as designed.

The HY 3001 hydrogen thyratron switches the current through the cathode/anode. The thyratron consists of a cathode, anode, and high voltage grid. Electrons are accelerated from the cathoe to the anode under the high voltage and collide with $H_2$ molecules, producing ions and electrons by the reaction

$$H_2 + e^- \longrightarrow H_2^+ + e^- \qquad (139)$$

The current is increased by several orders of magnitude. The plasma nuetralizes and the current pulse is terminated. As long as the grid voltage is held at a large negative voltage, no current flows. But, as its value is made less negative, elctrons begin to leave the cathode and eventually acquire enough energy to ionize the hydrogen gas. Breakdown occurs and a sharp pulse is created. A photograph of an oscilloscope trace of this current pulse as observed by Raytheon is presented in Appendix B.

The trigger for the thyratron is an EG&G TM-5 trigger module with a HY 6004 hydrogen thyratron that produces a 25 A/ 2.5 kV and 500 nsec output pulse, with a variable repetition rate to 20 kHz.

The cathode consists of "68 molybdenum pins, .03 inch in diameter, sealed to a high density alumina body using 7052

Corning glass" [3:40]. A 220 Ohm, 10 Watt resistor is connected to each pin. The pins are arranged in three rows with .083 inch seperation between rows and .33 inch seperation between pins in the same row. The flat aluminum anode is .4 inch below the cathode. This anode cathode seperation was chosen on the basis on tests that Raytheon conducted with the mini-TEA laser [3:41]. The total active volume is 7.5" x .166" x .4 " = .5 cubic inches = 8.16 cubic centimeters.

Gas Flow

This gas laser requires a flowing system for two reasons, (1) products of the chemical reaction must be removed from the cycle and fresh reactants supplied and (2) products of recation and heat of reaction must be convected from the optical region. The system is not sealed and gases are recirculated many times before being exhausted.

For maximum operation, a fresh $SF_6 + H_2$ gas supply should be provided for each discharge duration. This establishes a requirement for flow velocity [72]. It is important that reaction products be removed from the optical cavity and two processes accomplish this: (1) recombination processes such as

$$SF_5 + F \longrightarrow SF_6 \tag{140}$$

and

$$H + H \longrightarrow H_2 \tag{61}$$

and (2) convection of products from the active volume by high speed flows. Recombination processes are discussed in

the theory section on kinetics, pages 12-26. In general, these processes are slow and convection serves as the primary means for removing unwanted products.

If a uniform, constant gas flow is assumed, then the flow rate criteria yields

$$FLOW\ ^{\ell}/_{S} = VOLUME \times REP\ RATE \tag{141}$$

The flow will not be laminar and uniform for three main reasons; (1) a boundary layer will form on the electrodes, (2) the flow will be very turbulent, as a result of the physical design of the gas recirculating system, and (3) sudden heating of the gases during the electric discharge will create pressure waves within the gas mixture.

Dzakowicz and Hutzke estimate the required increase in flow rate due to processes (1) and (3) to be a factor of 2 - 5. [72].

The speed of sound in the $SF_6$+$H_2$ mixture may be calculated theoretically. The heat capacity of $SF_6$ at 300°K is 23.329 cal/mole °K [73]. Then, from an ideal gas approximation,

$$\eta = \frac{C_P}{C_P - R_u} \qquad R_u = 2\ ^{CAL}/_{MOLE\ ^\circ K} \tag{142}$$

and the speed of sound is

$$a_s = \sqrt{\frac{\eta R T}{M}} = 136\ ^{M}/_{S} \tag{143}$$

This establishes an upper limit on repetition rate for a subsonic, clean flow.

The flow of gases external to the HF laser is diagrammed in figure 17. Gases are stored in 100 lb. cylinders at 20 psig and fed by 3/4" plastic tubing to a control panel

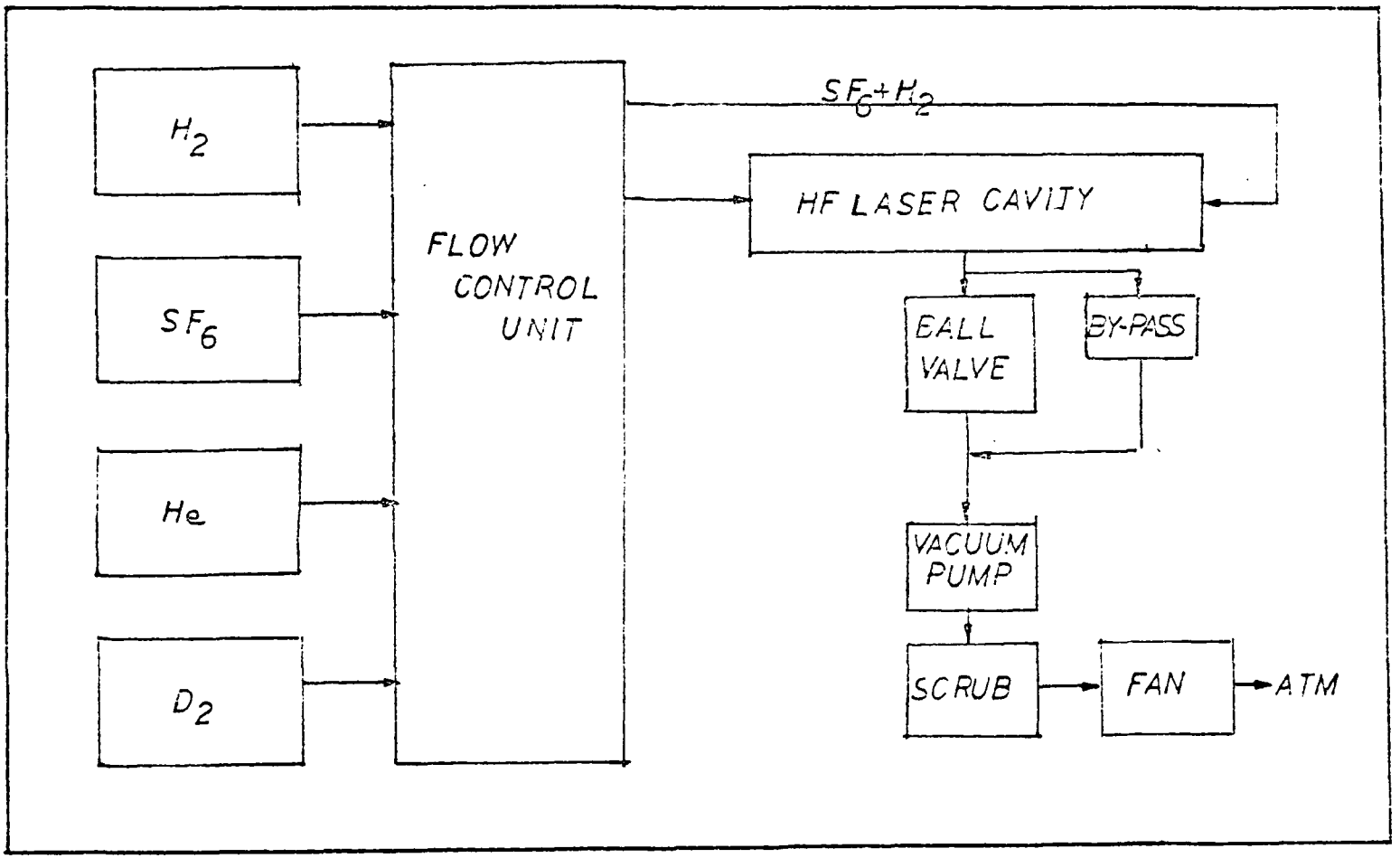


Figure 17.

HF Laser External Gas Flow

with Matheson 603 ($H_2$) and 605 ($SF_6$) flow meters to control the flow rate and mixture. Calibration charts for these flow meters are given in figure 18, from [3:88]. For the typical operating points of 20mm $H_2$ and 35 mm $SF_6$, the flow rates are 1.4 l/min and 5.6 l/min, respectively. The $SF_6$ + $H_2$ mixture is introduced into the HF laser across the $CaF_2$ brewster windows. The flow of gases within the laser is illustrated in figure 19 and discussed below.

Gases are exhausted through a 1 1/2" Hayward PVC Ball Valve and an Alcatel ZT 1060C vacumn pump to a chemical scrubber and exhausted to the atmosphere through a roof fan. The ball valve controls total gas pressure in the laser cavity.

Once gas is in the cylindrical laser housing, it flows in a circle past the discharge area, through a sulfur precipitator, chemical scrubber and heat exchanger. For low repetition rates, two Rotron Propimax 3B Model 754D fans with a 62.8 l/s capacity each, are used to recirculate the gases. The flow velocity within the cavity is

$$U = 2(62.8)(20\,CM^2) = 649\,M/S \tag{144}$$

The speed of sound from equation (143) is 136 m/s and then, the mach number is

$$M = \frac{U}{a} = .48 \tag{145}$$

The fresh gas flow rate is 7 l/min or .12 l/sec and on the average the gas remains in the laser cylinder for 523 cycles.

With this large number of cycles before exhaust, many contaminants will build up in the gas flow. The kinetic model presented in the theory section was based on a single

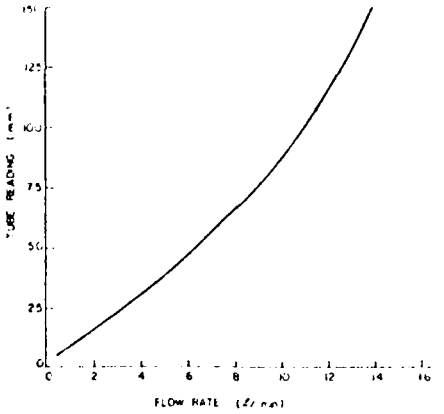


Hydrogen at 20 psig. Matheson 603 tube, glass ball.

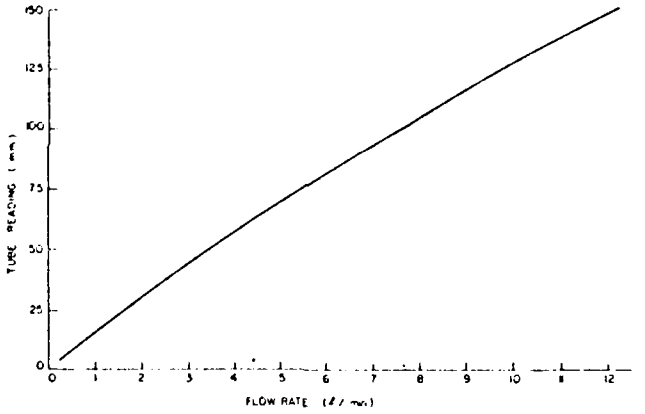


Sulfur hexafluoride at 20 psig. Matheson 605 tube, glass ball.

**Figure 18.**

**Flow Rate Calibration Charts [3:88]**

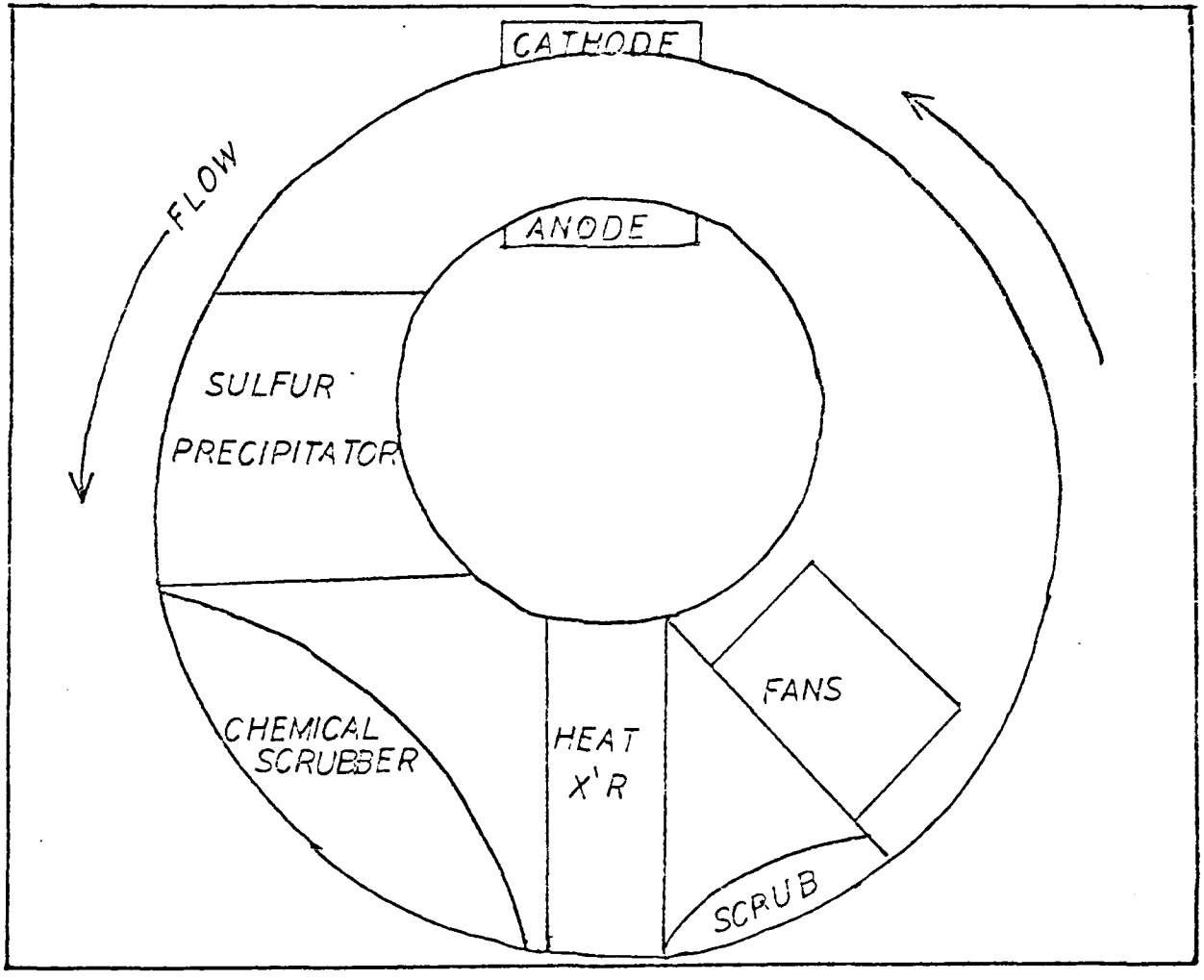


Figure 19.

HF Laser Internal Gas Flow

cycle and neglected the formation of S, $H_2S$, ground state HF, etc, which are formed downstream of the discharge volume after many cycles. In order to eliminate these unwanted products from the flow, a sulfur precipitator and chemical scrubber are included in the laser gas recirculating design. The sulfur precipitator is constructed of many, water cooled, aluminum plates. Two chemical scrubbers containing Linde 5A Molecular Sieves remove other contaminants. Note, as the laser is run for extended periods, particulates will build up on these collectors and their efficiency will be degraded. The odor of $H_2S$ was noticed in the laser exhaust and it is assumed that the precipitator and scrubber do not efficiently remove contaminants from the flow.

Cooling System

The electrical energy input to the laser is rather high:

$$P_{AV} = I_{AV} = 21\ W \quad (AVE.\ DISCHARGE\ POWER) \quad (146)$$

$$P_P = IV = 4\ MW \quad (PEAK\ DISCHARGE\ POWER) \quad (147)$$

$$P_{FAN} = 600\ W \quad (FAN'S\ POWER) \quad (148)$$

This energy heats the gas, cathode, and other components. Output power is very sensitive to gas temperature, see figure 20 [3: 13]. To cool the gas flow a Lytron Model 5120 Heat Exchanger (38W/°F) is included in the design.

Extreme temperatures will also damage the electrical components. These elements are air, water, and oil cooled. The gas recirculating fans are cooled by the high speed gases flowing past them and should not be operated with less than 50 torr total pressure in the cavity. The saturable

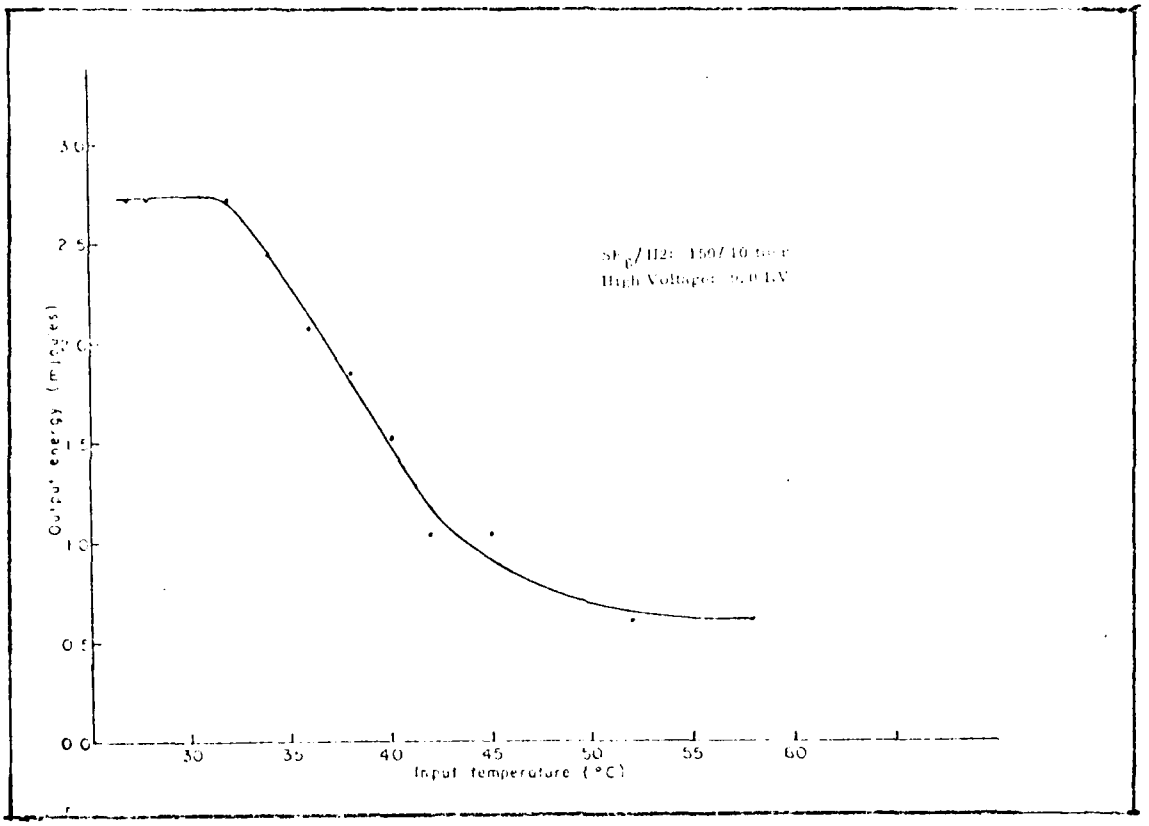


Figure 20.

HF Output Energy versus Temperature [3:13]

inductor and voltage doubling circuit is air cooled by a small fan. Gases are exhausted to atmosphere and convect heat from the laser.

The remaining cooling is completed by a water and oil (silicone, 20 cs viscosity) flow system as depicted in figure 21. Chilled water cools the heat exchanger and sulfur precipitator directly. The oil cools the cathode and thyratron in a closed flow system. The oil exchanges heat with the chilled water in a Young SSF-302-BY-2P heat exchanger and is pumped by a Little Giant Model 13 pump.

HF Laser Modifications

A number of modifications were made to the HF laser to complete the frequency investigation and to repair damaged components.

Optical Cavity

The power - frequency relations developed in the theory section were based on a single axial, TEM 00, $P_2(6)$ laser transition. The experiment also requires a controlled variation of HF frequency across the linewidth of 500 MHz. The HF laser normally operates multiline and multimode, however.

Two modifications to the optical cavity were made to solve these problems. An aperture was designed and installed to force the laser to the TEM 00 mode. A piezoelectric crystal was added to drive the output coupler mirror and control HF frequency. The $P_2(6)$ transition was selected with the grating replacing the OFHC copper mirror. A diagram of the modified optical cavity is shown in figure 22.

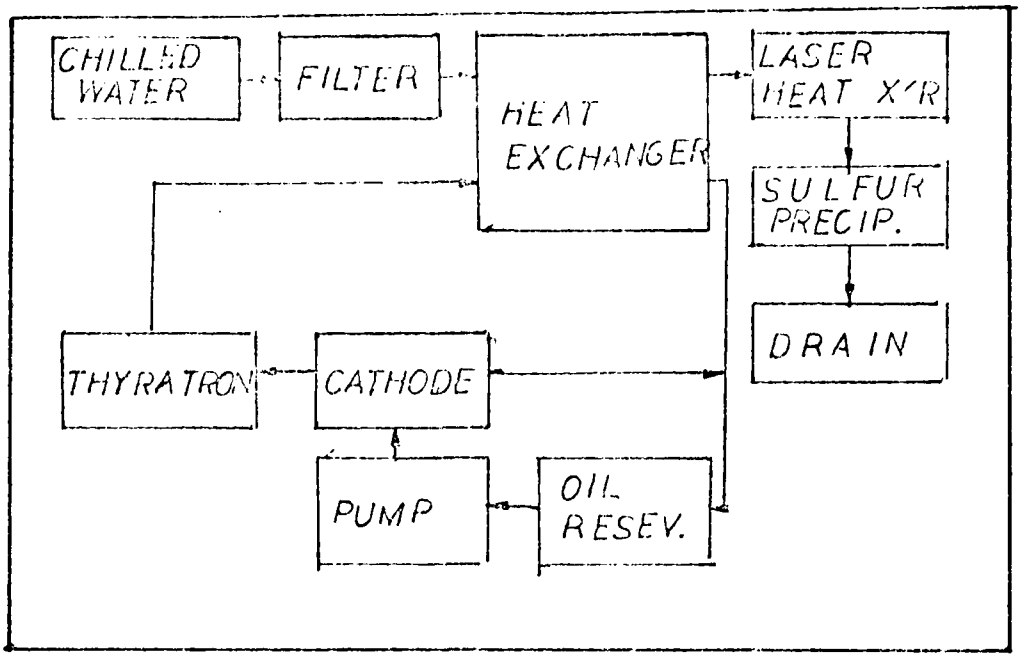


Figure 21.

HF Laser Cooling System

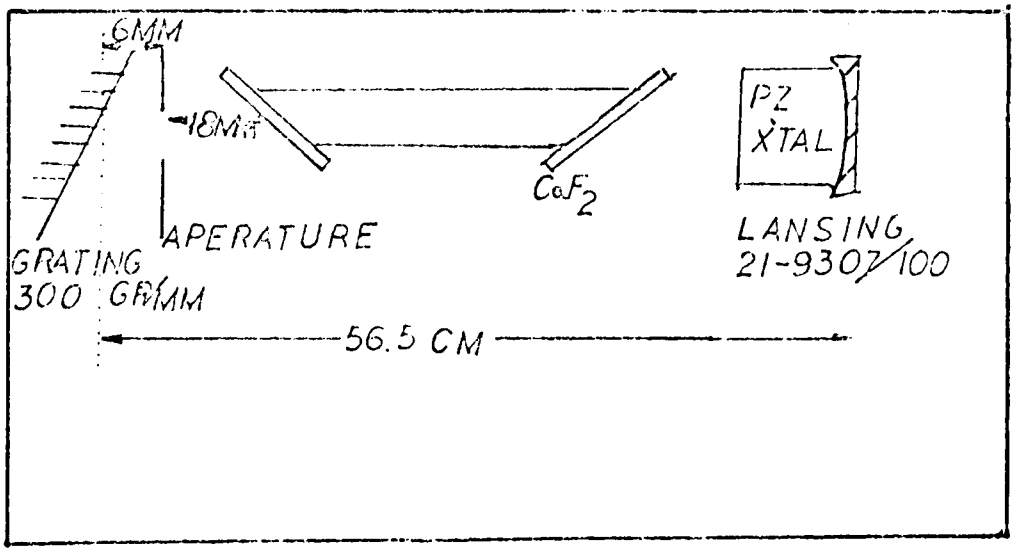


Figure 22.

Modified HF Optical Cavity

The variable aperture is continuously variable from .059 " to .709 ", with thirteen calibrated positions (.059, .086, .128, .159, .193, .221, .281, .328, .359, .406, .500, .709 inch). TEM 00 operatition is achieved for aperture diameters of .221 inches or less. The aperture is mounted in an aluminum plate and fixed to the grating mount with a vertic position control and centered horizontally on the discharge volume.

The HF frequency, , is varied by changing the cavity length, , with a variable voltage, 0 - 1.3 kV, applied to the piezoelectric crystal. A Lansing 80-214 Lock-in Stabilizer is used to supply the high voltage to the crystal. In the slow scan mode, this supply provides a linear ramp of 0 to - 1.3 kV in 44 seconds. The crystal returns to its unperturbed length in less than one second. Figure 23 shows a plot of the voltage applied to the crystal as a function of time.

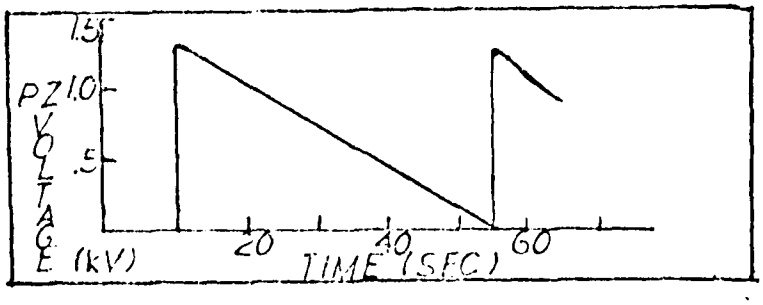


Figure 23.

PZ Voltage as a Function of Time

The crystal expands by 2.22 μm under a 1.3 kV applied voltage. This motion was detected with an Ealing Michelson interferometer as shown in figure 24.

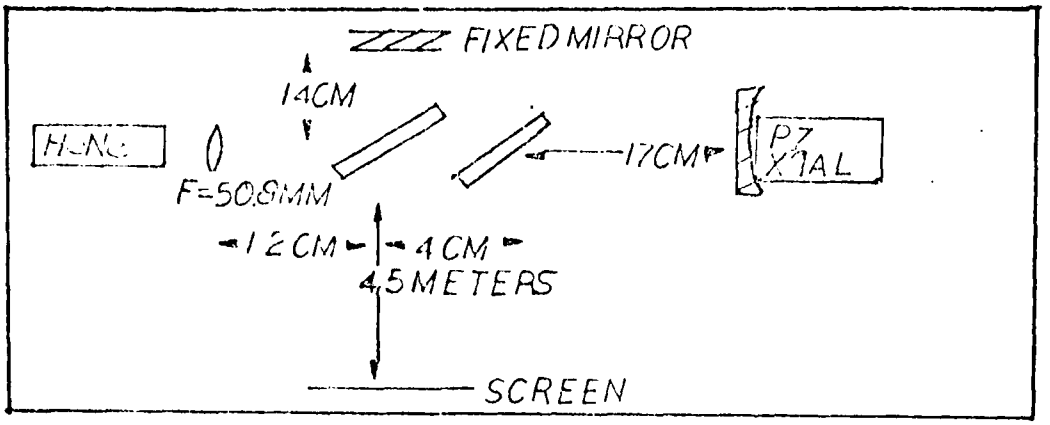


Figure 24.

Interferometer Test of PZ Crystal Motion

Fringes of 2.5 cm diameter were achieved at the screen and a shift of seven orders was observed as the voltage was was varied from 0 to -1.3 kV. The length change of the crystal is

$$\Delta L = m\frac{\lambda}{2} = 22\,\mu m \tag{149}$$

This nearly meets the requirement established by equation (18) for covering the 500 MHz linewidth of the HF gain curve.

The crystal was mounted on the laser with an adapter that screwed into the original mirror mount. The mirror was held to the adaptor by the same ring screw that originally held the mirror to the cavity.

The modified cavity length is 56.5 cm and from equation (17) the free spectral range is 268 MHz. The free spectral range is less than the linewidth and two axial modes will exist during extended periods of the piezoelectric crystal's sweep. Given the physical dimensions of the cylindrical housing, little can be done to increase the free spectral range.

When two axial modes exist, both will pump the $CO_2$ 000 - 101 transition. The mode on the low frequency end of the gain curve will pump much less efficiently, however. It has an offset frequency of 265 MHz greater than the first mode. Based on the model of pages 37-42 and equation (121), the ratio of pumping efficiency for the two axial modes is

$$\frac{\ln N_{\varphi q}/N_{\varphi_0}}{\ln N_{\varphi_q}/N_{\varphi_0}} = EXP-(\delta_q^2/\delta_0^2)/1.15 \sim 22\times10^{-3} \qquad (150)$$

and the lower frequency mode may be neglected.

Frequency stability of any mode could be enhanced by increasing the number of axial modes. If the free spectral range were to be decreased to 170 MHz (3-4 axial modes), the ratio as calculated in equation (150) would increase to 10 % and the second mode's interaction could not be neglected. The theory would be significantly complicated in this case. Note also, that decreasing the free spectral range limits the range over which the frequency can be effectively varied. The effect on $CO_2$ laser power at large offset frequency, $\delta$, would not be measureable. For these reasons, one or two axial modes is preferable.

The spot size of the HF beam is important, because the beam must be coupled into the $CO_2$ cell will sufficient intensity to establish the threshold population inversion. The HF beam is large and will be reduced with an optical system external to the HF cavity.

Several other problems were encountered with the optical cavity. Beam quality is rather poor due to aperturing, flow

turbulence, etc. Beam divergence is large, about 9 mrad. The control on optical alignment, particularly for the grating is poor. Finally, the output coupler was not truly flat on the external side, with a wedge angle of 7.3 mrad in the vertical direction and 14.6 mrad in the horizontal direction.

Electric Discharge

Repairs and modifications to the high voltage DC supply, high voltage diodes, and the thyratron trigger unit were required.

The DC voltage supply was modified to be included in the interlock system. This system prevents the laser from being run if the chilled water supply is off or if a five minute warm-up time for the thyratron is not provided. The DC supply was wired to this interlock system so that it could not be turned on if the interlock system was open circuit, or tripped. This KV DC supply require 240 Volt single phase power.

The high voltage diodes of figure 16 were unreliable and probably underrated (16-20 kV, required). The Solitron 8040 2A SLD - 30 diode failed twice during the investigation. Without this diode, the voltage doubling circuit does not function and the discharge is spatially nonuniform.

One replacement diode was available and was used to replace the first failure. The I - V characteristic for the defective and replacement diodes are shown in figure 25.

The second failure ocurred after repeated arcing in the voltage doubling circuit and extreme heating of the diode.

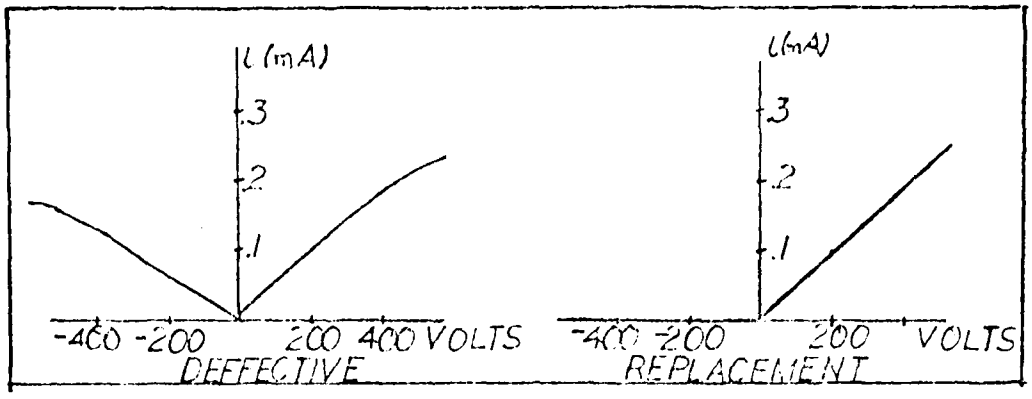


Figure 25.

I-V Characteristic of HV Diode (8040)

Three Varo VC 80 V diodes (8 kV, 2A, ea.) were used in series to replace the single Solitron diode.

Repeated problems in triggering the HY 3001 thyratron were encountered. Two distinct problems were involved. First, the EG&G TM-5 trigger unit with HY 6001 thyratron was inoperative and replaced. Secondly, the inetgrators and recording equipment require synchronization with the discharge pulse.

The EG&G TM-5 unit whould provide a 2.5 kV, 500 nsec pulse (unloaded). Two components within this unit failed, however. A 2N4401 transistor was defective and replaced. The HY 6001 thyratron was defective, probably due to its mounting design. The thyratron was located on its side and the grid was likely warped. No replacement thyratron was available and a new trigger system was designed.

An EG&G TM-30 trigger was available and used to trigger the HY 3001 thyratron. To match the output impedence of the TM-5 unit, a 28 ohm, wire wound resistor was put in series with the grid output of the TM-30 unit. The rise

time of the trigger pulse was increased by a factor of two to 2 μs by the inductance of this wire wound resistor. The magnitude of the trigger pulse was 2 kV and was sufficient to fire the laser thyratron.

The final solution employed for the integrator synchronization problem involved using two pulse generators with variable delay. The circuit is shown in figure 26.

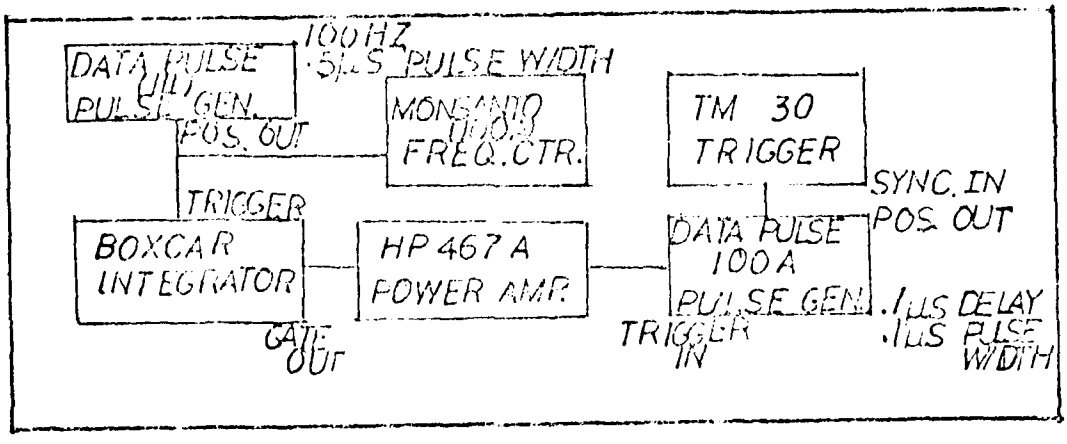


Figure 26.

Trigger Circuit

The first pulse generator is free-running and its variable repetiton rate determines the discharge repetition rate. The positive output of this generator triggers the boxcar integrator, whose gate output is used to trigger a second pulse generator with variable delay control. In this way, the boxcar integrator gate and laser pulse may be synchronized.

Substantial space-charge buildup in the TM30 circuit required grounding the wire wound resistor temporarily before laser turn on.

Gas Flow

A limited supply of $SF_6$ was available for this study,

approximately 300 lbs. Gas consumption without recirculation is 100 lbs/ 1.5 min [3:30]. With gas recirculation of 500 cycles, the 100 lb cylinder should last 12.5 hours. Even at this rate, the supply will only last 37.5 hours.

To decrease the $SF_6$ gas usage and increase laser time, a modification to the flow system was made. In the original design a 1 7/8" inner diameter stainless steel pipe was used to exhaust gases from the laser through the ball valve and vacumm pump. This pipe size was used to accomadate the gas flow required at 10 kHz repetition rates. Repetition rates of about 100 Hz were used in this experiemnt to conserve gas, provide sufficient signal-to noise averaging , and maintain sufficient energy/pulse to pump the $CO_2$ laser. This rate requires a 100 times smaller flow rate and a smaller exhaust pipe may be used.

The average flow velocity (radial average) of a flow in a pipe is

$$U = \frac{dP}{dz} a^2 \left(\frac{1}{4\mu}\right) \qquad (151)$$
[74]

where $a$ is the pipe radius, $\mu$ the gas viscosity, and $\frac{dP}{dz}$ the pressure gradient, axially. The volume flow rate is then

$$\frac{dP}{dz} \pi a^4 \left(\frac{1}{4\mu}\right) \qquad (152)$$

By reducing the pipe radius, much lower flow rates can be achieved. The same effect can be obtained by nearly closing the ball valve, but this adjustment becomes very sensitive for such slow rates.

On this basis, the modification of figure 27 was made. A cavity pressure of 1 torr was obtained with this modification

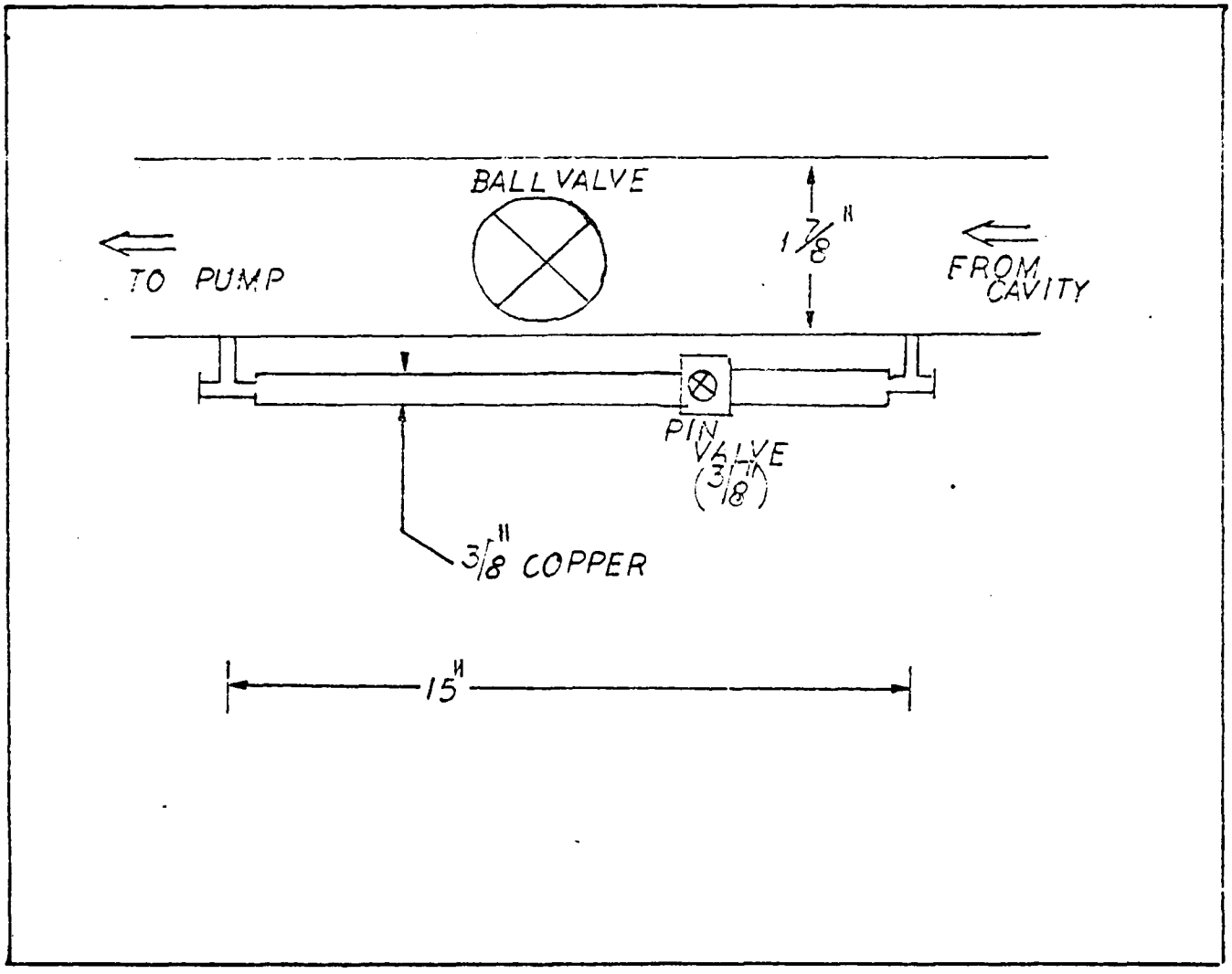


Figure 27.

By-Pass Valve Modification

and the ball valve closed. Two torr was maintained for several hours. The ball valve could not be completely closed when running the laser because a slightly greater flow rate was required. The pin valve was used as fine adjustment for flow rate.

HF Laser Operation, Safety, and Alignment

Appendix C lists the step-by-step procedure used for running the HF laser.

Several safety factors were considered. Deadly voltages and lethal energies are exposed during the operation of the laser. The trigger circuit, cathode area, and high voltage DC supply must be handled with extreme care. High voltage areas are clearly marked and shielded.

The interlock system was described on page 73.

The thyratron can "lock-on", continuously conducting current. If this occurs, the high voltage supply must be turned off within seconds to prevent damage to the power supply.

The gas recirculating fans are gas cooled and must not be operated with less than 50 torr total pressure in the laser cavity.

Several grounding wires are conveniently located for possible emergency use.

A gas detector (combustible products) was installed in the gas storage closet.

The safe eye exposure distance (SEED) is larger than the dimensions of the lab room:

$$SEED = \sqrt{\frac{2E_p}{\pi \theta_{1/2} PEL}} \qquad (153)$$

Evaluating equation (153) for

$$E_p = 1\ mJ$$
$$\theta_{1/2} = 6\ mrad$$
$$PEL \sim 10^{-1}\ J/cm^2$$

yields

$$SEED = 200\ M \tag{154}$$

The required optical density for goggles is

$$D = \log \frac{E_o}{E_p} = 4.4 \tag{155}$$

Goggles with $D = 4$ at 2.8 μm were available and were used when operating the laser.

The HF cavity was aligned with a HeNe laser. The laser is high gain and alignment is not particularly difficult. Once lasing is achieved, the power can be maximized by adjusting each of the mirrors. To achieve single line operation, the copper mirror is removed and replaced by the grating. Once the grating is in place, lasing can be established by merely adjusting the grating angle.

HF Laser Performance Characterization

The first set of experiments characterized the performance of the HF laser. Power was measured as a function of pressure, $SF_6/H_2$ mixture, repetition rate, discharge voltage, aperture diameter, and time. Beam quality and divergence were also investigated. The laser was operated under both multiline and single line (including the $P_2(6)$ transition) conditions.

Multiline operation was achieved with the OFHC copper mirror. A Raytheon Au:Ge Infrared detector was used to measure the energy/pulse. Pulse shapes were observed on a

Tektronix 555 Oscilloscope. A Princeton Applied Research Model 160 Boxcar Integrator with a 50 μs gate, 100 ms time base, and .3 ms time constant, was used to average the energy/pulse. The integrated output was displayed on a Fluke 8100A digital voltmeter. It is this averaged power that was measured as repetition rate, pressure, voltage, and mixture were varied.

Beam quality and divergence were investigated using the same set-up with the detector on a two degree of freedom ($X, Y$) translating mount. The detector was moved axially ($Z$) along the HF beam on a 90 cm optical rail. The coordinate axes are shown in figure 28.

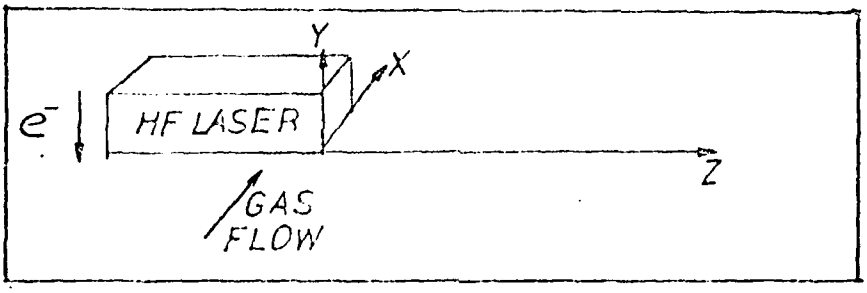


Figure 28.

Experimental Coordinate Axes

An absolute value for average energy/pulse was obatined with a Scientech Model 3604 Laser Power Meter thermal type energy detector with a sensitivity of 84.5 mV/W.

Single line operation was established with the 300 gr/mm grating replacing the copper mirror. A Lumonics Spex Mini-Mate monochromator with a 3 μm blaze, 300 gr/mm grating and 2.5 mm slits was used to choose the HF $P_2(6)$ transition. The

monochromator was calibrated by observing the location of the zeroeth through fifth orders of HeNe transmission. Based on $\lambda_{HeNe} = 0.6328\,\mu m$, the observed HeNe order separation of .5775 μm, and the observed zero order HeNe setting of -.008 μm, the relation between scale reading and actual wavelength is

$$\lambda_{ACTUAL} = 1.0958(\lambda_{SCALE} - .008\mu m) \qquad (156)$$

Three HF lines were observed at $\lambda_{ACTUAL}$ 2.851, 2,8074, and 2.7702 μm. These lines were identified as the $P_2(6)$, $P_2(5)$, and $P_2(4)$ transitions based on the comparisons of known wavelengths of the transitions, the seperation between these wavelengths, and the observed transitions in the Raytheon study [3:13,46]. This information is summarized in Table II.

Table II.

HF Line Identification

| Transition | λ(μm) | [3] @100μs | Wavelength Difference | This Study | Wavelength Difference |
|---|---|---|---|---|---|
| $P_3(6)$ | 2.9643 | | | | |
| $P_3(5)$ | 2.9256 | X | | | |
| $P_2(8)$ | 2.9111 | X | | | |
| $P_1(11)$ | 2.9103 | | | | |
| $P_1(4)$ | 2.8889 | | | | |
| $P_3(7)$ | 2.8706 | X | | | |
| $P_2(10)$ | 2.8657 | | | | |
| $P_1(6)$ | 2.8318 | X | .0365 | 2.8510 | .0436 |
| $P_2(5)$ | 2.7953 | X | | 2.8074 | |
| $P_2(8)$ | 2.7826 | X | .0349 | | .0372 |
| $P_1(4)$ | 2.7604 | X | | 2.7702 | |
| $P_2(7)$ | 2.7441 | X | | | |
| $P_1(3)$ | 2.7275 | | | | |
| $P_2(6)$ | 2.7075 | X | | | |
| $P_1(5)$ | 2.6730 | | | | |
| $P_1(4)$ | 2.6400 | | | | |

AD-A111 140 AIR FORCE INST OF TECH WRIGHT-PATTERSON AFB OH SCHOO--ETC F/G 20/5
CHARACTERIZATION OF AN HF-PUMPED CO2 LASER.(U)
OCT 81 G P PERRAM
UNCLASSIFIED AFIT/GEP/PH/81D-7 NL

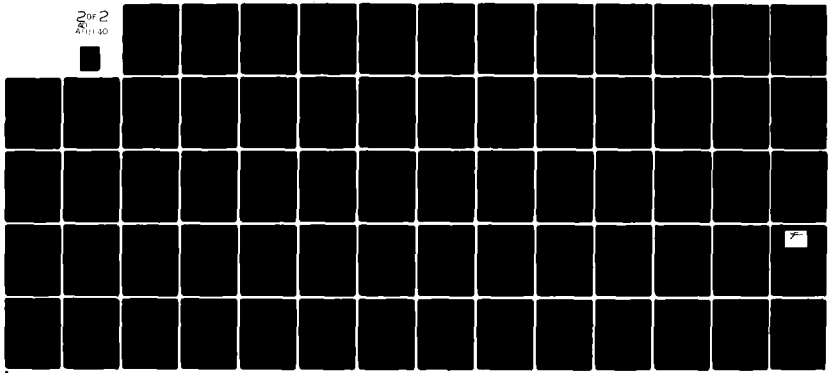

END
DATE FILMED
DTIC

Optical Pumping

After characterizing the HF laser and choosing the $P_2(6)$ transition, the HF beam was used to pump the $CO_2$ gas.

The results of the beam divergence measurements indicate the need for reducing the HF beam spot size. Originally, a telescope was used to couple the HF beam into the $CO_2$ cell with 4 mm diameter used by Raytheon in their study. With the optics available, this method did not reduce the HF beam size sufficiently.

To solve this problem, a 1 cm diameter $CO_2$ cell was designed and constructed as shown in figure 29. The HF beam was

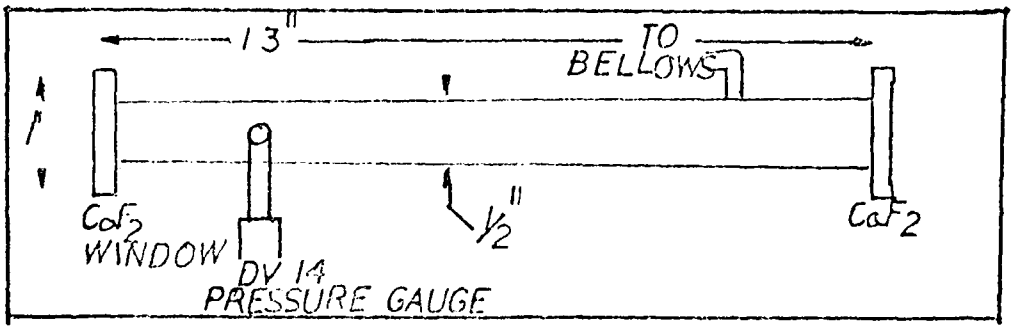


Figure 29

Redesigned $CO_2$ Cell

focused at the center of this cell with a one inch diameter $CaF_2$ lens. The two requirements of a small spot size and a collimation length of 40 cm led to the selection of a 250 mm focal length. (See Appendix D for the theoretical analysis used to make this selection.) This theoretical analysis predicted the 250 mm focal length lens would provide a spot size of less than 3.5 mm over a length of 40 cm at a distance of 14 -54 cm from the lens. Experimentally, a spot size of less than 6 mm was observed over this 40

cm range.

To fill the $CO_2$ cells and control pressure of the $^{12}C^{18}O_2$ gas, a pump system was designed (see figure 30). The two pyrex cells are connected to 1/4" piping by a flexible bellows. The $^{12}C^{18}O_2$ is stored in a 1 liter cylinder that can be cooled in a liquid nitrogen bath. The cells can be evacuated to about 1 torr with a DuoSeal Model R1406 vacuum pump. To reduce the pressure to 100 μm, a Varian Vac Sorb molecular sieve is cooled in a liquid nitrogen bath. An adaptor was designed and built from a non-rotating mini-flange flat to connect the 1/4" piping to the molecular sieve.

Power-Frequency Experiment

The optical set-up for the $CO_2$ power as a function of HF frequency experiment is illustrated in figure 31. The propogation of the HF, $CO_2$ and HeNe alignment beams are shown.

The main $CO_2$ cell is pumped by the HF laser directly. The incident HF beam is split and detected by a HgCdTe detector, D2. The transmitted HF beam is observed at the Raytheon Au:Ge detector, D4. The monochromator is used to determine the HF lasing transition and to filter out the $CO_2$ beam. The incident HF beam also travels through a second $CO_2$ cell. HF intensity is sufficiently low here that no lasing action is obtained and the absorbed HF beam is detected at a Santa Barbara Au:Ge detector, D1. There is a 2.8 μm filter in this leg of the optical path to remove the $CO_2$

The $CO_2$ cell lases and a forward and backward pulse is observed at D3 and D5 (InSb) detectors. A 4.3 μm filter

is used to eliminate the HF beam at D5. The second Lumonics monochromator is used to measure the $CO_2$ wavelength and select either the R(8) or P(10) 101 -100 transition. This monochrometer has a 150 gr/mm, 6 μm blaze grating and 1.25 mm slits.

The $CaF_2$, $F=25\,CM$, lens is used to focus the HF beam into the $CO_2$ cell, as described earlier. A $CaF_2$ lens focuses the HF incident beam on D2.

Finally, a HeNe, Spectra Physics Model 142 laser is used for alignment. After the absorption cell leg of the optical path was aligned, the HeNe laser was located as shown to align the main $CO_2$ cell and the monochrometers.

This set-up provided the necessary data for comparing the $CO_2$ power to HF freuqency. The amount of HF absorption was obtained by comparing intensities of incident (D2) and transmitted (D4) HF pulses. $CO_2$ forward and backward pulses were observed at D3 and D5. Finally, the HF frequency was measured by observing the HF absorption through the second $CO_2$ cell. The absorption should vary with frequency accoding to a doppler broadened lineshape. From this variation in absorption, the variation in frequency was measured.

The transmittance for each of the optical elements was measured with a Wilks Miran I Variable Filter IR Analyzer with a Wilks Preamplifier. The three $CaF_2$ beam splitters transmitted 90% at 4.3 microns and 95% at 2.8 microns at 45 ° incidence. The Raytheon 90-90574 2.8 micron filter transmitted 8% at 4.3 microns and 90% at 2.8 microns at normal incidence. The 4.3 micron filter is a flat gold and copper Laser Optics 3.6 - 8 micron filter and transmits

less than .5% at 2.8 microns and 95% at 4.3 microns at normal incidence. During alignment, the $CaF_2$ , $F = 25\ CM$ , lens transmittance was measured as 94% by detecting power with the thermal detector before and after the lens.

Each of the detected signals are amplified, displayed on an oscilloscope, averaged by a boxcar integrator, and recorded on an XY or strip chart recorder. The electrical wiring diagram for the entire experimental set-up is shown in figure 32.

The integrators are Princeton Applied Research CW-1 and 160 boxcar integrators. The gate widths were chosen to match the widths of the detected pulses. The faster PAR 160 integrators were used with the faster detectors (D2, D5). Time constants were chosen to reduce noise as plotted on the recorders. The settings for each integrator are listed in table III.

Table III

Boxcar Time Settings

| Integrator | Model | Gate Width | Time Base | Time Constant |
|---|---|---|---|---|
| I2 | PAR 160 | 500 ns | 20 µs | .3 ms |
| I3 | PAR 160 | 1.6 µs | 2 µs | 1 ms |
| I4 | CW-1 | 10 µs | 50 µs | .3 ms |
| I5 | CW-1 | 10 µs | 1 ms | 3 ms |

HF absorption was measured as the auxiliary cell was filled with $^{12}C^{18}O_2$ at pressures from 0 - 7 torr. Integrated

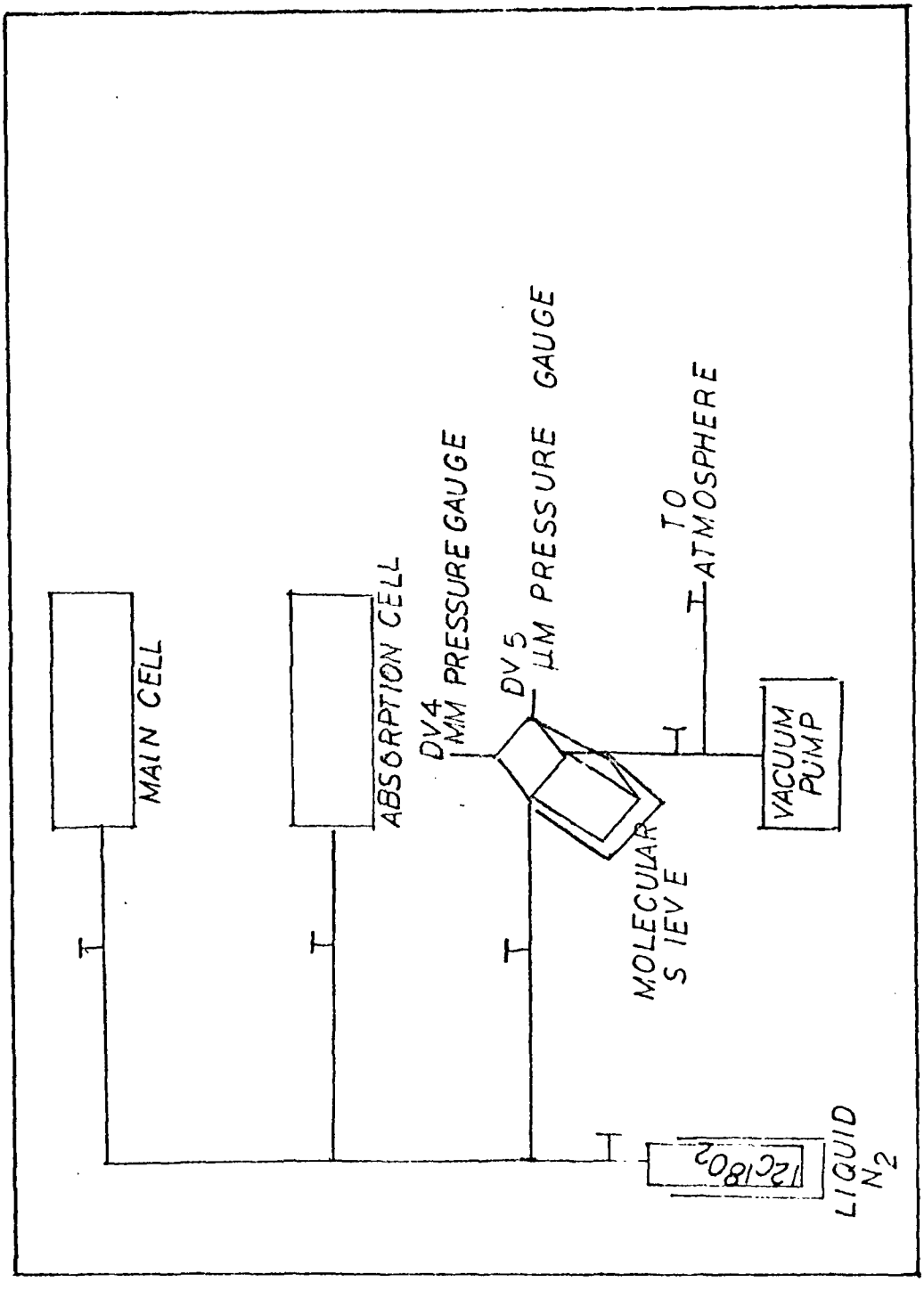


Figure 30.

$CO_2$ Gas Pumping System

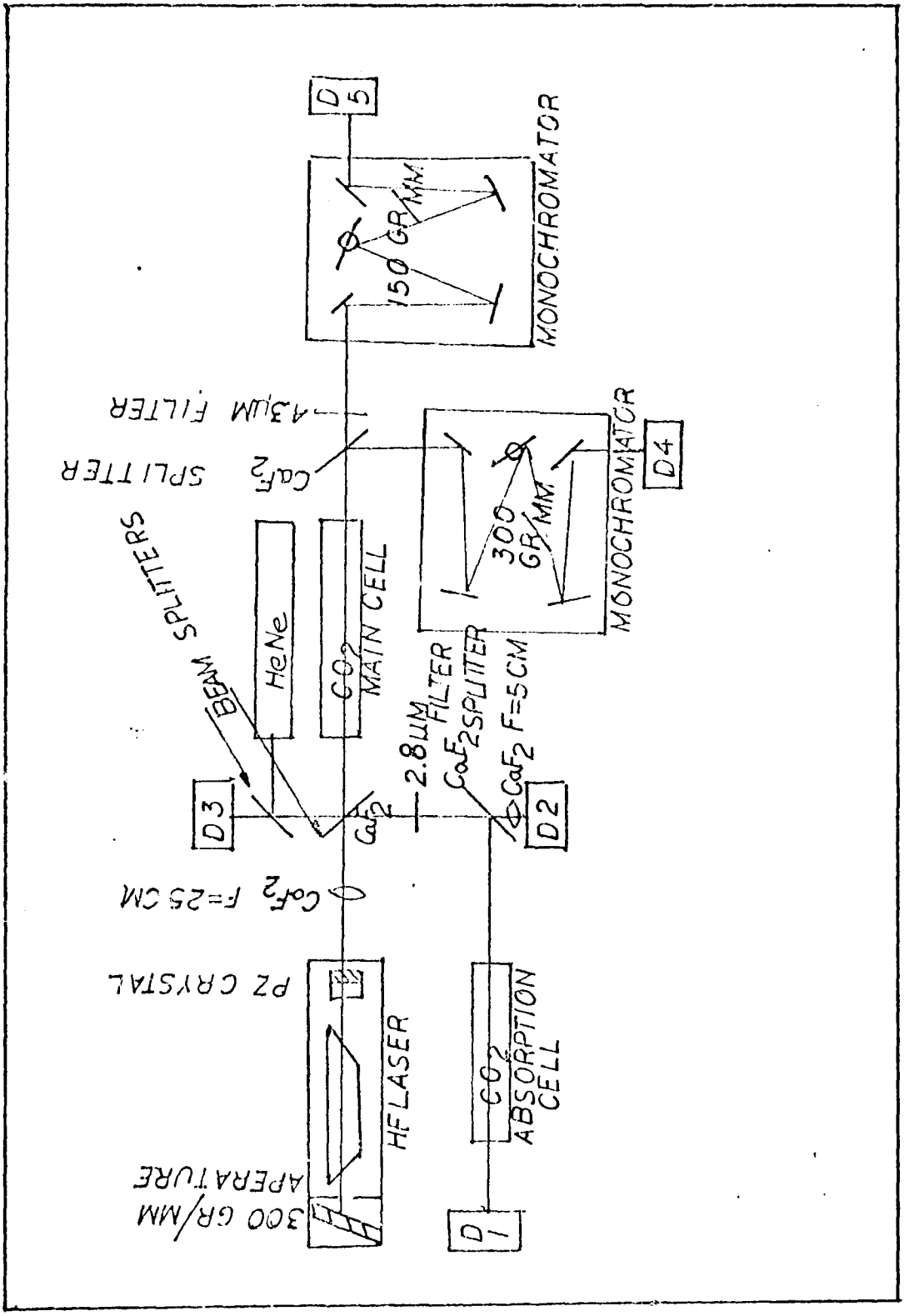


Figure 31.

Optical Set-up for Freuency Experiment

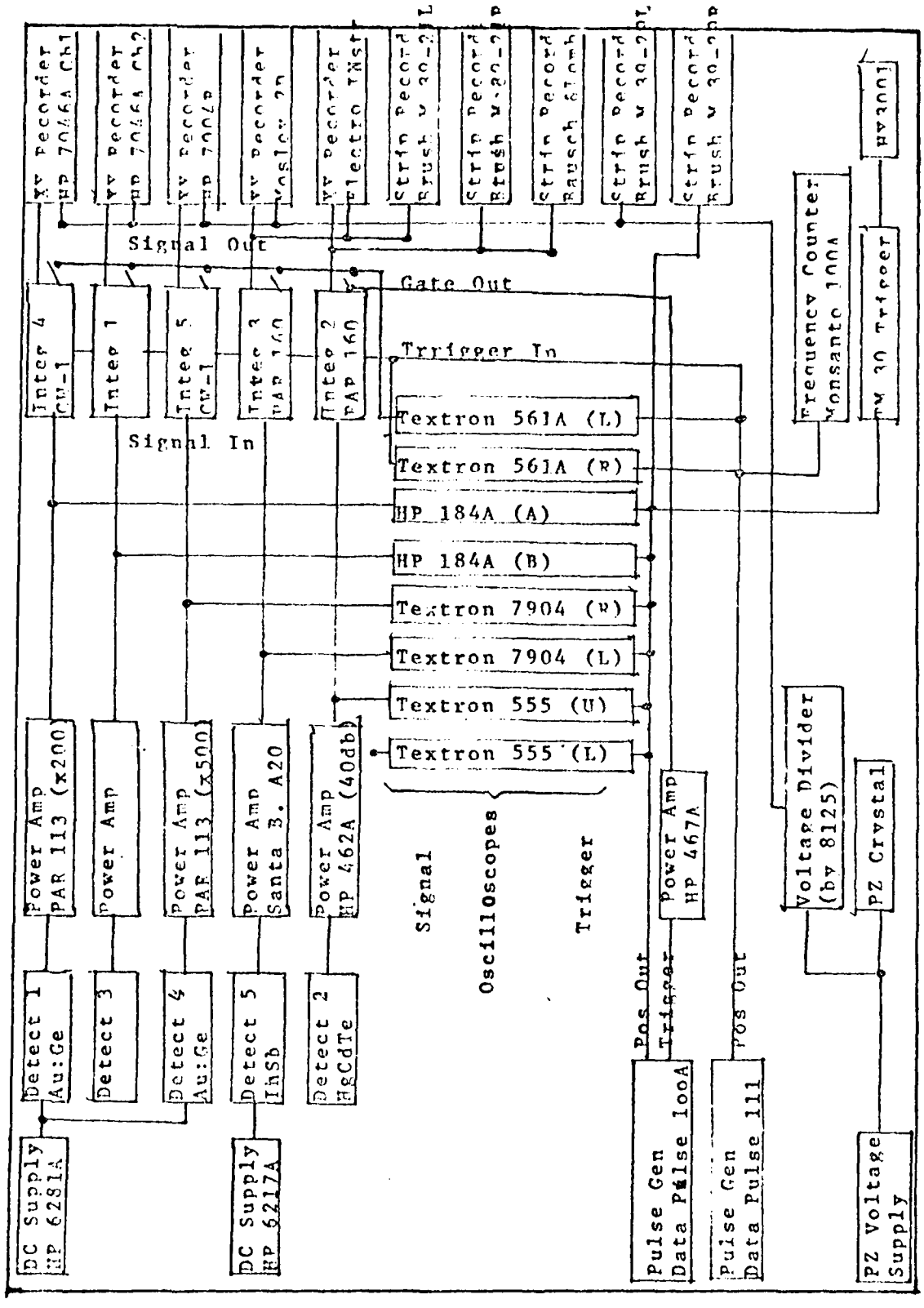


Figure 32

Electrical Wiring Diagram

power from detectors D1 and D2 were recorded on the HP 7046 XY recorder. Immediately after changing the pressure, the HF beam was blocked to mark the pressure reading.

The main $CO_2$ cell was then slowly filled with $^{12}C^{18}O_2$. $CO_2$ lasing was observed at 7 torr. HF and $CO_2$ pulse shapes dectected at D1, D2, D4, and D5 were photographed from oscilliscope traces. Dectectors D2 and D4 were sufficiently fast to resolve 20-200 nsec pulse shapes.

From the oscilloscope traces, it was observed that $CO_2$ lasing was erratic. A $CO_2$ pulse was observed for every 3-5 HF pulses. The HF pulses varied considerably in magnitude from pulse to pulse and $CO_2$ lasing was achieved only on the stronger HF pulses. The pulse-to-pulse variation in HF power was measured by displaying multiple pulses from detector D2 on oscilliscope channel 1.

HF absorption was measured as the PZ crystal voltage was swept from 0 to - 1.3 kV in 44 sec. No correlation between power and PZ crystal voltage was observed, indicating a frequency instability in the HF laser pulse on a time scale small compared to the integration period of 1 ms.

The nature of the power and frequency instability was investigated and its dependence on repetition rate, discharge voltage, and pressure recorded.

The data and results of these experiments are presented in the following section. Conclusions and recommendations will be made after considering these results.

## Results and Conclusions

The results of the experiments described in the previous section are now presented and compared to the theory established in the first section and to prior experimental studies. Conclusions concerning the system and its operation are drawn. Finally, a summary of the investigation, results, and conclusions is presented. The HF laser characterization, the pulse shape and kinetic model, and the optically pumped $CO_2$ laser will be discussed individually.

### HF Laser Characterization

The experiments characterizing the HF pump laser studied the dependence of HF power on the $SF_6$:$H_2$ mixture, total cavity pressure, discharge voltage, repetition rate, and aperture size, and analyzed beam quality and beam divergence. Power and frequency stability are discussed in the section on the optically pumped laser.

Figure 33 illustrates the dependence of HF power on the $SF_6$ flow rate, for a fixed $H_2$ flow rate of 1.4 l/min. There is a slight decrease in power at lower $SF_6$ flow rates, indicating the reduction in atomic fluorine concentration and the resultant decrease in vibrationally excited HF concentration. Results from the Raytheon investigation are also shown in figure 33. These results indicate a reduction in HF power above 80% $SF_6$, where hydrogen becomes the limiting specie in the cold reaction (21). Throughout this investigation, a 79% $SF_6$ mixture was used.

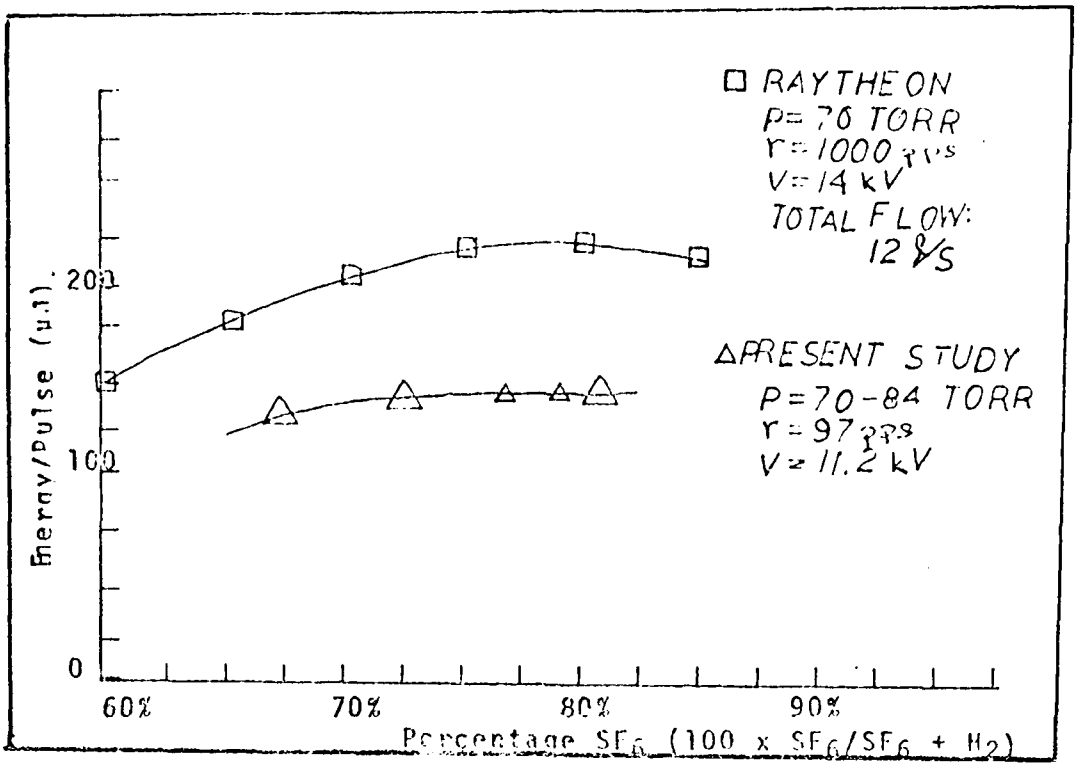


Figure 33.

HF Multiline Energy versus $SF_6/SF_6+H_2$ Mixture

Figure 34 depicts the HF output power - total cavity pressure relationship. At 11.2 kV discharge voltage, 97 pulses/sec repetition rate, and 79% $SF_6$, no variation in power with pressure was observed over a 30 torr range. No study of this relationship was undertaken by Raytheon. Throughout this study, a total pressure of 70 - 90 torr was maintained.

Figure 35 illustrates the dependence of HF power on discharge voltage as observed in this experimental study at 100 pulses/sec and in the Raytheon study at 4000 pulses/sec. The peak in this curve depends on repetition rate and moves to higher voltages at lower repetition rates [3:42-43]. The peak occurs at 12 kV at 4000 pps, but no peak is observed at 100 pps. The 100 pps curve is very flat from 10 - 16 kV and the peak likely occurs above the 16 kV recommended

voltage limit. 11 - 12 kV was chosen as the operating point for the current experiments.

The input power is $V/R^2$ ,where $V$ is the discharge voltage and $R$ is the resistance of the gases between the cathode and anode. A larger discharge voltage provides a greater input power and current to dissociate $SF_6$. Larger powers result. A larger discharge voltage also yields a greater average electron energy (see equation (28)). The reaction rates for electron attachment to $SF_6$ decrease as electron energy increases (see Appendix A). The associated reduction in flourine reduces HF output power. These two effects are competir

At high repetition rates, the discharge circuitry can become power limited. In this case, current will be fixed and only the electron energy effect will be important. As repetition rate increases, current limiting occurs sooner and the peak shifts to lower voltages.

There is a voltage below which no discharge occurs. Since electron attachment increases with decreasing voltage, it is not ionization that limits the discharge, but rather the discharge circuit itself. At low voltages, the current reduction may reduce the population inversion below threshold conditions. A determination of which effect is dominant was not completed.

The energy per pulse and average power versus repetition rate are presented in figures 36 and 37. The average energy per pulse decreases linearly in the range 0 -600 pps, and has a long shallow tail to 1000 pps. High repetition rates

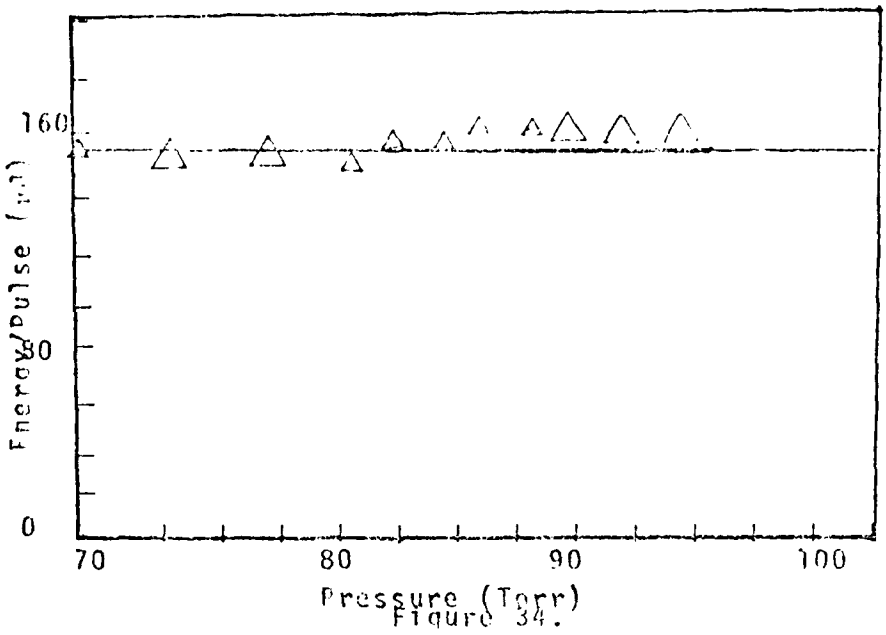


Figure 34.

Figure 34.
HF Energy versus Cavity Pressure

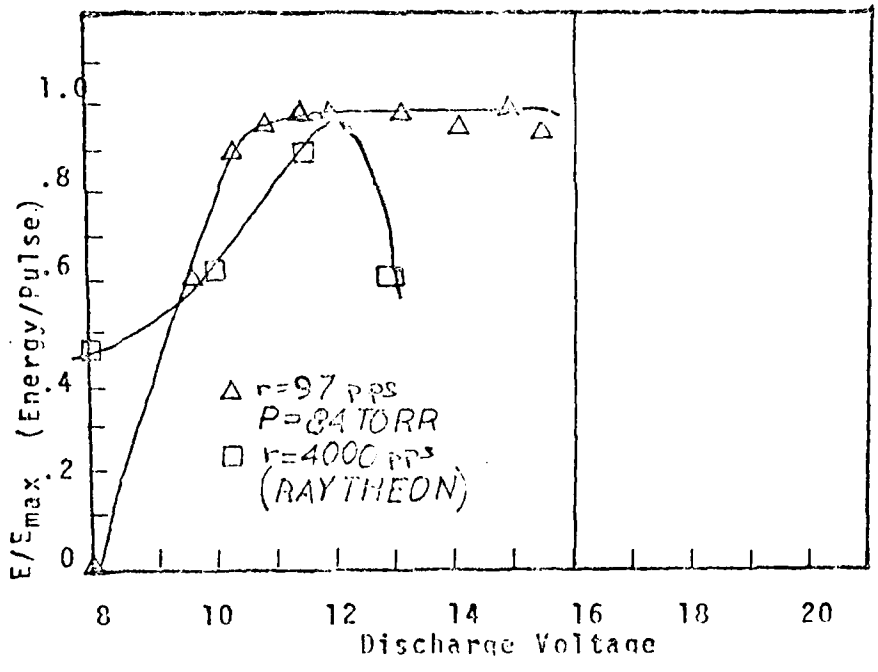


Figure 35
HF Energy versus Discharge Voltage

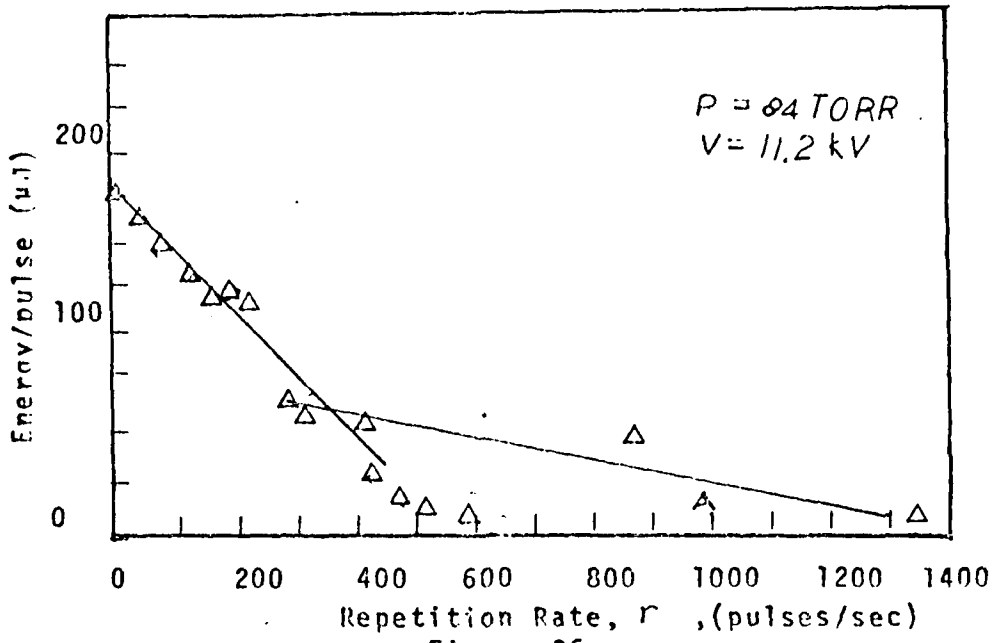


Figure 36.
HF Energy versus Repetition Rate

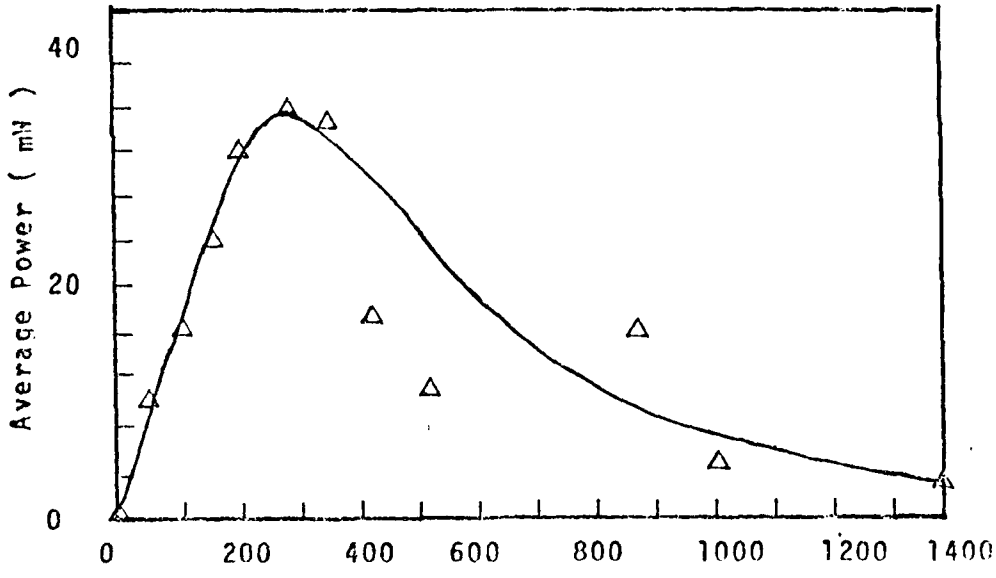


Figure 37.
HF Average power versus Repetition Rate

were not studied, due to the modifications for flow rate and limited gas supply.

Discharge voltage drops with increased repetition rate for a fixed DC supply because of increased loading. A constant 11.2 kV was maintained throughout this repetition rate study, however.

Average power is related to the energy per pulse by the repetition rate, $\Upsilon$ ,

$$P_{AVE} = E_{PULSE} X \Upsilon \qquad (157)$$

Average power is plotted against repetition rate in figure 37. The results from the Raytheon study of power versus repetition rate indicate a much wider curve; over a 10,000 pps range with a peak at 3000 pps. These results appear to be obtained by maximizing power with respect to discharge voltage, pressure, mixture, and flow rate at each repetition rate.

Average power increases initially to 300 pps, simply due to the increased number of pulses per second. The average power falls above 300 pps largely due to increased contaminants ($H_2O$, $H_2S$) in the flow. Also, the chemical scrubber is less efficient at higher repetition rates [3:43]. The increased power input will also increase the gas temperature and decrease output power. The fixed flow rate will affect power only if an incomplete exchange of gases in the electrode volume occurs between pulses. This is not the case at these low repetition rates.

Three HF vibrational-rotational transitions were observed

to lase; the $P_2(6)$, $P_2(5)$, and $P_2(4)$ transitions (see page 81 and table II). The results already presented include all of these transitions. The total multiline energy per pulse observed was 156 μJ.

The $P_2(6)$ transition was studied by itself. 88μJ was measured as the average energy per pulse. With a .221" diameter aperture, the measured average energy per pulse was 37.5 μJ. TEM 00 operation was achieved with this .221" aperture. A plot of energy/pulse versus aperture size in shown in figure 38.

No $\upsilon=1$ to $\upsilon=0$ transitions were observed. Raytheon observed no $P_1(J)$ transitions above 2000 pps, due to the decreased efficiency of the chemical scrubber [3:43]. It is likely that the chemical scrubber's performance has been degraded to the point that it will not remove sufficient ground state HF to establish a population inversion between the $\upsilon=1$ and $\upsilon=0$ levels even at 100 pps.

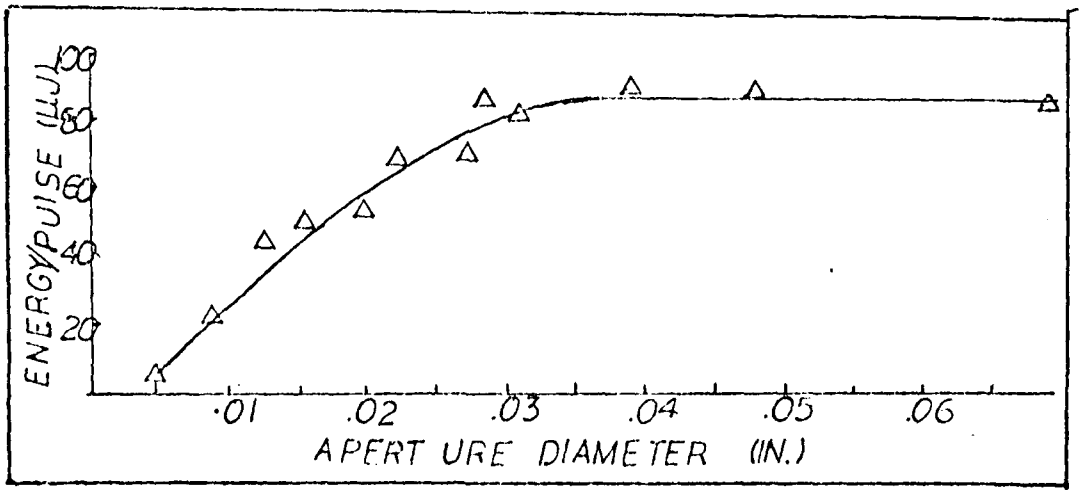


Figure 38.

Energy/Pulse vs Aperture Diameter

The spatial distribution of power within the HF beam was investigated for three cases: (1) multiline operation, (2) single $P_2(6)$ line, TEM 00 mode operation, and (3) with external focusing optics for the $P_2(6)$ TEM 00 case. No similar investigation was reported by Raytheon.

Figures 39 - 44 present representative spot shapes for the three cases. From the full set of spot size measurements as a function of axial distance, beam divergence was calculated and the spot sizes versus axial position are shown in figures 45 - 46. A time resolved study of the pulse shapes was not conducted.

The multiline HF beam profile is certainly non-Gaussian. This is not merely a result of higher order transverse modes. Spatial inhomogeneities in the lasing medium also contribute to the features of the beam profile. The uniformity of the discharge is important as well.

Turbulence within the gas flow and local nonuniformities in the concentrations of reactants and contaminants will affect the local gain. Purely random fluctuations will not persist and therefore will not be evident in the measured profiles, however.

Several persistent features in the profiles are observed. The multiline profiles exhibit a "flat top" across about one-half of the FWHM in the vertical direction. This is a result of aperturing by the cathode - anode structure. In the horizontal direction, the profiles exhibit a long tail in the up-flow direction. This is likely a result of a nonuniform electric discharge.

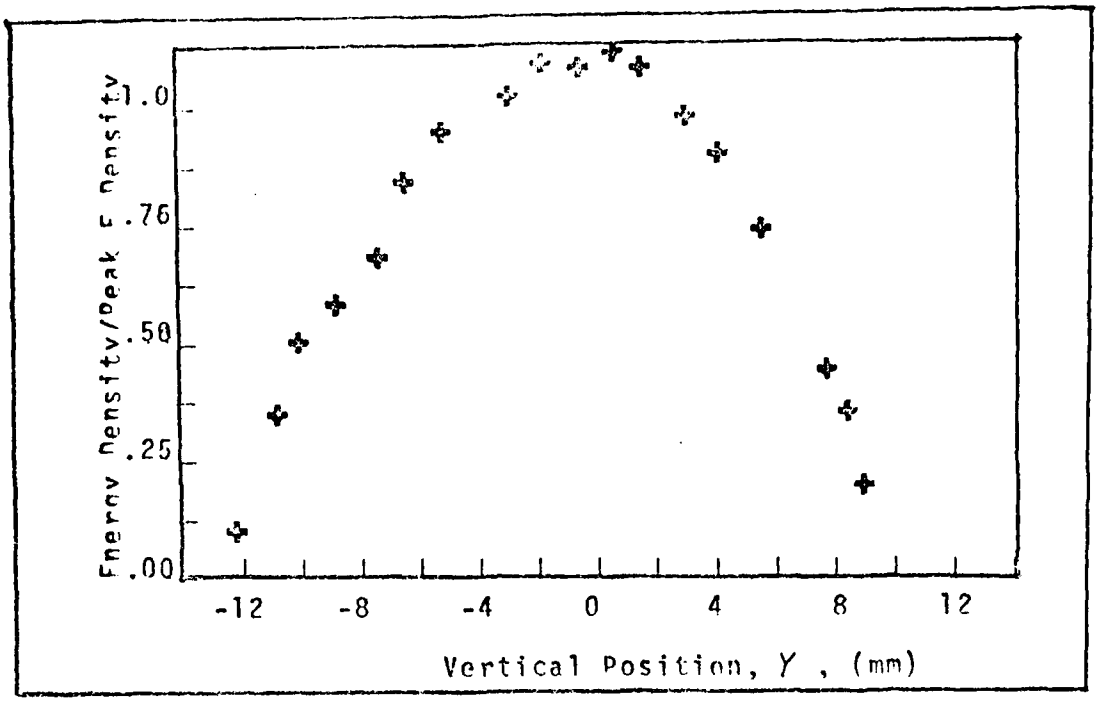


Figure 39
HF Spot Shape: Multiline - Vertical

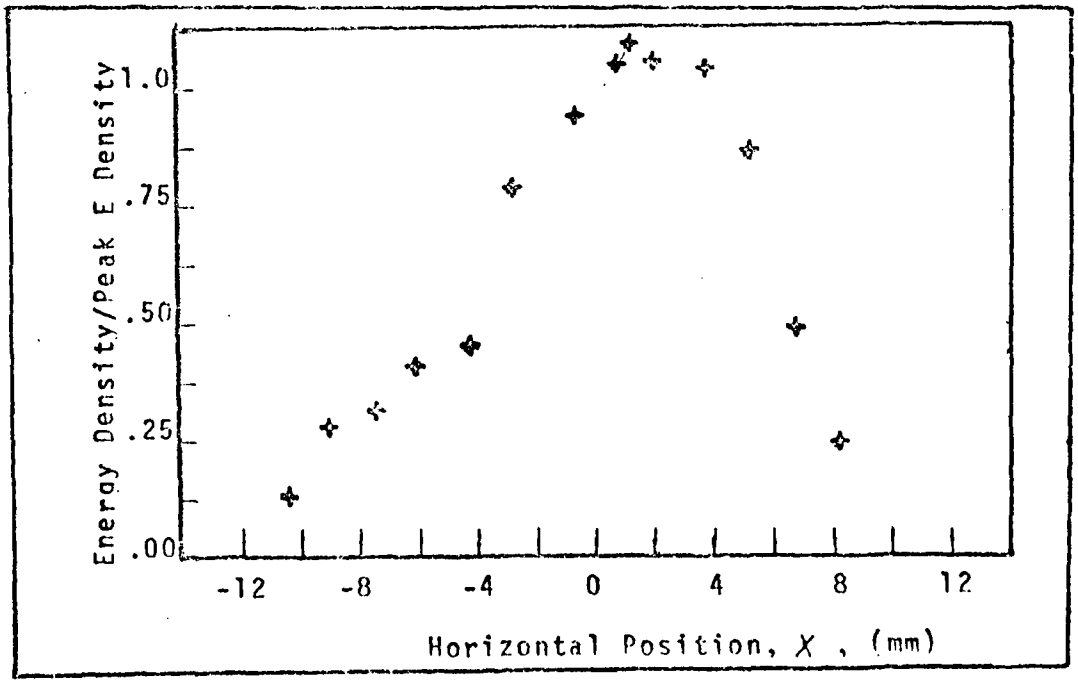


Figure 40.
HF Spot Shape: Multiline - Horizontal

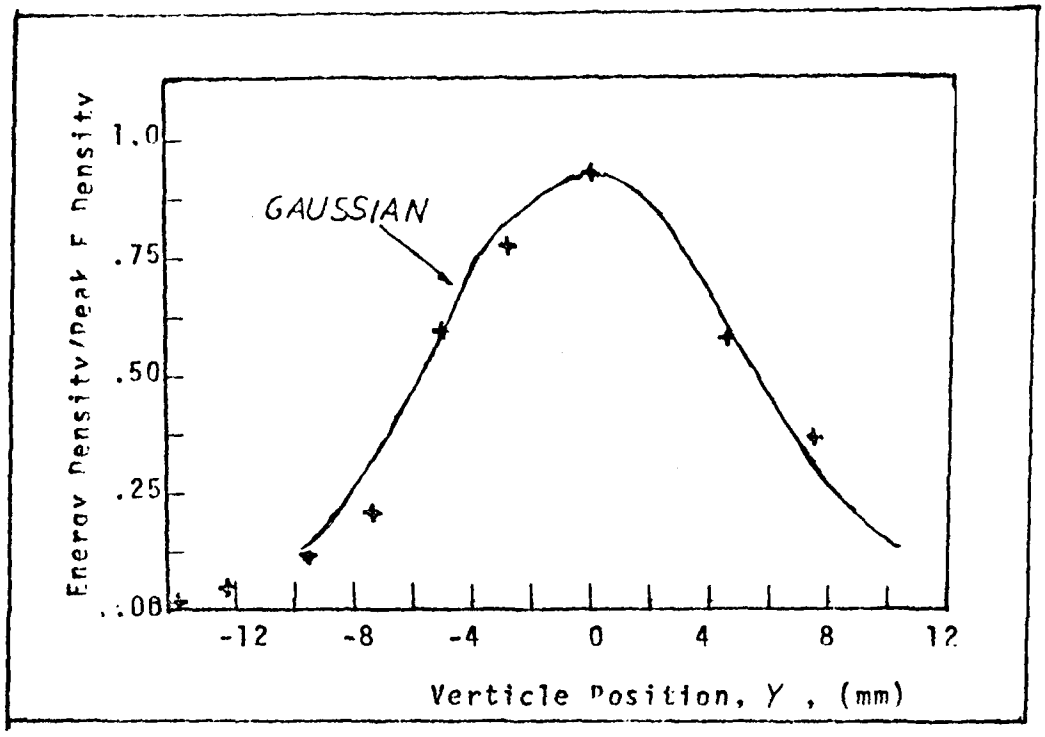


Figure 41.
HF Spot Shape: Singleline - Vertical

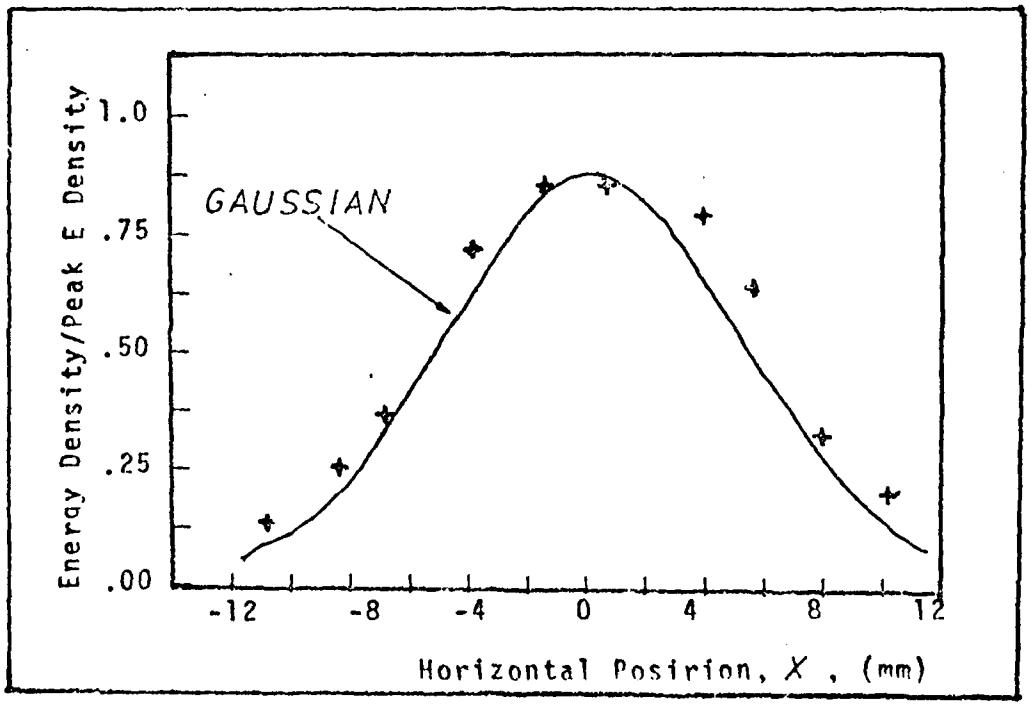


Figure 42.
HF Spot Shape: Singleline - Horizontal

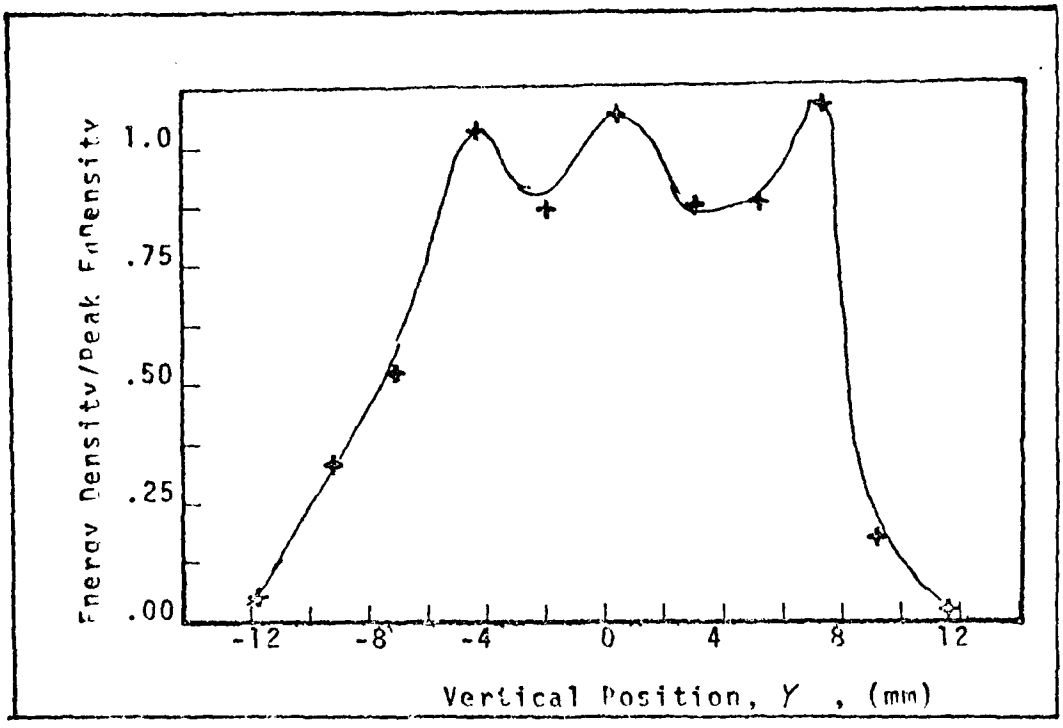


Figure 43.
HF Spot Shape: Focused-Vertical

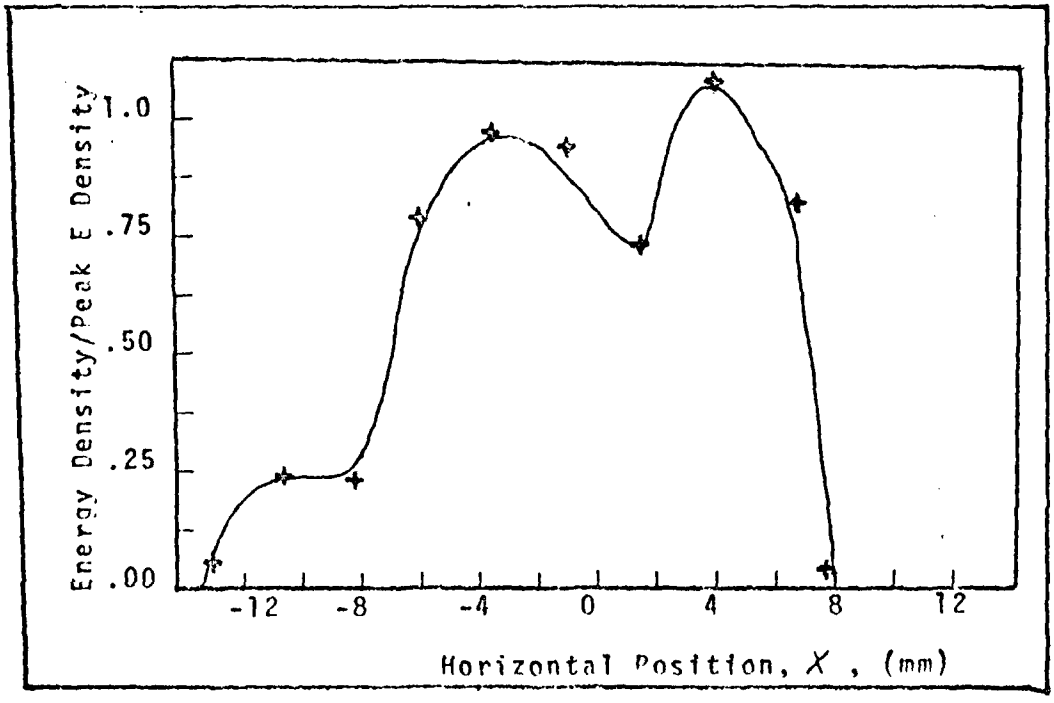


Figure 44.
HF Spot Shape: Focused - Horizontal

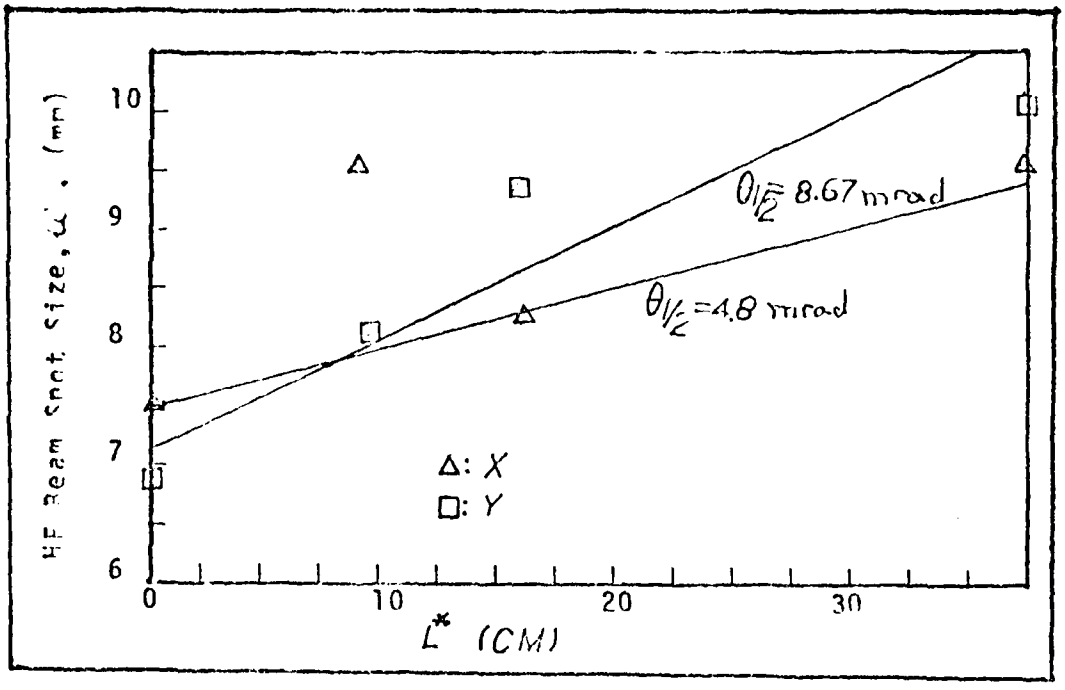


Figure 45.
HF Beam Divergence: Multiline

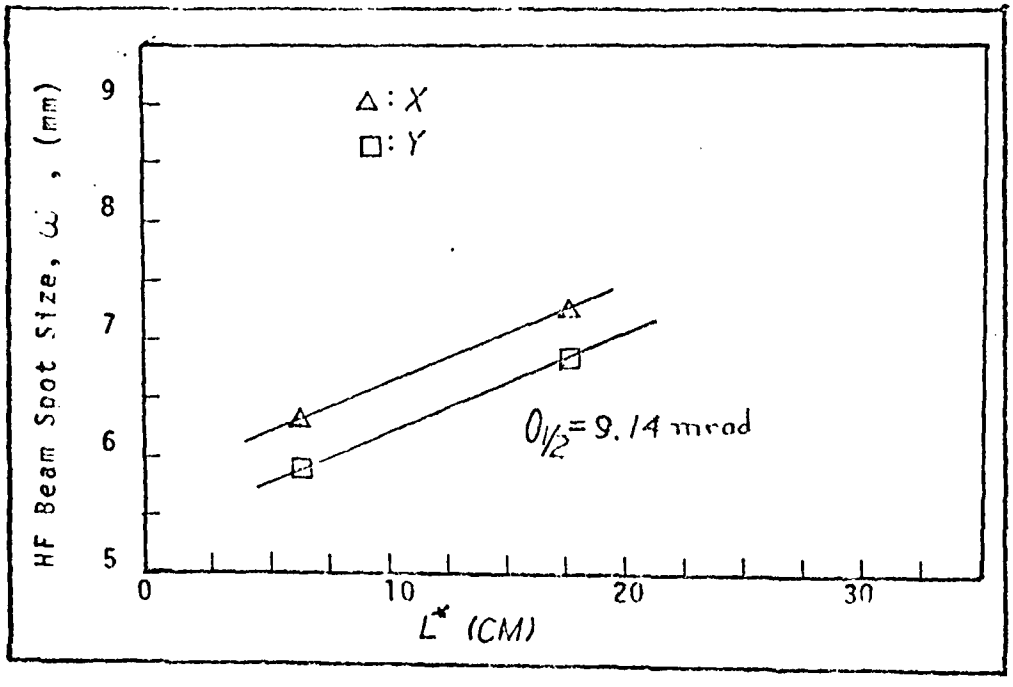


Figure 46.
HF Beam Divergence: $P_2(6)$ TEM 00

The single $P_2(6)$ transition with the .221" diameter aperture corresponds very nearly to a gaussian profile, indicating the TEM 00 mode.

The focused $P_2(6)$ beam has several peaks in its spatial energy distribution. This poor beam quality is probably due to imperfect lensing.

The full set of beam profiles at various axial locations were used to establish the beam divergence. The spot size was taken as the half-width at the 1/e power point of each profile.

The far field condition is

$$Z \gg \frac{\pi \omega_o^2}{\lambda} = 1.3 \text{ METERS} \tag{158}$$

where $\omega_o$ is the beam waist, $\omega_o = 1.09\omega_{m}$ [3:48]. None of the beam profiles were measured in the far field. In the near field, the spot size as a function of axial distance, $Z$, is

$$\omega = \omega_o \sqrt{1 + \left(\frac{\lambda Z}{\pi \omega_o^2}\right)^2} \tag{159}$$

where $\omega_o$ is the beam waist [34]. Then,

$$\delta\omega = \omega_o Z \frac{\lambda}{\pi \omega_o^2} \tag{160}$$

Or,

$$\Delta\omega = \frac{\lambda}{\pi\omega_o} \Delta Z \frac{1}{\sqrt{1 + \left(\frac{\pi\omega_o^2}{\lambda Z}\right)^2}} \tag{161}$$

Let

$$L^* = \frac{Z}{\sqrt{1 + \left(\frac{\pi\omega_o^2}{\lambda Z}\right)^2}} \tag{162}$$

Then

$$\Delta\omega = \theta_{1/2} \Delta L^* \tag{163}$$

where $\theta_{1/2}$ is the far field beam divergence.

The plots in figures 55 and 56 are based on this new variable $L^*$ , to find the far field beam divergence from the near field measurements. The resulting beam divergences are summarized in table IV.

Table IV.

Beam Divergence

| Case | | (mrad) |
|---|---|---|
| Multiline | Y | 8.7 |
| | X | 4.8 |
| $P_2(6)$ TEM 00 | Y | 9.1 |
| | X | 9.1 |

Raytheon gives a value of 1.4 mrad , based on a theoretical calculation and the cavity design [3:49].

Pulse Shapes

The power pulse shapes for HF and $CO_2$ are illustrated in figures 47-48. The data is taken from photographs of oscilloscope traces and the calibration from voltage to power, 60 W/Volt, is based on the total area under the power curve ,

$$E = \int P\,dt \tag{164}$$

equal to the average energy per pulse of 37.5 μJ.

For the HF pulse, the full-width at half-maximum is 106 ns, total energy, 37.5 μJ, and peak power .46 kW. For the $CO_2$ pulse, the FWHM is 26 ns. No total energy calibration

for the $CO_2$ curve was possible because the thermal energy detector was insufficiently sensitive to measure the lower power $CO_2$ signal. In contrast, Raytheon observed a 90 ns $CO_2$ pulse for a 100 us, 1.8 mJ HF pump pulse.

The reduced $CO_2$ pulse width observed in this study is a result of reduced intensity of the HF pump pulse. Threshold lasing conditions for the $CO_2$ gas are reached only at the peak of the most intense HF pulses. The time interval over which threshold pumping is achieved is reduced to a small interval across the top of the HF pulse.

This conclusion is supported by several observations. The pulse-to-pulse variation in HF power is as large as a factor of six. $CO_2$ lasing was observed for one out of 3-5 HF pulses. The pulse shapes of figures 47 and 48 suggest a reasonable value for threshold pumping of 300 $W/cm^2$.

Figure 49 compares the pulse shape predicted by the kinetic theory of figure 3 and the observed HF pulse normalized to a 1.5 mJ total energy. The zero of the time scale for the actual HF pulse is taken at 140nsec, to align the peaks of the two pulses. No measurement of the delay between electric discharge initiation and pulse initiation or of delays in the wiring or equipment were made.

The FWHM of the two curves agree very closely. The two curves diverge slightly at low power. No consideration of losses or threshold pumping was included in the kinetic model and this probably accounts for the divergence at lower powers.

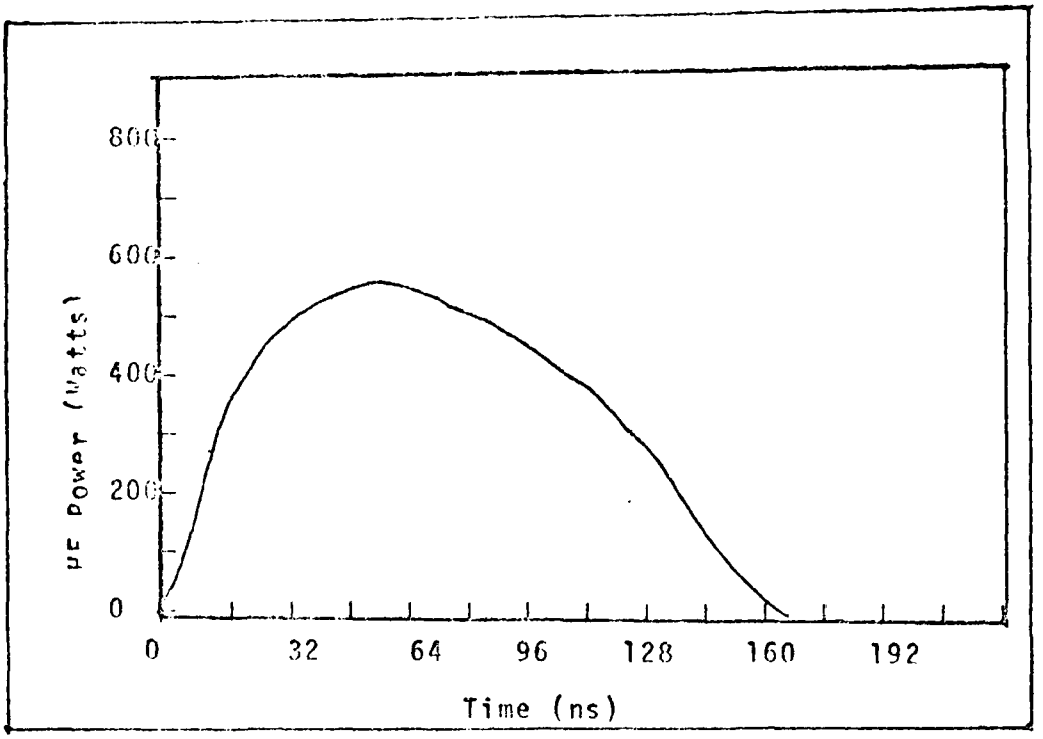


Figure 47.
HF Pulse Shape

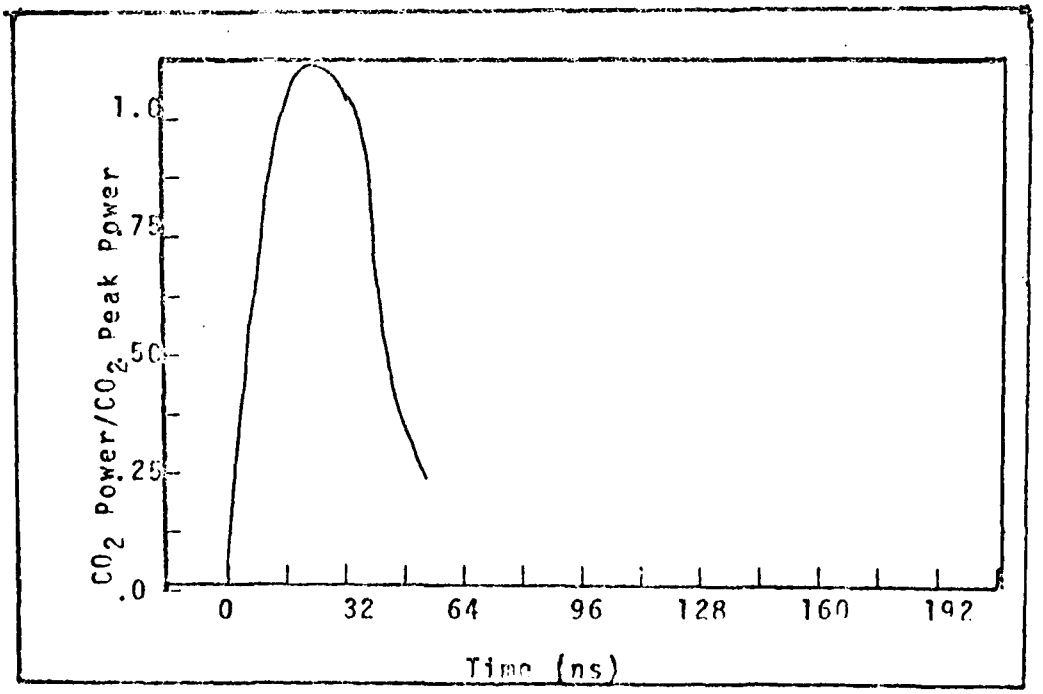


Figure 48.
$CO_2$ Pulse Shape

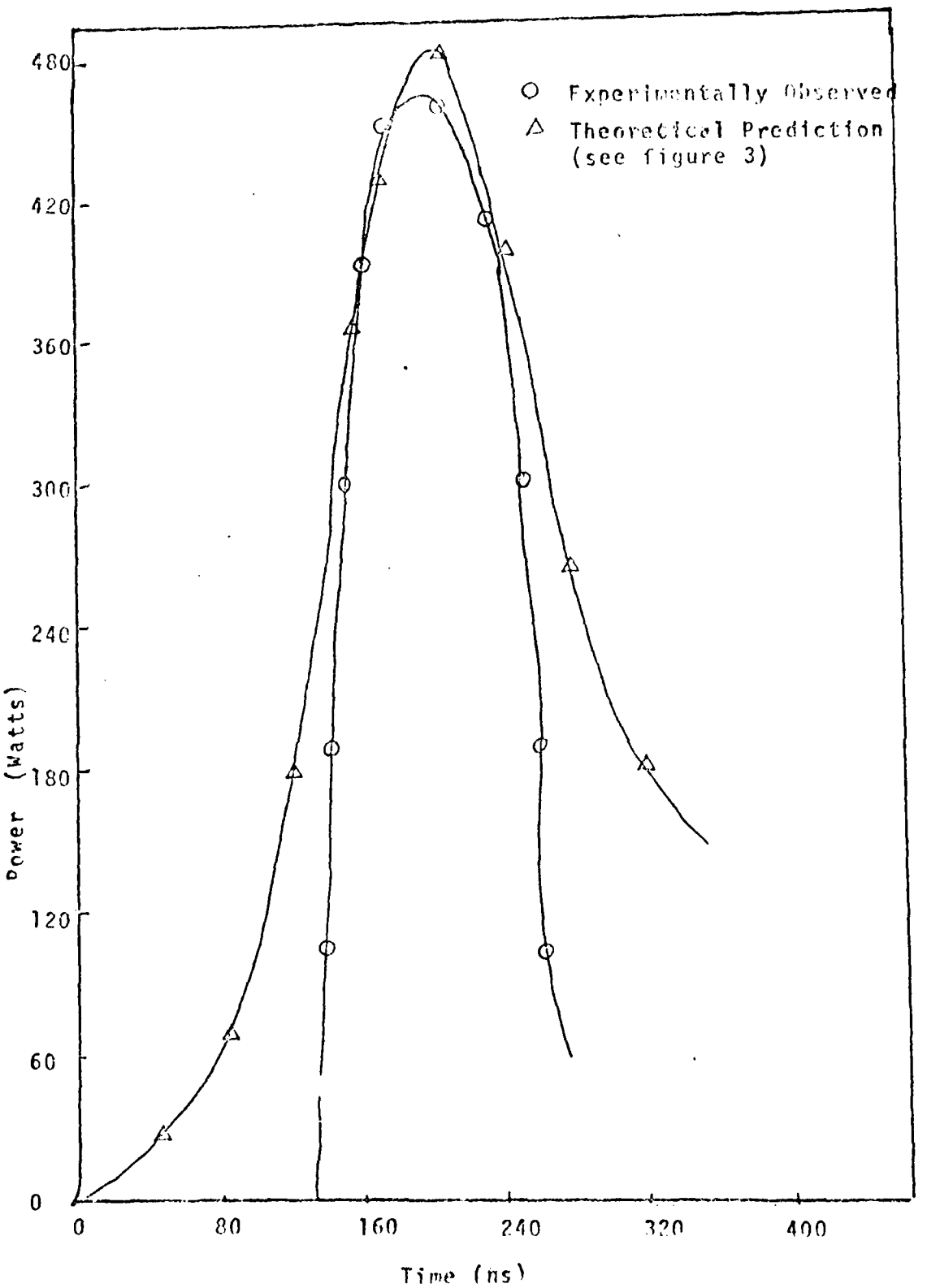


Figure 49.
HF Pulse Shapes

The HF pulse was normalized to 1.5 mJ total energy which is a factor of forty greater than observed in the current study. The difference in magnitude is a result of a number of factors. First, no losses were included in the theoretical model. Aperturing, scattering, and alignment losses were not considered. Certainly the aperture installed in the cavity to force the beam to the TEM 00 mode reduces the output power. Without the aperture , an energy of 88 mJ was measured. Secondly, the model neglected the formation of $H_2S$ and other contaminants in the flow. $H_2S$ is particulary efficient at depopulating excited HF molecules. This cause of reduced power may indeed be significant. Raytheon obtained an 1.8 mJ $P_2(6)$ pulse energy with clean chemical scrubbers.

Optical Pumping

The absorption of the HF $P_2(6)$ laser transition by the $^{12}C^{18}O_2$ molecules as observed experimentally ( $\triangle$ ), predicted theoretically ( $\circ$ ), and as observed by Raytheon ( $\square$ ) are presented in figure 50. The absorption coefficient is related to incident and transmitted power by

$$\alpha = \frac{1}{L} \ln \frac{P_{TRANS}}{P_{INC}} \qquad (165)$$

The three curves have significantly different slopes and illustrate the effect of saturation. The HF intensity in the Raytheon experiment was $10^4$ larger than in this study. The 000 - 101 transition is saturated at this higher intensity (see page 53). In the saturated case, a significant number of $CO_2$ molecules are pumped to the 101 level, reducing the total number of absorbers that the remainder of the HF

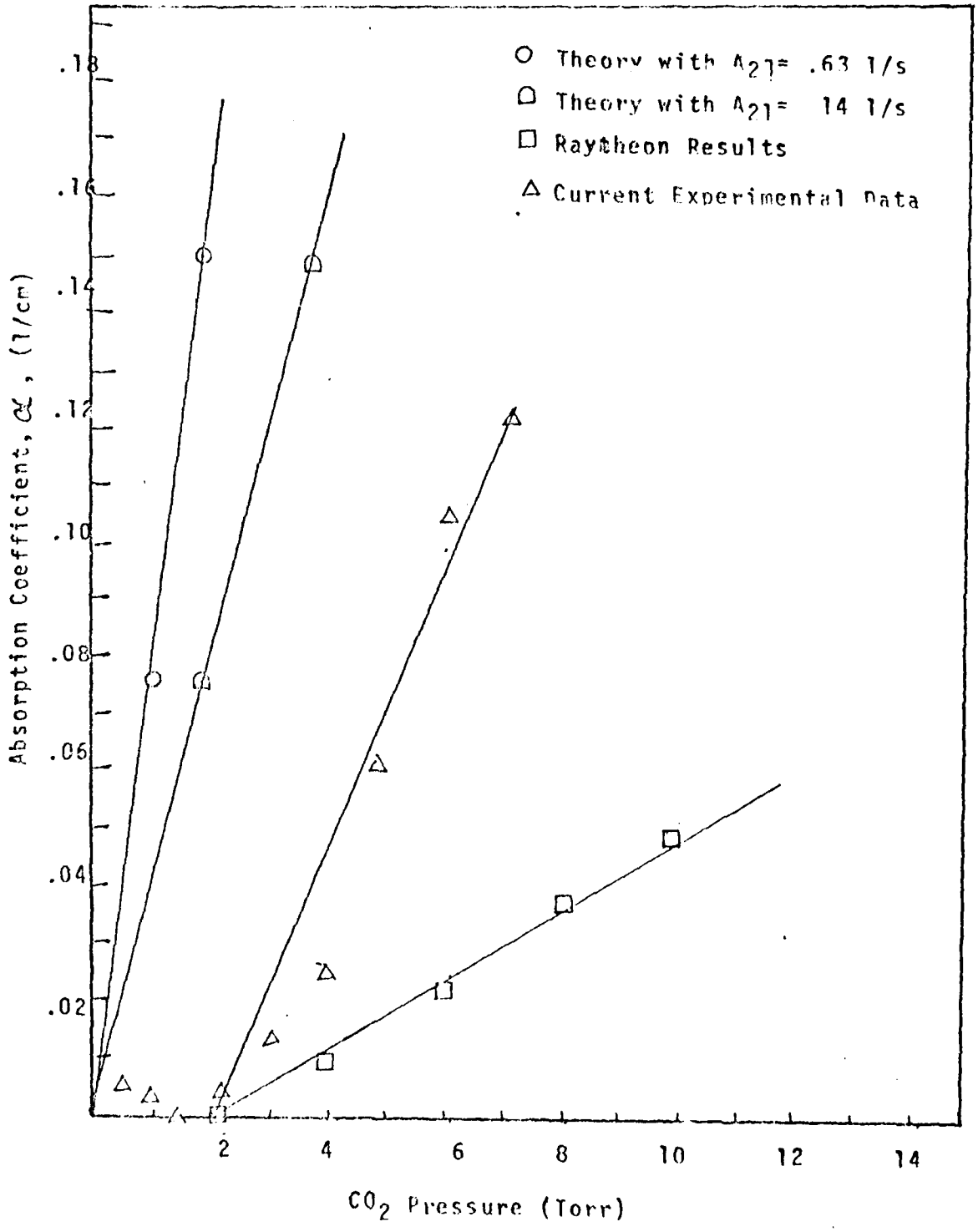
Theory with $A_{21}$= .63 1/s
Theory with $A_{21}$= 14 1/s
Raytheon Results
Current Experimental Data
Absorption Coefficient, $\alpha$, (1/cm)
.18
.16
.14
.12
.10
.08
.06
.04
.02
2
4
6
8
10
12
14
$CO_2$ Pressure (Torr)

Figure 50.

pulse observes. This reduces the total absorption of the HF beam. Therefore, the Raytheon curve should lie below the results from this study.

The same reasoning explains why the theory curve is substantially above both of the experimental curves. The theory assumed no population of the upper level, $N_2 = 0$. That is, the result holds for a negligibly intense probe beam. Note that the slope of the theoretical curve is sensitive to the value of the Einstein coefficient for the 100 - 000 transition (eq. 112.). The second value for $A_{21} = 4.5$ [29] is 22 times larger than the value given by refernce [62] and used on page 38. There is a substantial uncertainty in the value of this coefficient.

Instability

Throughout this investigation, problems with power fluctuation were encountered. This was most pronounced in the $CO_2$ absorption of the HF beam. The instability was also observed in oscilloscope traces. An example trace is shown in figure 51.

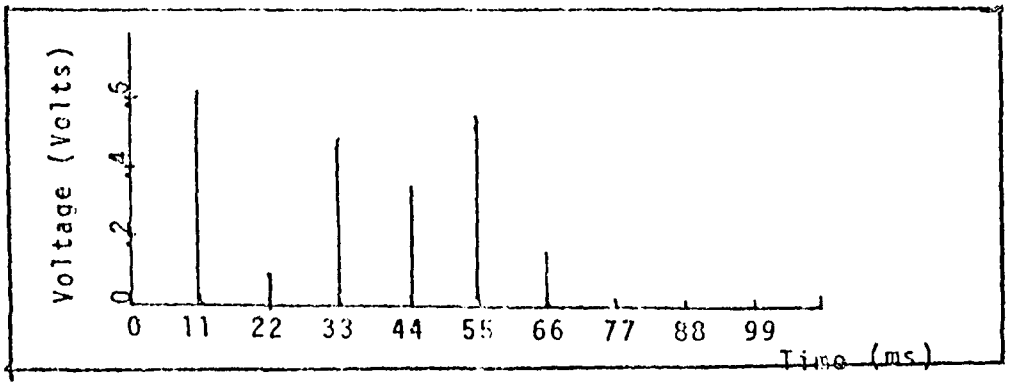


Figure 51.

HF Power Instability

The HF power varies on a pulse-to-pulse basis by as much as a factor of six. This variation is partially explained by a nonuniform $SF_6/H_2$ gas flow with contaminants and by varying electric discharge quality.

There exists an instability in HF frequency as well. This is most readily noted by observing the fluctuation in % absorption of the HF beam in the $CO_2$ cell with all variables held constant. The problems of power instability are removed by looking at the ratio of transmitted to incident power. This plot of transmitted to incident power as a function of time is shown in figure 52. A plot for a slow sweep of the PZ crystal voltage is also presented. The only explanation for the variations observed in these plots is a substantial frequency instability. Note that no correlation between frequency and PZ crystal voltage is observable, indicating that the frequency stability completely obscures the frequency changes caused by the PZ crystal.

The variation in the magnitude of the power instability as a function of repetition rate, discharge voltage, and pressure was studied and the results are presented in figures 53 -55. The best operating point is 20 pps, 14 kV, and 88 torr. Operating at 12 kV and 80 torr is nearly as good, but a 100pps repetition rate is a little high. Even at the optimum operating point, the signal to noise ratio is

$$\frac{S}{N} = 20R3 \qquad (166)$$

The frequency instability is a severe problem. With no

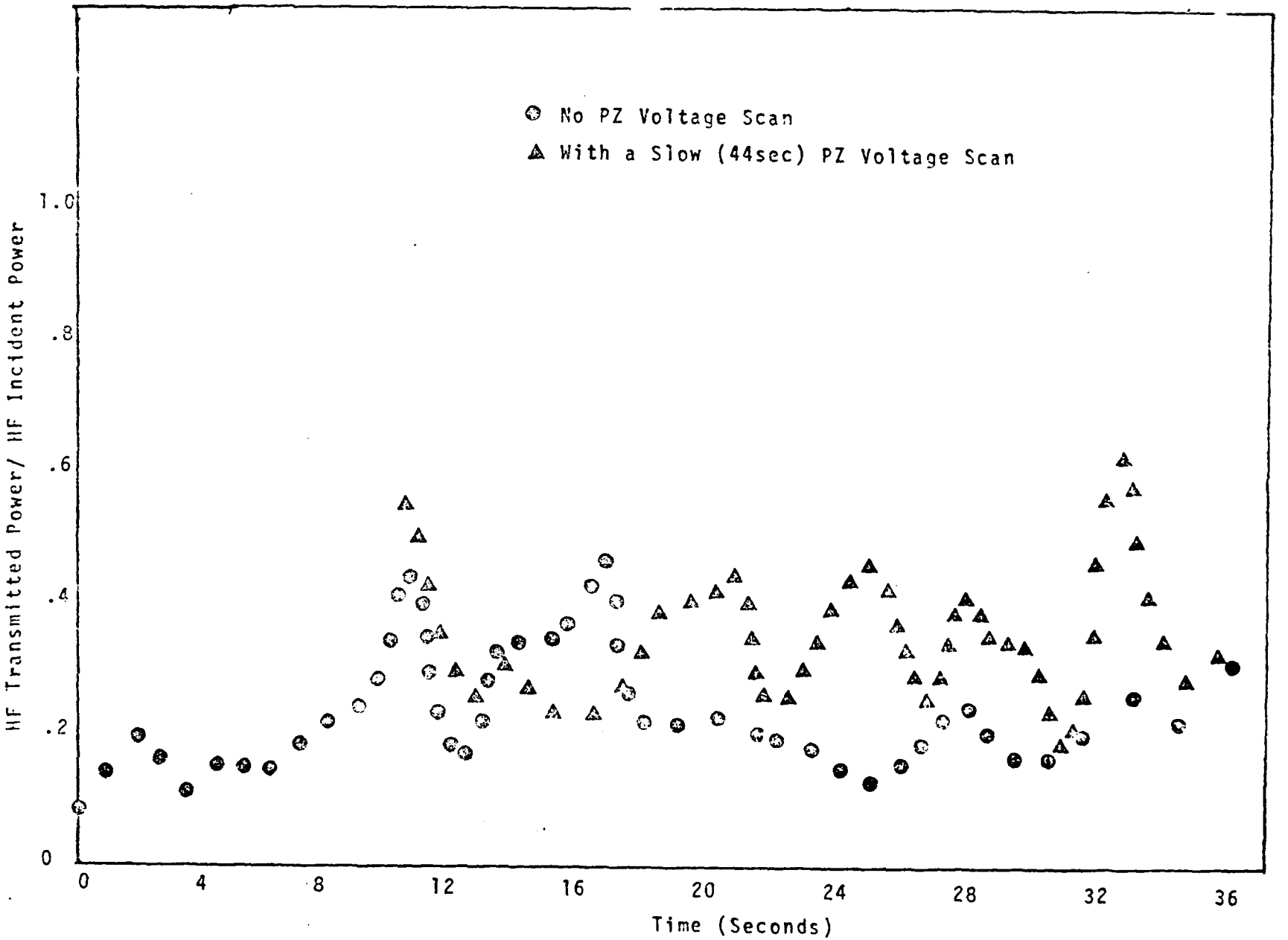


Figure 52
*HF Frequency Stability*

control over frequency, the actual frequency must be measured throughout time and correlated to the $CO_2$ power. Even more importantly, the RF frequency must be stable during the period of integration, otherwise only an average frequency power is observed. The frequency instability is worse than 1 ms, the period of integration in this study. No study of $CO_2$ output power with RF frequency was possible in this investigation. Recommendations concerning this problem are presented in the conclusions section.

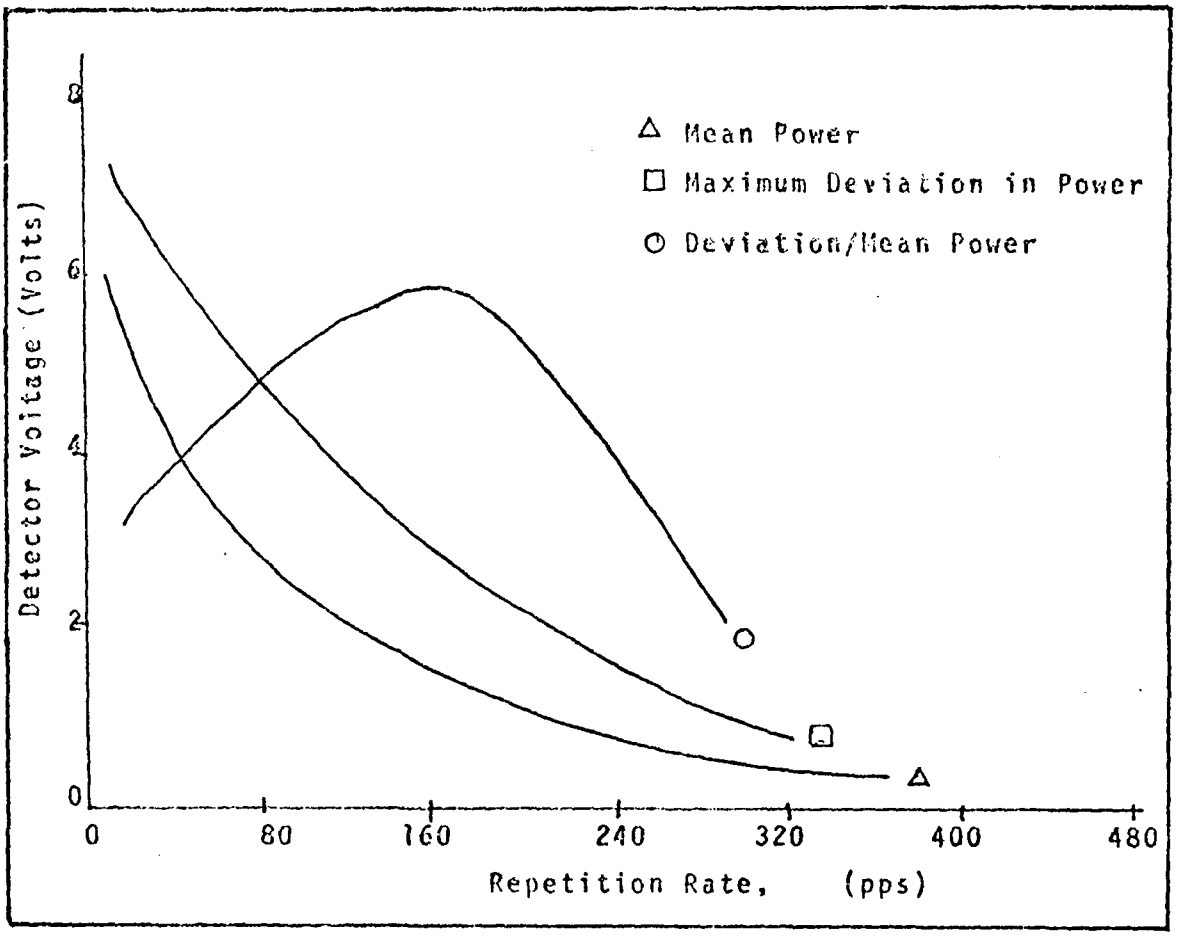


Figure 53

Power Instability versus Rep Rate

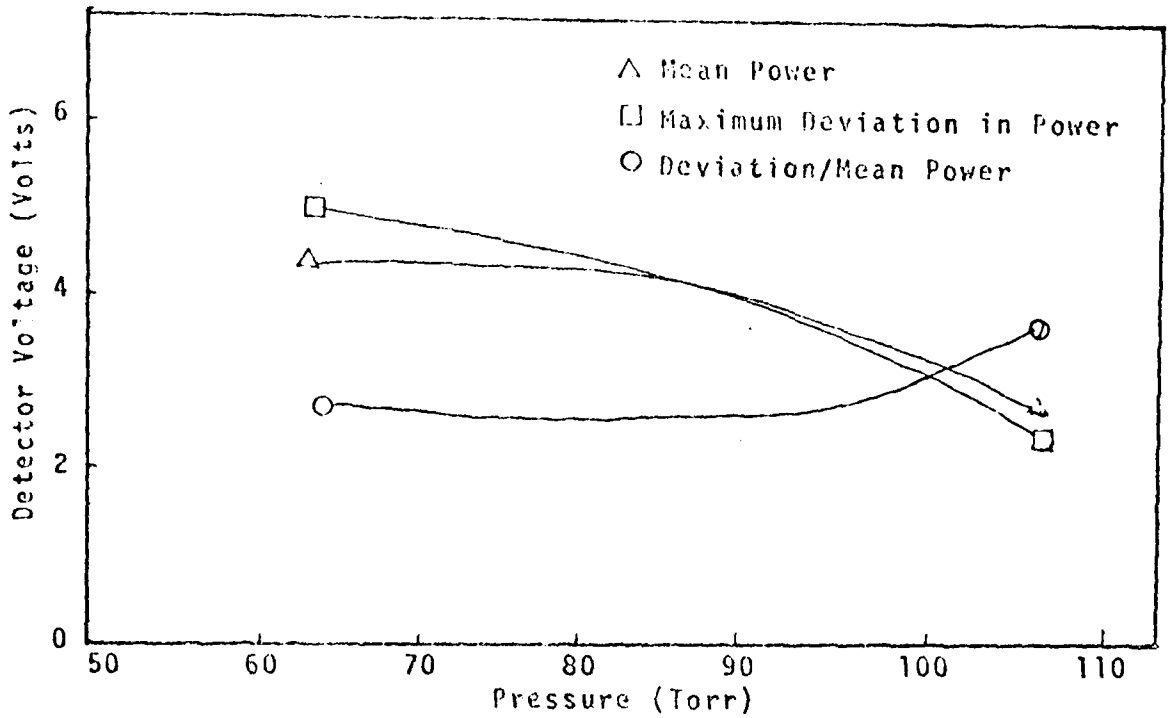


Figure 54
Power Instability vs Pressure

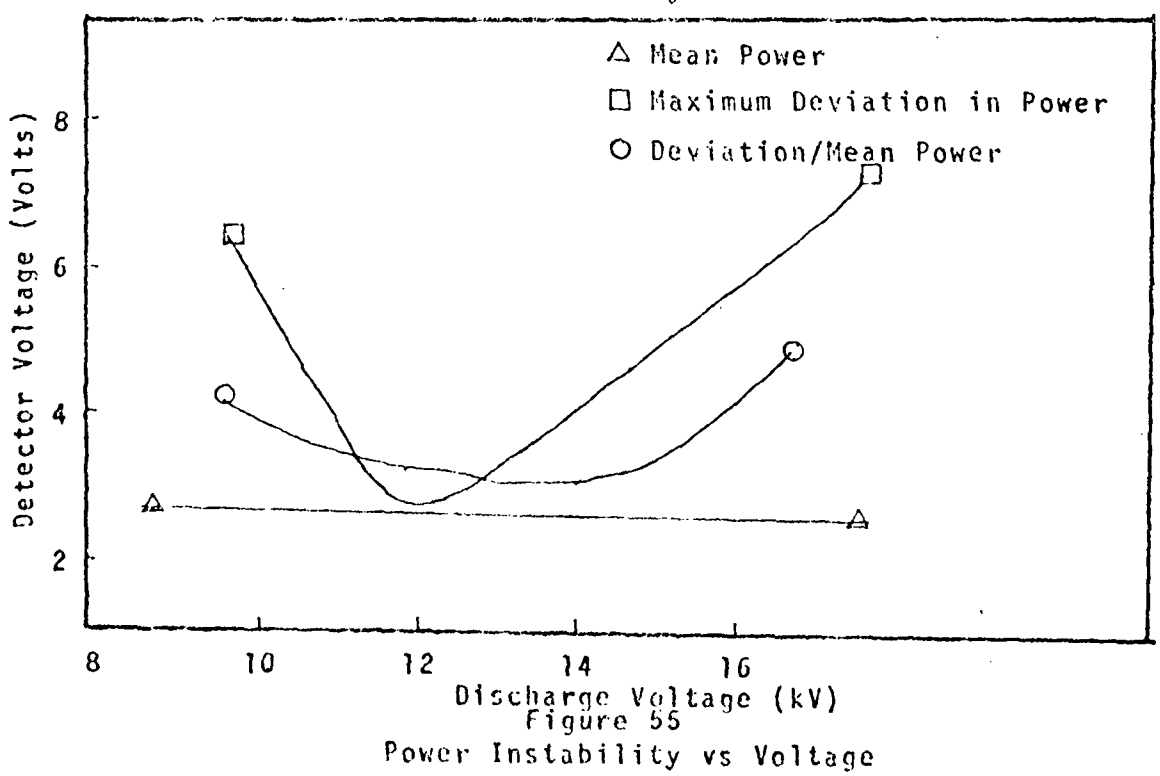


Figure 55
Power Instability vs Voltage

## Conclusions and Recommendations

A complete study of the HF-pumped $CO_2$ laser developed by the Raytheon Corporation has been completed. Background theory for the design and performance of the laser system has been presented and applied. The HF laser's performance was experimentally characterized and output power maximized with respect to repetition rate, discharge voltage, pressure, gas mixture, and stability. Optical pumping of the 101 level of $^{12}C^{18}O_2$ by the HF $P_2(6)$ transition established lasing action to the 100 $CO_2$ level. The optical pumping was studied through an absorption experiment. No measurement of $CO_2$ output power as a function of HF frequency was made, due to a large HF frequency instability. Discrepencies between thoery and experiment on this frequency dependence was explained however. Pulse shapes were observed and shown to agree with the kinetic model developed in this study.

The HF laser was modified to conduct these investigations. The gas flow rate was controlled to reduce $SF_6$ consumption. The optical cavity was modified to accomodate an aperture and piezoelectric crystal for control of the cavity length. The trigger and discharge circuitry were repaired and modified. Reliability of the laser was addressed in the main text, including discussions of the discharge circuit and gas recirculation and scrubbing.

In this modified form, the laser's performance was maximized for power at 79% $SF_6$/21% $H_2$ , 88 torr total pressure,a 12 kV discharge voltage, and a 300 pps repetition rate. Stability in HF power was enhanced by reducing the repetition rate to 20 - 60 pulses/sec. Only 7 l/min flow rates were used. A

total multiline energy per pulse of 156 μJ was achieved with lasing on the $P_2(4)$, $P_2(5)$, and $P_2(6)$ transitions. An 88 μJ $P_2(6)$ single line energy was achieved and TEM 00 operation of the $P_2(6)$ transition achieved with an aperture of .221" diameter.

A beam divergence of 5-8 mrad multiline and 9mrad for the $P_2(6)$ transition was measured. Beam quality is rather poor, exhibiting the effects of aperturing, inhomogeneous gas flow and a nonuniform electric discharge.

A pulse-to pulse variation in power of a factor of six was the best power stability achieved. Frequency stability is worse than 200 MHz over a millisecond time interval.

Optical pumping of $^{12}C^{18}O_2$ by the HF $P_2(6)$ transition produced $CO_2$ lasing from the $(10°1)_{II}$ level to the $(10°0)_{I}$ level. Pumping was near threshold conditions, and as a result, $CO_2$ lasing was erratic, low intensity, and exhibited a shortened pulse width of 26 ns. No investigation of the effect of HF frequency on $CO_2$ power was possible, due to the large HF frequency instability.

The optical pumping was studied through an absorption experiment. The absorption coefficient was shown to vary linearly with pressure over the 0 -7 torr pressure range, as predicted by the presented theory. The magnitude of the absorption is less than predicted due to saturation.

HF and $CO_2$ pulse shapes were observed with FWHM of 106 ns and 26 ns, respectively. The HF pulse width agrees well with the kinetic model presented. This model was based on the HF cold reaction and electron attachment to

$SF_6$ to produce atomic flourine.

Throughout this study, results were compared with the experimental data obtained by Raytheon, using the same HF laser and basic set-up. The issue of $CO_2$ power depending on HF frequency was addressed and the apparent contradiction between theory and prior experimental results explained.

Raytheon observed no significant variation in $CO_2$ power with changes in HF frequency over a 300 MHz range. A number of factors explain this observation. First, and foremost, the HF laser's frequency is unstable and the random fluctuation in frequency completely obscurs the effect of a piezoelectric crystal. The frequency varies greatly during the period of observation and no meaningful power observations are possible without actively stabilizing the HF cavity. Secondly, under the conditions of the Raytheon study, the $CO_2$ transition is saturated as suggested by the authors of the Raytheon report. Calculations presented in the theory section support this claim of saturation. Finally, the $CO_2$ cell was not pumped uniformly in the Raytheon study , the beam was not Gaussian, and several axial modes were present in the HF pump beam.

Several recommendations may be made based on these results and conclusions.

The HF laser's performance could be enhanced by reducing contaminants in the $SF_6/H_2$ gas flow. A design modification to allow frequent cleaning of the chemical scrubbers would be a great advantage. Reducing the concentration of contaminants, particularly $H_2S$ would enhance power and power

stability.

To investigate the dependence of $CO_2$ power on HF frequency, an active method of stabilizing the HF cavity is proposed. In this way the frequency instability problem could be overcome and the HF frequency easily controlled.

A direct investigation of the low signal gain of the optically pumped $CO_2$ system should be undertaken to validate the optical pumping theory presented on pages 43-47. Studying the ratio of forward to backward $CO_2$ powers may also provide insight into the nature of the optical pumping.

## Conclusion

An optically pumped molecular laser was operated and characterized. The HF pump laser's performance was documented and the kinetics of the elctric discharge analyzed. The optical pumping scheme was studied by absorption measurements. The apparent contradiction between theory and experiment on the dependence of $CO_2$ power on HF frequency was resolved, but the frequency-power dependence was not experimentally established.

## Bibliography


1. Grasyuk, A.Z., Letokhov, V.S., and Lobko, V.V., "Molecular Infrared Lasers Using Resonant Laser Pumping (review)," Soviet Journal of Quantum Electronics, 10(11), 1317 - 1338, (Nov 1980).

2. Jones, C.R., "Optically Pumped Mid-IR Lasers," Laser Focus, 68-74, (Aug 1978).

3. Rudko, R.I., Bua, D.P., Drozdowicz, Z., and Linhares, S.J., "Electric-Pulse-Initiated Chemical Laser," AFWAL-TR-81-1054 under contract F33615-77-C-1046, (1981).

4. Kompa, K.L., and Pimentel, G.C., "Hydroflouric Acid Chemical Laser," Journal of Chemical Physics, 47, 857-858, (1967).

5. Spencer, D.J., Tacobs, T.A., Mirels, H., and Gross, W.F., "Continuous Wave Chemical Laser," International Journal of Chemical Kinetics, 1, 493-494, (1969).

6. Deutsch, T.F., "Molecular Laser Action in Hydrogen and Deuterium Halides," Applied Physics Letters, 10, 234-236, (Apr 1967).

7. Batowskii, O.M., Vasil'ev, G.K., Makarov, E.F., and Tal'roze, V.L., "Chemical Laser Operating on Branched Chain Reaction of Flourine with Hydrogen", JETP Letters, 9, 200-201, (1969).

8. Jensen, R.J., "Electric Discharge Initiated $SF_6 + H_2$ and $SF_6$ + HBr Chemical Lasers", Chemical Physics Letters, 7, 627-629, (1970).

9. Brandelik, J.E., and Paulson, R.F., "Operation of an HF ($SF_6 + H_2$) TE Laser at 10 kHz Pulse Repetition Rates", IEEE Journal of Quantum Electronics, QE-13, 933-934, (Dec 1977).

10. Buazek, C.J., Freiberg, R.J., Hinchen, J.J., Chenausky, P.P., and Wayne, P.J., "Premixed cw Chemical Laser", Applied Physics Letters, 17, 514-516, (Dec 1970).

11. Jacobson, T.V., Kimbell, G.H., and Snelling, D.R., "A High-Repetition Rate Chemical Laser", IEEE Journal of Quantum Electronics, QE-2, 496-497, (Apr 1973).

12. Voinov, A.M., Doubysh, L.E., Kazakevich, A.T., Mel'nikov, S.P., and Sinyankii, A.A., "High Pressure Radiation-Chemical Laser Initiated by a Fast Electron Beam From a Coaxial High-Voltage Diode", Soviet Journal of Quantum Electronics, 7, 234-235, (Feb 1977).

13. Spencer, D.J., Mirels, H., Jacobs, T.A., and Gross, R.W.F., "Preliminary Performance of a cw Chemical Laser", Applied Physics Letters, 16, 235-237, (Mar 1970).

14. Bashkin, A.S., Orayevskii, A.N., and Tovarnshov, V.N., "Energy Characteristic of an Electron-Beam-Initiated HF Chemical Laser", Soviet Journal of Quantum Electronics, 7, 94-95, (Jan 1977).

15. Pummer, H., Breitfeld, W., Redler, H, Klema, G.,and Kompa, K.L., "Parametric Study of a 10-J Hydrogen Flouride Laser", Applied Physics Letters, 22, 319-320, (Apr 1973).

16. Pummer, H. and Kompa, K.L., "Investigation of a 1-J Pulse Discharge-Initiation HF Laser", Applied Physics Letters, 20, 356-357, (May 1972).

17. Wenzel, R.G., and Arnold, G.P., "A Double-Discharge-Initiated HF Laser", IEEE Journal of Quantum Electronics, QE-8, 26, (Jan 1972).

18. Chester, A.N., "Chemical Lasers, A status Report:, Laser Focus, 28, 25, (1971).

19. Gross, R.W.F., and Bott, J.F., Handbook of Chemical Lasers, New York, John Wiley and Sons, 1976.

20. Hinchen, J.J., "Operation of a Small Single-Mode Stable cw Hydrogen Flouride Laser", Journal of Applied Physics, 45, 1818, (Apr 1974).

21. Mann, D.E., Thrush, B.A., Lide, D.P., Ball, J.J., and Acquista, N., "Spectroscopy of Florine Flames. I. Hydrogen Flourine Flow and the Vibrational-Rotational Emission Spectrum of HF", Journal of Chemical Physics, 34, 420-431, (Feb 1969).

22. Pressley, Handbook of Lasers with selected Data on Optical Technology, Cleveland: CRC Press, (1971), 317-318.

23. Buchwald, M.I., Jones, C.P., Fetterman, H.R., and Schlossberg, A.P., "Direct Optical Pumping of Multiwavelength $CO_2$ Laser", Applied Physics Letters, 29, 300-302, (Sep 1976).

24. Yariv, Amnon, Quantum Electronics, (Second Edition), New York: John Wiley and Sons, 1967.

25. Peterson, L.M., Arnold, C.B., and Lindquist, G.H., "Pulse HF Chemical Laser Linewidth Measurements using Time-Resolved Bleachable Absorption of HF Gas", Applied Physics Letters, 24, 615-617, (June 1974).

26. Siegman, A.E., An Introduction to Lasers and Masers,New York: McGraw-Hill, 1971, 120.

27. Chester, A.N. and Moss, L.D., "Study of the HF Chemical Laser by Pulse-Delay Measurements", IEEE Journal of Quantum Electronics, QE-8, 1-13, (Jan 1972).

28. Sienko, M.J. and Plane, R.A., Chemistry, (Fifth Edition), New York: McGraw-Hill, 1976.

29. Omenetto, N., Analytical Laser Spectroscopy, New York: John Wiley and Sons, 1979, 128-129.

30. Davies J.T. and Vaughan, J.M., "A New Tabulation of the Voigt Profile", Astrophysical Journal, 137, 1302-1305, (1963).

31. Milonni, D.W., "Saturation of Anomolous Dispersion in cw HF Lasers", Applied Optics, 20, 1571-1578, (May 1981).

32. Herget, W.F., Deeds, W.E., Gails, M.M., Lovell, P.J., Nielson, A.H., "Infrared Spectrum of Hydrogen Flouride: Line Positions and Line Shapes Part II. Treatment of Data and Results", Journal of the Optical Society of America, 52, 1113-1119, (Oct 1962).

33. Jaffe, B., Cook, W.R., Jaffe, H., Piezoelectric Ceramics, New York: Academic Press, 1971.

34. Pedrotti, L.S., Class Notes from PH 7.43, Spring 1981, AFIT, WPAFB, OH.

35. Warren, W.R., "Reacting Flow and Pressure Recovery Processes in HF/DF Chemical Lasers", Acta Astronautica, 1, 813-834(1973).

36 Miresl, H., Hofland, R., and King, M.S., "Simplified Model of cw Diffusion Type Chemical Laser", AIAA Journal, 11, 156-164, (Jan 1973).

37. Cotton, F.A. and Wilkinson, G., Advanced Inorganic Chemestry, New York: John Wiley and Sons, 1962, 534-539.

38. Weast, Handbook of Chemestry and Physics, (55th ED), Cleveland: CRC Press, 1974.

39. McDaniel, E.W., 'Collision Phenomenon in Ionized Gases, New York: John Wiley and Sons, 1964, 39.

40. Rohr, K., "Absolute Differential Cross Sections for $e^-$ - $SF_6$ scattering in the alg and tlu Resonance Region," Journal of Physics B, 12, L185-L188, (1979).

41. Lockett, A., Los Alamos Scientific Laboratory, cited as a private communicationby [42].

42. Lyman, J.L., "Computer Model of the $SF_6$ - $H_2$ Electric Discharge Chemical Laser", Applied Optics, 12, 2736-2747,(1973).

43. Fehsenfeld, T.C., "Electron Attachment to $SF_6$", Journal of Chemical Physics, 53, 2000-2004, (Sep 1970).

44. Hatsuzawa, H. and Sakamoto, S., "Long-lived Electron Beam Pre-Irradiation Effect in a Impact $SF_6/H_2$ Laser", Japanese Journal of Applied Physics, 19 L509-L512, (Sep 1980).

45. McGeehan, J.P., O'Neill, R.C., and Craggs, J.D., "Negative Ion/Molecule Reactions in Sulphur Hexaflouride", Journal of Physics D, 8, 153-160, (1975).

46. Ahearn, A.J. and Nanney, N.B., "The Formation of Negative Ions of Sulfur Hexaflouride", Journal of Chemical Physics, 21, 119-124, (Jan 1953).

47. Asundi, R.K., and Craggs, J.D., "Electron Capture and Ionization Phenomenon in $SF_6$ and $C_7F_{14}$", Proceedings of the Royal Physical Society, 83, 611-618, (1964).

48. Curran, R.K., "Low energy Processes for $F^-$ Formation in $SF_6$", Journal of Chemical Physics, 34, 1969, (1961).

49. Fenimore, C.P., and Jones, G.W., "Decomposition of Sulfur Hexaflouride in Flows by Reaction with Hydrogen Gas", Combustion Flame, 8, 231, (1964).

50. Yariv, A., Introduction to Optical Electronics, (Second Ed), New York: Holt, Rinehart and Winston, 1976.

51. Golger, A.L. and Letokhov, V.S., "Population inversion Due to Saturation of Absorption in Molecular Rotational-Vibrational Transitions", Soviet Journal of Quantum Electronics, 3, 15-20, (1973).

52. Bushnell, A.H., Jones, C.P., Buchwald, M.I., Gundersen, M., "New HF Laser Pumped Molecular Lasers in the Middle Infrard", IEEE Journal of Quantum Electronics, QE-15, 208-209, (Apr 1979).

53. Osgood, P.M., "1 mJ Line Tunable Optically Pumped 16 Micron Laser", Applied Physics Letters, 28, 342-345, (May 1978).

54. Osgood, R.M., "optically Pumped 16 micron Laser", Applied Physics Letters, 28, 342-345, (Mar 1976).

55. Chang, T.Y., and Wood, O.R., "Optically Pumped 33 atm $CO_2$ Laser", Applied Physics Letters, 23, 370-372, (Oct 1973).

56. Wang, J.H.S., Finzi, J, and Mstrup, F.N., "CW Optically Resonance Pumped Transfer Laser in DF-$CO_2$ System", Applied Physics Letters, 31, 35-37, (July 1977).

57. Banwell, C.N., Fundamentals of Molecular Spectroscopy, (Second Edition), London: McGraw-Hill, 1972, 90.

58. Patel, "Gas Lasers", Lasers: A Series of Advances, Vol 3., edited by Levine, A.K., New York: Marcel Dekkowicz, (1970),

59. Subolev, M.N., and Sckovikov, V.V., "$CO_2$ Lasers", Soviet Physics Uspekhi, 10, 153-170, (1967).

60. Gordon, Howard and McCubbin, T.K., "The 2.8 μm Bands of $CO_2$", Journal of Molecular Spectroscopy, 19, 137-154, (1966).

61. Oberly, R. and Rao K.N., " Near IR Absorption Spectrum of Oxygen-18 Enriched $CO_2$", Journal of Molecular Spectroscopy, 40, 356-366, (1971).

62. Statz, H., Tang, C.L., Koster, G.F., "Transition Probabilities between lower states in Carbon Dioxide", Journal of Applied Physics, 37, 4275-4280, (1966).

63. Javan, A., "Theory of a Three Level Maser", Physical Review, 107, 1579-1589, (Sep 1957).

64. Feld M.S., and Javan, A., "Lase Induced Line Narrowing Effects in Coupled Doppler-Broadened Transitions", Physical Review, 177, 540-562, (Jan 1969).

65. Panock, R.L. and Temkin, R.J., " Interaction of Two Laser Fields with a Three Level Molecular System", IEEE Journal Of Quantum Electronics, QE-15, 170-178, (Mar 1979).

66. Drozdowciz, Z., Temkin, R.J., Lax, B., "Laser Pumped Molecular Lasers- Part I:Theory" IEEE Journal of Quantum Electronics, QE-15, 170-178, (March 1979).

67. Drozdowicz, Z., Temkin, R.J., Lax, B., "Laser Pumped Molecular Lasers- Part II: Submillimeter Laser Experiments", IEEE Journal Of Quantum Electronics, QE-15, 865-869, (Sep 1979).

68. Dicke, R.H., "Coherence in Spontaneous Radiative Processes", Physical Review, 93, 99-110, (Jan 1954).

69. Skibanowitz, N., Herman, I.P., MacGillvary, J.C., and Feld, M.S., "Observation of Dicke Superradiance in Optically Pumped HF Gas", Physical Review Letters, 30, 309-312, (Feb 1973).

70. Friedberg, R. and Hartmann, S.R., "Superradiant lifetime, Its definitions and relation to Absorption Length", Physical, Review A, 13, 495-496, Jan 1976.

71. Discussion with Capt Cook, Air Force Institute of Technology, AFIT/ENP, WPAFB, OH, 45433, (9 Sep 1981).

72. Dzakowicz, G.S. and Wutzke, S.A., "High-Pulse-Rate Glow-Discharge Stabalization by Gas Flow", Journal of Applied Physics, 44, 5061-5063, (Nov 1973).

73. Stull, D.D. and Prophet, H., JANAF Thermochemical Tables, (Second Edition), National Bureau of Standards, NSRDS-NBS 37, (June 1971).

74. Tritton, D.J., Physical Fluid Dynamics, New York: Von Nostrand Reinhold Co., 1977, 11.

75. Dolgov-Sovel'ev, G.G., Polyakov, V.A., and Chanik, G.M., "Laser Emission in the 2.8 μm Range involving Vibrational-Rotational Transitions in the HF Molecule", Soviet Physics JETP, 31, 643-645, (Oct 1970).

76. Dorko, E.A., Professor, Air Force Institute of Technology, Class note from PH 6.61, Fall Quarter, 1980.

77. Compton, R.N., Christophorov, L.G., Hurst, G.S., and Reinhardt, P.W., "Nondissociative Electron Capture in Complex Molecules and Negative Ione Lifetimes", Journal of Chemical Physics, 45, 4635-4639, (Dec 1966).

78. Curan, R.K., "Low-energy Process for $F^-$ Formation in $SF_6$", Journal of Chemical Physics, 34, 1069, (1961).

79. Cirrigan, S.J.B., "Dissociation of Molecular Hydrogen by Electron Impact", Journal of Chemical Physics, 43, 4381-4386, (Dec 1965).

80. Kondratiev, V.N., Rate Constants of Gas Phase Reactions, translated by Holtshring, National Bureau of Standards, 1972.

81. Igoshin, V.I., "Numerical Analysis of an HF-HCl Chemical Laser Utilizing the $ClF + H_2$ Chain Reaction", Kvantovoya Elektron, 6, 528-538, (Mar 1979).

82. Fettis, G.C., Knox, J.H., Trotman-Dickerson A.F., "The transfer reactions of Halogen Atoms", Canadian Journal of Chemestry, 38, 1643-1647, (Oct 1960).

83. Suchard, S.N., Kerber, R.L., Emanuel, G., Whittier, J.S., "Effect of $H_2$ pressure on Pulsed $H_2 + F_2$ Laser. Experiment and Theory", Journal of Chemical Physics, 57, 5065-5075, (Dec 1972).

84. Mercer, P.D., and Protchard, H.O., "The Gas Phase Flourination of Hydrogen-Methane Mixtures", Journal of Physical Chemestry, 63, 1468-1470, (Sep 1959).

85. Dodonov, A.F., Lavouskaya, G.K., Morozov, I. I., Wlbright, R.L., Tal'roze, V.L., and Lyubimova, A,K.", Mass-spectrometric Measurements of the Rate Constant of Elementary Reactions of Hydrogen Atoms with Chlorine and Flourine.", Kinetics and Catalysis, 1, 677-684.

86. Levy, J.B., and Copeland B.K.W., "The kinetics of the Hydrogen-Flourine Reaction III. The Photochemical Reactions", Journal of Physical Chemestry,72, 3168-3177, (Sep 1981).

87. Sarner, F.S., Propellant Chemestry, New York: Reinhold Publishing Corp, 1966, 119.

88. Guzov, I.P., Kormer, S.B., L'vov, L.V., Punin, V.T., Sinitsyn, M.V., Stankeev, E.A., and Urlin, V.D., "Measurements of the Recombination Constant of Atomic Flourine", Soviet Journal of Quantum Electronics, 6, 1112-1119, (Sep 1976).

89. Modica, A.P., and Sillers, S.J., "Experimental and Theoretical Kinetics of High-Temperature Flourocarbon Chemestry", Journal of Chemical Physics, 48, 3283-3289, (Apr 1968).

90. Bennet, J.E. and Blackmore D.R., "The measurement of the Rate of Recombination of Hydrogen Atoms at Room Temperature by Means of esr Spectroscopy", Proceedings of the Royal Physical Society A , 305, 553-574, (1968).

91. Jacobs, T.A., Giedt, R.R.,and Cohen, N., "Kinetics of Decomposition of HF in Shock Waves", Journal of Chemical Physics, 43, 3688-3693, (Nov 1965).

92. Hancock, J.K., and Green W.H., "Vibrational Reactivation of HF in pure HF and in HF-Additive Mixtures", Journal of Chemical Physics, 57, 4625-4639, (Dec 1972).

93. Hinchen J.J., "Vibrational Relaxation in Hydrogen and Deuterium Flourides", Journal of Chemical Physics, 59, 233-240, (July 1973).

94. Quigly, G.P. and Wolga, G.J., "The deactivation of HF(1) and DF(1) by O, Cl, and F atoms", Journal of Chemical Physics, 63, 5263-5268, (Dec 1975).

95. Cohen, N., "A Review of Rate Coefficients for Reactions in the $H_2$-$F_2$ Laser System", TR-0172(2279), 2 Sep 1973, The Aerospace Corporation, El Segundo, California.

## Appendix A

### Rate Constants for the $SF_6$+$H_2$/Electric Discharge Laser

Table V lists the reaction rate constants and characteristic times for the major reactions in the $SF_6 + H_2$, electric discharge laser of this investigation. The characteristic time for bimolecular reactions is given by

$$\tau = \frac{1}{k[M]} \tag{167}$$

and for three-body recombination as,

$$\tau = \frac{1}{k[M][M]} \tag{168}$$

These are the same characteristic times developed for the HF cold reaction (bimolecular) and the fluorine recombination (trimolecular) reaction in equations (59) and (55), respectively.

All rates and characteristic times will be evaluated at:

$T = 300^\circ K$
$T_e = 25{,}500^\circ K$
$[SF_6] = 4 \times 10^{-6}$ MOLES/CM$^3$ $\quad n_e = 4 \times 10^{-11}$ MOLES/CM$^3$
$[H_2] = 1 \times 10^{-6}$ MOLES/CM$^3$

All energies are in kCal/mole, temperature in °K, concentrations in moles/cubic cm, and rate constants in units of cubic cm/mole sec, unless otherwise noted. The first rate coefficient listed for each reaction is the one used in the kinetic model and the calculation of HF power pulse shape, as given in Appendix B.

Table V
$SF_6 + H_2$ / Electric Discharge Rate Constants

| Reaction | Rate Constant $(K)$ | Time Constant $(\tau)$ | Reference |
|---|---|---|---|
| 1. $SF_6 + e^- \rightarrow SF_6^-$ | $K = 2.32 \times 10^{16}\left(\frac{236.3}{T_e - 2287}\right)$ $= 2.4 \times 10^{14}$ | $\tau = 1/K n_e = 95\ \mu s$ | [32] |
| | Calculated from experiment of [77]. P=100 torr; E/N=$10^{17}$ V/ | | |
| | $K = 3.35 \times 10^{14}$ | | [33] |
| | P=.1 - 1.5 torr; Helium Buffer; Electron Beam | | |
| 2. $SF_6 + e^- \rightarrow SF_5^- + F$ | $K = (5.881 - 7.093 \times 10^{-4} T_e + 3.253 \times 10^{-9} T_e^2 - 1.826 \times 10^{-14} T_e^3) \times 10^{14}$ $= 2.4 \times 10^{14}$ | $\tau = 1/K n_e = 95 \mu s$ | [32] |
| | Calculated from experiment of reference [78]. | | |
| | $K = 2.2 \times 10^{12}$ | | [33] |
| | P=.1 - 1.5 torr; Helium Buffer; Electron Beam | | |
| 3. $SF_6 + e^- \rightarrow SF_5^+ + F + e^-$ | $K = 5.55 \times 10^{16} e^{-236850/T_e}$ $= 5.1 \times 10^{12}$ | $\tau = 1/K n_e = 4.5\ ms$ | [32] |
| 4. $SF_6 + e^- \rightarrow SF_5 + F + e^-$ | $K = 1.12 \times 10^{15} e^{-56400/T_e}$ $= 1.2 \times 10^{14}$ | $\tau = 1/K n_e = 189\ \mu s$ | [32] |
| | Calculated from experiment of [74]. P=$10^{-6}$ torr. | | |

Table V
$SF_6 + H_2$ / Electric Discharge Rate Constants
(Continued)

| Reaction | Rate Constant ($K$) | Time Constant ($T$) | Reference |
|---|---|---|---|
| 5. $SF_6 + e^- \rightarrow SF_5 + F^-$ | $k = 2.32 \times 10^{14}\left(\frac{236.3}{T_e - 2287}\right)$ $= 2.4 \times 10^{12}$ | $\tau = 1/k n_e = 9.5\ ms$ | [32] |
| 6. $H_2 + e^- \rightarrow H + H + e^-$ | $k = 10^{16} e^{-100,000/T_e}$ $= 1.98 \times 10^{14}$ | $\tau = 1/k n_e = 116\ \mu s$ | [32] |
| 7. $H + e^- \rightarrow H^+ + e^- + e^-$ | $k = 1.11 \times 10^{16} e^{-182,088/T_e}$ $= 8.5 \times 10^{12}$ | $\tau = 1/k n_e = 2.6\ ms$ | [32] |
| 8. $H_2 + e^- \rightarrow H_2^+ + e^- + e^-$ | $k = 10^{16} e^{-196,000/T_e}$ $= 4.8 \times 10^{12}$ | $\tau = 1/k n_e = 4.8\ ms$ | [32] |
| 9. $SF_6 + H \rightarrow SF_5 + HF(0)$ | $k = 2 \times 10^{15} e^{-30/RT}$ $= 3.9 \times 10^{-7}$ | $\tau = 1/k H \gg 1s$ | [33] |
| | $k = 2.\times 10^{16} e^{-30 \pm 5/RT}$ $= 3.9 \times 10^{-7}$ | | |
| 10. $SF_6 + M \rightarrow SF_5 + F + M$ | $k = P\left(8\pi RT\left(\frac{1}{M_{SF_6}} + \frac{1}{M_M}\right)\right)^{1/2} \times \sigma_{ab}^2 e^{-E_a/RT}$ $\simeq 1.05 \times 10^{-41}$ ($E_a = 76$ kcal/mole) | $\tau = 1/k M \gg 1s$ | |
| 11. $SF_5 + M \rightarrow SF_4 + F + M$ | $k = P\left(8\pi RT\left(\frac{1}{M_{SF_5}} + \frac{1}{M_M}\right)\right)^{1/2} \times \sigma_{ab}^2 e^{-E_a/RT}$ $\simeq 1.8 \times 10^{-34}$ ($E_a = 66$ kcal/mole) | $\tau = 1/k M \gg 1s$ | |

Table V
$SF_6 + H_2$ / Electric Discharge Rate Constants
(Continued)

| Reaction | Rate Constant $(K)$ | Time Constant $(T)$ | Reference |
|---|---|---|---|
| 12. $H_2 + M \rightarrow H + H + M$ | $k = P/(8\pi RT(\frac{1}{M_{H_2}} + \frac{1}{M_M}))^{1/2} \times \sigma_{ab}^2 e^{-E_a/RT}$ | | |
| | $= 1.9 \times 10^{-10}$ | $\tau = 1/kM >>> 1s$ | |
| 13. $F + H_2 \rightarrow HF(v) + H$ | $K(v=0) = 1.2 \times 10^{13} \times 10^{-3601/T}$ | | |
| | $= 3.7 \times 10^{12}$ | | |
| | $K(v=1) = 2.4 \times 10^{13} \times 10^{-3501/T}$ | | |
| | $= 7.5 \times 10^{12}$ | | |
| | $K(v=2) = 8.2 \times 10^{13} \times 10^{-3501/T}$ | | |
| | $= 2.5 \times 10^{13}$ | | |
| | $K(v=3) = 4.1 \times 10^{13} \times 10^{-3501/T}$ | | |
| | $= 1.3 \times 10^{13}$ | $\tau = 1/k_{H_2} = 200$ ns | [27], [95] |
| | $k = \sum_v k(v) = 1.2 \times 10^{14} e^{-(1.7 \pm .2)/RT}$ | | |
| | $= 6.93 \times 10^{12}$ | | [80] |
| | $K = 1.62 \times 10^{11} e^{-1.6/RT}$ | | |
| | $= 1.11 \times 10^{13}$ | | [81] |
| | $K = 10^{14} e^{-1.71/RT}$ | | |
| | $= 5.67 \times 10^{12}$ | | [82] |
| | $K(0) : K(1) : K(2) : K(3) = .15 : .3 : 1 : .5$ | | [12] |
| | $K(0) : K(1) : K(2) : K(3) = .15 : .29 : 1 : .5$ | | [27] |
| | $k(v=1) = 3.7 \times 10^{13} e^{1.6/RT}$ | | |
| | $K(v=2) = 3.26\ k(v=1)$ | | |
| | $K(v=3) = 1.63\ K(v=1)$ | | [83], [95] |

Table V
$SF_6 + H_2$ / Electric Discharge Rate Constants
(Continued)

| Reaction | Rate Constant $(K)$ | Time Constant $(T)$ | Reference |
|---|---|---|---|
| 14. $H + F_2 \rightarrow HF(v) + F$ | $k = (2.5 \times 10^{-10}) e^{-(2.4 \times 2.3)/RT} \times (6.02 \times 10^{23})$ | | |
| | $= 9.2 \times 10^{12}$ | $\tau = 1/k F_2 \geq 109$ ns | [85] |
| | $k = 1.8 \times 10^{12}$; $E_a = 15$ kcal/mol | | [86] |
| | $k = 1.58 \times 10^{12}$ | | [80] |
| | $k = 10^{13.48} e^{-4.2/RT}$ | | [80] |
| | $= 2.75 \times 10^{10}$ | | |
| | $k = 10^{12.72} T^{1/2} e^{-4/RT}$ | | [80] |
| | $= 6.25 \times 10^{12}$ | | |
| | $k = (1.1 - 7.7) \times 10^{12}$ | | [12:59] |
| 15. $H + F + M \rightarrow HF + M$ | $k = 10^{16.69} e^{-3.05/RT}$ | | |
| | $= 2.9 \times 10^{13}$ | | [80] |
| | $k = 10^{15.03} T^{1/2}$ | | |
| | $= 1.8 \times 10^{16}$ | $\tau = \frac{3.4}{k F M} \geq 20 \mu s$ | [80] |
| | $k = 7.5 \times 10^{18} T^{-1}$ | | |
| | $= 2.5 \times 10^{16}$ | | [87] |
| | $k = 10^{18} T^{-1}$ | | |
| | $= 3.3 \times 10^{15}$ | | [81] |

Table V
$SF_6 + H_2$ / Electric Discharge Rate Constants
(Continued)

| Reaction | Rate Constant ($K$) | Time Constant ($T$) | Reference |
|---|---|---|---|
| 16. $F + F + M \rightarrow F_2 + M$ | $k = 10^{14} T^{-2}$ $= 1.7 \times 10^{15}$ | $\tau = \frac{3.4}{K_{F+M}} \geq 20\mu s$ | [81] |
| | $k = 8.1 \times 10^{19} - 1.9 \times 10^{13}$ | | [88] |
| | $k = 3.6 \times 10^{15} - 7.2 \times 10^{15}$ | | [88] |
| | $k = 1.46 \times 10^{11} e^{1321/RT}$ $= 9.8 \times 10^{19}$ | | [89] |
| 17. $H + H + M \rightarrow H_2 + M$ | $k = 2.5 \times 10^{18} T^{-1}$ $= 8.3 \times 10^{15}$ | $\tau = \frac{3.4}{K_{H+M}} = 41\mu s$ | [32] |
| | $k = 3.5 \times 10^{19} T^{-1}$ $= 1.2 \times 10^{17}$ | $\tau = \frac{3.4}{K_{H+M}} = 2.8\mu s$ | [32] |
| | $k = 10^{18} T^{-1}$ $= 3.3 \times 10^{15}$ | | [83] |
| | $k = 2.7 \times 10^{15}$ | | [90] |
| 18. $HF(v) + H \rightarrow H_2 + F$ | $k = 1.2 \times 10^{13} T^{.15}$ $(v \geq 5)$ | | [32] |
| | $k = 10^{19.05} T^{-1} e^{-134/RT}$ | $\tau >> 1s$ | [91] |
| 19. $HF(v) + M \rightarrow HF(v-1) + M$ | | | |
| a. $M = H_2$ | $k = 5 \times 10^4 T^{2.06} v$ $= v(6.34 \times 10^9)$ | $\tau = \frac{1}{K_{H_2}} \geq 158\mu s$ | [32] |

Table V
$SF_6 + H_2$ / Electric Discharge Rate Constants
(Continued)

| Reaction | Rate Constant $(K)$ | Time Constant $(T)$ | Reference |
|---|---|---|---|
| (9a cont) | $K = 6.41 \times 10^{1} T^{3.51} e^{-3.906/RT}$ $= 4.23 \times 10^{7}$ | | [83] |
| | $K = v(1.6 \times 10^{4}) T^{2.28}$ $= v(7.11 \times 10^{9})$ | | [12] |
| | $K = 5.98 \times 10^{7}$ | | [92] |
| | $K = 6.96 \times 10^{7}$ | | [93] |
| b. M9 = HF | $K = v\, 10^{4.39} T^{2.3} + 10^{13} T^{-.4}$ $= (1+\frac{v}{700})\, 10^{12}$ | $\tau = \frac{1}{K_{HF}} \geq 1\mu s$ | [32] |
| | $K = 5 \times 10^{7} v(v+2) T^{1.5}$ $= 7.8 \times 10^{11}$ $(v=1)$ | | [83] |
| | $K = 1.5 \times 10^{8}$ | | [93] |
| | $K = 1.16 \times 10^{8}$ | | [92] |
| | $K = 1.31 \times 10^{8}$ | | [94] |
| c. M9 = F | $K = 1.5 \times 10^{10} T$ $= 4.5 \times 10^{12}$ | $\tau \geq 200ns$ | [83] |
| | $K = 1.5 \times 10^{10} e^{-1.1/RT}$ $= 2.4 \times 10^{9}$ | | [32] |

Table V
$SF_6 + H_2$ / Electric Discharge Rate Constants
(Continued)

| Reaction | Rate Constant ($K$) | Time Constant ($T$) | Reference |
|---|---|---|---|
| 19 d. $M = SF_6$ | $K = v(5.45 \times 10^{-4}) T^{4.056}$ $= 6.1 \times 10^{6}(v)$ | $\tau = \frac{1}{K_{SF_6}} = 16.5\,ms$ | [32] |
| e. $M = H$ | $K = f(v,v') 10^{13.9} T^{-.08} e^{-.675/kT}$ $\simeq 1.6 \times 10^{13}$ $(f(v) \sim 1)$ | $\tau = \frac{1}{K_H} = 62\,ns$ | [32] |
| | $f(3,0) = .95$ $f(2,0) = .73$ $f(3,1) = .73$ $f(2,1) = .51$ $f(3,2) = .62$ $f(1,0) = .33$ | | |
| 20. $HF + M \rightarrow H + F + M$ | $K = 1.33 \times 10^{18} T^{-1} e^{-(135.4 - E_v)/kT}$ $\simeq 10^{-83}$ | $\tau >>> 1S$ | [32] |
| 21. $HF(v) + HF(v') \rightarrow$ $HF(v-1) + HF(v+1)$ | $K = v(v+2) 5 \times 10^{7} T^{1.5}$ $= 7.8 \times 10^{11}$ $(v=1)$ | $\tau = \frac{1}{K_{HF}} \geq 1.3\mu s$ | [32] |
| | $K = 1.6 \times 10^{15} v'(v+1) \frac{1}{T}$ $= 10^{13}$ | | [12] |
| 22. $HF(v) + H_2(v') \rightarrow$ $HF(v+1) + H_2(v'-1)$ | $K = 10^{6} T^{1.5}$ $= 5.2 \times 10^{9}$ | | [32] |
| | $K = 10^{8} T^{1.5}$ $= 5.2 \times 10^{11}$ | $\tau = \frac{1}{K_{H_2}} = 2\mu s$ | [83] |

Table V
$SF_6 + H_2$ / Electric Discharge Rate Constants
(Continued)

| Reaction | Rate Constant $(K)$ | Time Constant $(T)$ | Reference |
|---|---|---|---|
| 23. $A^- + B \rightarrow A + B^-$<br>$A^+ + B \rightarrow A + B^+$ | $K \sim 1.9 \times 10^{14} \sqrt{T/\mu_{AB}}$<br>$\sim 2.6 \times 10^{16}$ | $\tau \approx 20$ ns | [32] |

## Appendix B

### Numerical Solution of the HF Laser Kinetic Model Equations

The set of differential equations modeling the $SF_6 + H_2$ in the electric discharge are as presented on page 26:

$$\frac{d[SF_6]}{dt} = -(K_1+K_2+K_3+K_4+K_5)\,n_e\,[SF_6] \tag{75}$$

$$\frac{d[H_2]}{dt} = -K_6\,n_e\,[H_2] - \sum_U K_{10}(U)\,[F]\,[H_2] \tag{76}$$

$$\frac{d[H]}{dt} = 2K_6\,[H_2]\,n_e - K_8\,n_e\,[H] + \sum_U K_{10}(U)\,[F]\,[H_2] \tag{77}$$

$$\frac{d[F]}{dt} = +(K_2+K_3+K_4)\,n_e\,[SF_6] + \sum_M K_9(M)\,[F][M] - \sum_U K_{10}(U)\,[F]\,[H_2] \tag{78}$$

$$\frac{d[F]}{dt} = +K_5\,n_e\,[SF_6] - \sum_M K_9(M)\,[M]\,[F] \tag{79}$$

$$\frac{d[HF(U)]}{dt} = +K_{10}(U)\,[F]\,[H_2] - K_{11}(U)\,[HF(U)]\,[F] \tag{80}$$

$$+K_{11}(U+1)\,[HF(U+1)]\,[F] - \sum_{U'<U} K_{12}(U,U')\,[HF(U)]\,[H] + \sum_{U'<U} K_{12}(U',U)\,[H]\,[HF(U')]$$

with the initial conditions

$$[H] = [F] = [\bar{F}] = [HF] = 0 \quad [SF_6] = 4[H_2] = 4\times 10^{-6}\ \frac{MOL}{CM^3} \tag{81}$$

The current forcing function is

$$n_e = \frac{1}{e}\int_{t_1}^{t_2} i(t)\,dt \tag{82}$$

Equation (82) is approximated by

$$n_e = \frac{1}{e}\left(\frac{i(t_2)+i(t_1)}{2}\right)\Delta t \qquad \Delta t = 20\ ns \tag{169}$$

The current, $i(t)$, is obtained from the pulse shape for current as observed by Raytheon and shown in figure 56. The results of applying equation (169) to the pulse shape of figure 56 are presented in Table VI.

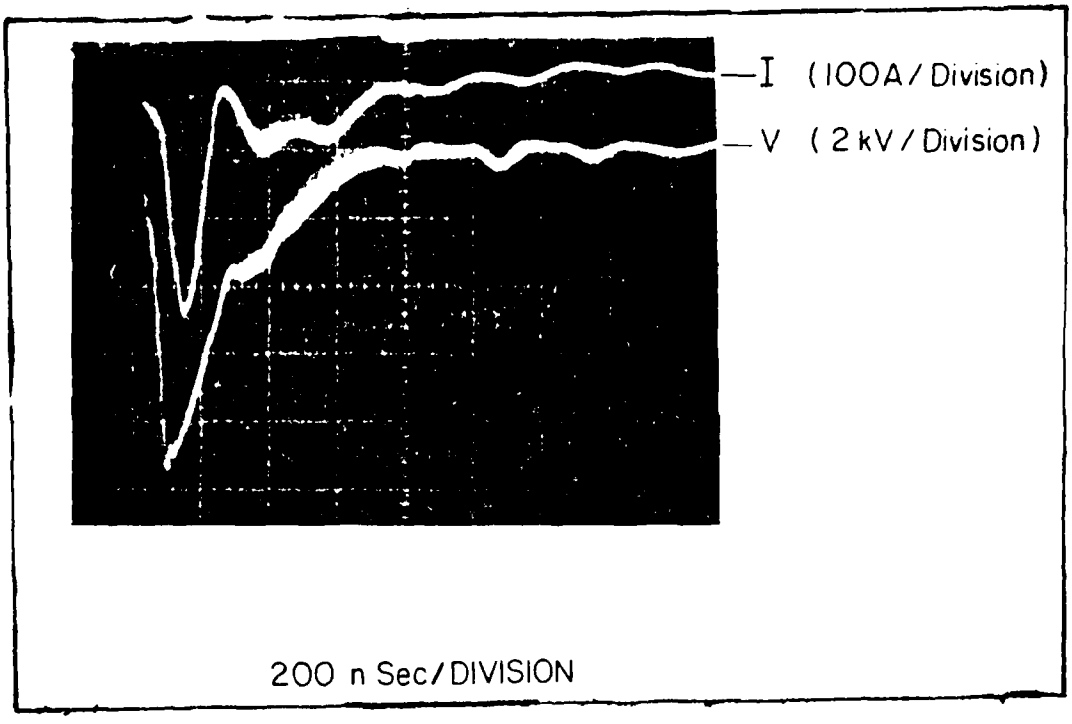


Figure 56.

Discharge Current Pulse Shape

Equation (75) can be solved directly,

$$\frac{d}{dt}SF_6 = -\left(\sum_1^5 K_i\right)\eta_e(t)\,dt \tag{75}$$

$$SF_6(t) = SF_6(0)\,EXP\left[-\sum_1^5 K_i \int \eta_e(t)\,dt\right] \tag{170}$$

$$\sum_1^5 K_i = 6.1 \times 10^{14}\ \frac{CM^3}{MOLE\text{-}S} \tag{171}$$

From Table VI, $\eta_e \sim 10^{-13}\ \frac{MOL}{CM^3}$ and $\Delta t = 20\ nS$, and the argument of the exponent is of the order $10^{-6}$. Therefore,

$$SF_6(t) = SF_6(0) \tag{172}$$

is a very good approximation for the times of interest.

Equation (79) can now be solved directly, with the use of equation (172):

$$\frac{d}{dt}F^- + \sum_M K_9(M)\,M\,F^- = K_3 SF_6\,\eta_e(t) \tag{173}$$

$$\sum_M K_9(M)\,M \approx K_9(M^*)\sum M = K_9' \tag{174}$$

$$\frac{dF^-}{dt} + K_9' F^- = K_3 SF_6 \eta_e(t) \tag{175}$$

Using an integrating factor of $S = e^{K_9' t}$ yields,

$$F^-(t) = e^{-K_9' t} \int K_3 SF_6(0) \eta_e(t) e^{K_9' t} dt \tag{176}$$

To evaluate this expression with a discrete summation approximation is difficult because the argument of the exponent is very large, $K_9' t \sim 10^4$ . Therefore, the following technique is adopted. Let

$$\eta_e(t) = \sum_0^\infty a_i t^i \tag{177}$$

with the initial condition, $\eta_e(t) = 0$ , gives

$$\eta_e(t) = \sum_1^\infty a_i t^i \tag{178}$$

Then,

$$\begin{aligned} F^-(t) &= K_3 SF_6(0) e^{-K_9' t} \sum_1^\infty a_i \int t^i e^{K_9' t} dt \\ &= K_3 SF_6(0) \sum_{i=1}^\infty \left[ a_i \left( \sum_{r=0}^{i} (-1)^r \frac{i!\, t^{i-r}}{(i-r)!\, K_9'^{r+1}} \right) \right] \\ &= \frac{K_3}{K_9'} SF_6(0) \left[ a_1 \left(1 - \frac{1}{tK_9'}\right) t + a_2 \left(1 - \frac{2}{tK_9'} + \frac{2}{(tK_9')^2}\right) t^2 + \ldots \right] \\ &= \frac{K_3}{K_9'} SF_6(0) \left[ \sum_1^\infty a_i t^i + \mathcal{O}\left(\frac{1}{K_9' t}\right) \right] \end{aligned} \tag{179}$$

But, $\frac{1}{K_9' t} \leq 10^{-4}$, even at times of 20 nsec. Then,

$$F^-(t) \cong \frac{K_3}{K_9'} SF_6(0) \eta_e(t) \tag{180}$$

From Appendix A,

$$K_9' = 1.3 \times 10^{11}\ 1/S \quad K_3 = 5.1 \times 10^{12} \frac{CM^3}{MOLE\text{-}S} \quad SF_6(0) = 4 \times 10^{-6} \frac{MOL}{CM^3} \tag{181}$$

And finally,

$$F(t) = 3.9 \times 10^{-4} n_e(t) \tag{182}$$

Equations (76) - (78) do not depend on the solution of equation (80) and may be solved independantly. A step-by-step numerical integration will be used to evaluate these functions of time. With this numerical approximation, the system of equation (76) - (78) become

$$\Delta = (K_6 X_1 n_e(t) + K'_{10} X_1 X_3)\Delta t \tag{183}$$

$$\Delta = (2K_6 X_1 n_e(t) - K_8 X_2 n_e(t) + K'_{10} X_1 X_2)\Delta t \tag{184}$$

$$\Delta = (K^2 S F_6 n_e(t) + K_9 (3.9 \times 10^{-4}) n_e(t) - K'_{10} X_1 X_2)\Delta t \tag{185}$$

Where

$$X_1 = [H_2] \qquad X_2 = [H] \qquad X_3 = [F]$$

$$K'_{10} = \sum_{v=0}^{3} K_{10}(v) \qquad K^2 = K_2 + K_3 + K_4$$

$$\Delta t = 20 \text{ ns} \qquad X_1(0) = 10^{-6} \text{ MOL/CM}^3$$

$$X_2(0) = X_3(0) = 0$$

This system was evaluated in a step by step fashion with the 20 ns time interval on a HP-25 programmable calculator. The results are presented in table VII.

The remaining equations to be solved are those for the population of HF vibrational energy levels from equation (80). For the $v = 2$ to $v = 1$ transition, it is not important to consider the $v = 0$ level. Again, a step-by-step integration of the equations given by (80) yields the following system of equation. The system was solved, again using the HP-25 calculator with a step interval of 20 nsec. A table of the concentrations of HF($v$) and of the population inversion

is presented in table VIII. These results are then used to calculate and plot the power pulse shape given in the main text in figure 3.

Table VI

Electron Number Density

| Time (nsec) | Current (Amps) | $n_e(t)$ $(2.08\times10^{-15}$ MOLE/CM$^3)$ |
|---|---|---|
| 0 | 0 | 1.25 |
| 20 | 20 | 3.13 |
| 40 | 30 | 4.38 |
| 60 | 40 | 6.25 |
| 80 | 60 | 13.75 |
| 100 | 160 | 28.75 |
| 120 | 300 | 39.00 |
| 140 | 325 | 40.00 |
| 160 | 315 | 36.56 |
| 180 | 270 | 29.38 |
| 200 | 200 | 18.75 |
| 220 | 100 | 10.00 |
| 240 | 60 | 4.38 |
| 260 | 10 | 0.63 |
| 280 | 0 | 1.25 |
| 300 | 20 | 3.75 |
| 320 | 40 | 6.88 |
| 340 | 70 | 9.38 |
| 360 | 80 | 10.63 |
| 380 | 90 | 10.94 |
| 400 | 85 | 10.31 |
| 440 | 75 | 9.06 |
| 480 | 65 | 7.81 |

Table VII

Hydrogen and Fluorine Concentrations

| Time (nsec) | $[H_2]$ $(10^{-11} \frac{MOLE}{CM^3})$ | $[H]$ $(10^{-11} \frac{MOLE}{CM^3})$ | $[F]$ $(10^{-11} \frac{MOLE}{CM^3})$ |
|---|---|---|---|
| 20 | 10.0 | .62 | 1.87 |
| 40 | 10.0 | 2.49 | 6.15 |
| 60 | 10.0 | 5.72 | 11.4 |
| 80 | 10.0 | 10.8 | 18.2 |
| 100 | 10.0 | 20.7 | 34.8 |
| 120 | 10.0 | 40.9 | 70.2 |
| 140 | 9.99 | 72.3 | 113. |
| 160 | 9.99 | 112.0 | 148. |
| 180 | 9.99 | 155. | 170. |
| 200 | 9.98 | 199. | 177. |
| 220 | 9.98 | 238. | 166. |
| 240 | 9.97 | 272. | 145. |
| 260 | 9.97 | 299. | 120. |
| 280 | 9.97 | 320. | 94. |
| 300 | 9.97 | 336. | 75. |
| 320 | 9.97 | 351. | 64. |
| 340 | 9.97 | 366. | 61. |
| 360 | 9.96 | 381. | 61. |

Table VIII

HF Concentration and Population Inversion

| Time (nsec) | HF(1) $10^{12}$ MOL/CM$^3$ | HF(2) $10^{12}$ MOL/CM$^3$ | HF(3) $10^{12}$ MOL/CM$^3$ | HF(2)-HF(1) $10^{12}$ MOL/CM$^3$ |
|---|---|---|---|---|
| 20 | 2.80 | 9.54 | 4.78 | 6.74 |
| 40 | 9.19 | 31.4 | 15.7 | 22.2 |
| 60 | 17.0 | 58.1 | 29.1 | 41.1 |
| 80 | 27.2 | 92.8 | 46.5 | 65.6 |
| 100 | 52.0 | 177. | 88.8 | 125. |
| 120 | 105. | 358. | 179. | 253. |
| 140 | 169. | 567. | 288. | 398. |
| 160 | 221. | 754. | 377. | 533. |
| 180 | 254. | 865. | 432. | 611. |
| 200 | 264. | 899. | 449. | 635. |
| 220 | 248. | 841. | 419. | 593. |
| 240 | 216. | 732. | 364. | 516. |
| 260 | 179. | 604. | 299. | 425. |
| 280 | 140. | 470. | 232. | 330. |
| 300 | 111. | 373. | 182. | 262. |
| 320 | 94.8 | 316. | 153. | 221. |
| 340 | 90.4 | 300. | 145. | 210. |
| 360 | 90.2 | 299. | 144. | 209. |

## Appendix C

### HF Laser Operating Instructions

This appendix lists the HF laser turn-on procedure used in this study. The procedure differs from that of refernce [3:84-89], due to the modifications made to the laser. The starred entries note changes and/or additions to the operating procedure dictated by these modifications.

* (1) Turn on the 400 cycle power generator
* (2) Turn on the red warning light (outside lab door) on
* (3) Turn room exhaust fan on
* (4) Turn roof fan for vacumm pump and the vacumm pump on
(5) Turn the chilled water supply on
* (6) Turn the two pulse generators and their power amp on
* (7) Turn on Boxcar Integrator #3 and establish triggering.
(8) Turn on Voltage Doubler Fan and Fluid Cooling Pump
* (9) Ground the TM 30 wire wound resistor, momentarily
(10) Turn resevoir heater on, 75%. WAIT 5 MINUTES.
* (11) Turn TM 30 unit on
* (12) Turn gas detector on
* (13) Check the gas pressure in the HF laser, (Approx 1 torr).
* (14) Turn the HV DC 220 Voltage-Single Phase circuit breaker on
(15) Open the $SF_6$ and $H_2$ gas bottles and main gas line valves
(16) Let $SF_6$, and then $H_2$ gas, into the cavity; select mixture
* (17) Adjust the By-Pass valve for the desired pressure
(18) At 60 torr or better, turn on the gas recirculating fans
* (19) Set resevoir setting at 85 - 90 %
(20) Turn the HV DC supply on an raise voltage to desired level.
* (21) Check for discharge, power pulse.

The laser turn off procedure is the reverse of the above listed procedure.

## Appendix D

### HF Beam Propogation

The theory of gaussian beam propogation will be used to calculate the beam spot size as a function of axial distance for two different focusing lenses. The following model is used:

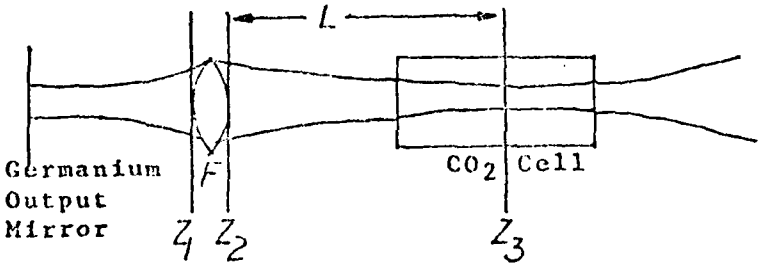


At $Z_i$ , $W = W_i$ and $R = R_i$ . From the results of the beam diveregence experiments, $W_1$ = 6mm, $R_1$ = 95.3cm. The focusing lens is $F_1$=25cm or $F_2$ = 50cm.

For a thin lens,

$$\frac{1}{Q_2} = \frac{1}{Q_1} + \frac{1}{F} \tag{186}$$

where

$$\frac{1}{Q(Z)} = \frac{1}{R(Z)} - \frac{i\lambda}{\pi W^2(Z)} \tag{187}$$

Then

$$\frac{1}{R_2} - \frac{i\lambda}{\pi W_2^2} = \left(\frac{1}{R_1} - \frac{1}{F}\right) - \frac{i\lambda}{\pi W_1^2} \tag{188}$$

and equating the real an imagniary parts of equation (188)

$$\frac{1}{R_2} = \frac{1}{R_1} - \frac{1}{F} \qquad \text{and} \quad W_2 = W_1 \tag{189}$$

Translating the beam through the distance $L$ to $Z_3$:

$$Q_3 = Q_2 + L \tag{190}$$

But,

$$Q_2 = \frac{1}{\left(\frac{1}{R_1} - \frac{1}{F}\right) - i\frac{\lambda}{\pi\omega_1^2}} = \frac{R_1 F \pi \omega_1^2}{\pi\omega_1^2(F - R_1) - i\lambda R_1 F} \tag{191}$$

And thus,

$$Q_3 = Q_2 + L = \frac{R_1 F \pi\omega_1^2 + L(F - R_1)\pi\omega_1^2 - i\lambda R_1 F L}{\pi\omega_1^2(F - R_1) - i\lambda R_1 F} \tag{192}$$

or,

$$\frac{1}{Q_3} = \frac{\pi\omega_1^2(F - R_1) - i\lambda}{\pi\omega_1^2(R_1 F + LF - R_1 L) - i\lambda R_1 F L} \tag{193}$$

Equation (193) can be rewriten as

$$\frac{1}{Q_3} = \frac{(F - R_1)(R_1 F + LF - R_1 L) + \lambda\frac{R_1 F L}{\pi\omega_1^2}}{(R_1 F + LF - R_1 L)^2 + \left(\lambda\frac{R_1 F L}{\pi\omega_1^2}\right)^2} + i\frac{\left(\lambda - \frac{R_1 F}{\pi\omega_1^2}\right)R_1 F}{(R_1 F + LF - R_1 L)^2 + \left(\lambda\frac{R_1 F L}{\pi\omega_1^2}\right)^2} \tag{194}$$

From equation (186)

$$\frac{1}{Q_3} = \frac{1}{R_3} - i\frac{\lambda}{\pi\omega_3^2} \tag{195}$$

Define the position, $L$, by $Z$ specifying the beam waist.

Then,

$$\frac{1}{R_3} \to 0 \qquad \omega_3 \to \omega_0 \tag{196}$$

Equating the real parts of equation (194) and (195) yields

$$L = -(F - R_1)R_1 F\left[\left(\lambda\frac{R_1 F}{\pi\omega_1^2}\right)^2 + (F - R_1)^2\right] \tag{197}$$

Equating the imaginary parts of equations (194) and (195) yields

$$\frac{i\lambda}{\pi\omega_0^2} = i\frac{\left(\lambda\frac{R_1 F}{\pi\omega_1^2}\right)R_1 F}{(R_1 F + LF - R_1 L)^2 + \left(\lambda\frac{R_1 F L}{\pi\omega_1^2}\right)^2} \tag{198}$$

Or, simplifying equation (198),

$$\omega_0 = \omega_1\left[\frac{(R_1 F + LF - R_1 L)^2 + \left(\lambda\frac{R_1 F L}{\pi\omega_1^2}\right)^2}{(R_1 F)^2}\right]^{1/2} \tag{199}$$

Now, substitute equation (197) into equation (199). After simplification,

$$\omega_o = \omega_1 \left[ \frac{\left(\lambda \frac{R_1 F}{\pi \omega_1^2}\right)^2}{\left(\lambda \frac{R_1 F}{\pi \omega_1^2}\right)^2 + (R_1 - F)^2} \right]^{1/2} \tag{200}$$

For the initial values of $R_1$ and $\omega_1$ quoted in the first paragraph,

$$\left(\lambda \frac{R_1 F}{\pi \omega_1^2}\right)^2 = .58 \text{ AND } 1.16 \tag{201}$$

for $F = 25CM$ and $F = 50CM$, respectively.

Since,

$$\lambda \frac{R_1 F}{\pi \omega_1^2} \ll R_1 - F \tag{202}$$

$$\omega_o \approx \omega_1 \left( \frac{\lambda R_1 F / \pi \omega_1^2}{R_1 - F} \right) = \frac{\lambda}{\pi \omega_1} \frac{R_1 F}{R_1 - F} \tag{203}$$

and

$$\omega_o = 7.4 \times 10^{-5} CM \text{ AND } 3.4 \times 10^{-4} CM \tag{204}$$

for $F = 25$ CM and 50 CM, respectively.

From equation (197), the value of $L$ is 33.9 CM or 105.2 CM for $F = 25CM$ and $F = 50$ CM focal lengths.

Equation (199) can be used to obtain the spot size at $Z = L \pm 20$ CM,

$$\omega_3 \approx \omega_1 \left( \frac{R_1 F + \lambda F - R_1 \lambda}{R_1 F} \right) = \omega_1 \left( 1 + L \left( \frac{1}{R_1} - \frac{1}{F} \right) \right) \tag{205}$$

For $F = 25CM$, $\omega_3 = 3.5$mm and for $F = 50CM$, $\omega_3 = 1.1$mm, at the ends of the $CO_2$ cell, if the cell is centered at the beam waist, $Z = 33.9$ CM and 105.2 CM, respectively.

The location, $L=105.2CM$, is rather large for the laboratory and the beam size of $\omega_3 3.5_{mm}$ at the ends of the $CO_2$ should be satisfactory. Thus, the $F=23CM$ focal length lens will be used to focus the HF beam into the $CO_2$ cavity.

# VITA

Glen Paul Perram was born on 6 May 1958 in Phoenix, Arizona. He graduated from Westland High School in Columbus, Ohio in 1976 and attended the School of Engineering, Cornell University, from which he received the degree of Bachelor of Science, with distinction, in May 1980. Upon graduation, he received a commission in the USAF as a distinguished graduate of the AFROTC program and entered the School of Engineering, Air Force Institute of Technology in June 1981.

Permanent Address: 331 King Edward West
Columbus, Ohio 43228

SECURITY CLASSIFICATION OF THIS PAGE (When Data Entered)

| REPORT DOCUMENTATION PAGE | READ INSTRUCTIONS BEFORE COMPLETING FORM |
|---|---|
| 1. REPORT NUMBER: AFIT/GEP/PH/81D-2 | 2. GOVT ACCESSION NO: DD-A111 182 | 3. RECIPIENT'S CATALOG NUMBER |
| 4. TITLE (and Subtitle): CHARACTERIZATION OF AN HF-PUMPED $CO_2$ LASER | 5. TYPE OF REPORT & PERIOD COVERED: MS Thesis; 6. PERFORMING ORG. REPORT NUMBER |
| 7. AUTHOR(s): Glen P. Perram, 2Lt USAF | 8. CONTRACT OR GRANT NUMBER(s) |
| 9. PERFORMING ORGANIZATION NAME AND ADDRESS: Air Force Institute of Technology, Wright-Patterson AFB, OH 45433 AFIT/EN | 10. PROGRAM ELEMENT, PROJECT, TASK AREA & WORK UNIT NUMBERS |
| 11. CONTROLLING OFFICE NAME AND ADDRESS | 12. REPORT DATE: December 1981; 13. NUMBER OF PAGES: 160 |
| 14. MONITORING AGENCY NAME & ADDRESS (if different from Controlling Office) | 15. SECURITY CLASS. (of this report): Unclassified; 15a. DECLASSIFICATION/DOWNGRADING SCHEDULE |

16. DISTRIBUTION STATEMENT (of this Report)

APPROVED FOR PUBLIC RELEASE AFR 190-17

Approved for public release; distribution unlimited.

Fredric C. Lynch

17. DISTRIBUTION STATEMENT (of the abstract entered in Block 20, if different from Report)

20 JAN 1982 Fredric C. Lynch

FREDRIC C. LYNCH, Major, USAF
Director of Public Affairs

18. SUPPLEMENTARY NOTES

Prepared in cooperation with the Avionics Laboratory, AFWAL, WPAFB, OH 45433 (Dr. W Schuebel and J. Brandelik/AADO/AFWAL).

19. KEY WORDS (Continue on reverse side if necessary and identify by block number)

HF Pumped $CO_2$ laser, Optically Pumped $CO_2$ laser, $^{12}C^{18}O_2$ laser at 4.3 microns, kinetics of an $SF_6 + H_2$ / electric discharge HF chemical laser.

20. ABSTRACT (Continue on reverse side if necessary and identify by block number)

Optical pumping of the 000 - $(10^0 1)_{II}$ transition in $^{12}C^{18}O_2$ by the $P_2(6)$ transition of an $SF_6$:$H_2$ electric discharge HF chemical laser was used to establish a population inversion between the $(10^0 1)_{II}$ and $(10^0 0)_{I}$ levels of $^{12}C^{18}O_2$ and lasing at 4.3 microns.

The HF pump laser was characterized and maximum power

DD FORM 1 JAN 73 1473 EDITION OF 1 NOV 65 IS OBSOLETE

SECURITY CLASSIFICATION OF THIS PAGE (When Data Entered)

achieved at 79% $SF_6$/ 21% $H_2$, 89 torr total pressure, a 12 kV discharge voltage, and 300 pulses/sec. Lasing on the $P_2(4)$, $P_2(3)$, and $P_2(2)$ transitions was observed with a beam divergence of 7 mrad. A pulse-to-pulse variation in output power of a factor of 1/3 and a frequency instability greater than 200 MHz/msec was observed. A 1.6 micro-Joule, 150 nsec pulse was observed initially.

The $P_2(3)$ TEA CO HF beam at 37.5 micro-J was coupled into a .5 inch diameter pyrex cell with 7 torr $^{12}C^{18}O_2$ with a 25 cm focal length $CaF_2$ lens. A 26 nsec $CO_2$ pulse was observed in the forward propagating direction. $CO_2$ lasing was erratic, due to near threshold pumping conditions.

A theoretical model of the kinetics of the $SF_6$ + $H_2$/ electric discharge was established. Pulse widths predicted by this theory and those observed experimentally agree well. The predicted power amplitude is larger than observed, due to losses not included in the model.

The dependence of $CO_2$ output power on HF frequency was not observed experimentally. The contradiction between established theory and previous experimental results was explained, however.


END
DATE
FILMED
3-82
DTIC